

ulm university universität
uulm

On the Noise Behavior of PLL-based Frequency Synthesizers

DISSERTATION

zur Erlangung des akademischen Grades eines

DOKTOR-INGENIEURS
(DR.-ING.)

der Fakultät für Ingenieurwissenschaften
und Informatik der Universität Ulm

von

Gurpreet Singh Sangha
aus Tohana, Indien

Gutachter:	Prof. Dr. rer. nat. Michael Hoffmann
	Dr.-Ing. Christoph Scheytt
Amtierender Dekan:	Prof. Dr.-Ing. Klaus Dietmayer

Ulm, 12. Oktober 2010

This work was completed during my time as research assistant at the Institute of Microwave Techniques at the University of Ulm. My special thanks goes to my PhD supervisor Prof. Michael Hoffmann for his guidance and support. During the difficult stages, he was always there supporting me and showing me that there is light at the end of the tunnel.

I am very grateful to Dr. Christoph Scheytt for being the second referee for this work.

Moreover, I would like to thank Prof. Wolfgang Menzel for his valuable advices during my PhD research.

I hereby would also like to thank all the members of the Institute of Microwave Techniques for the kindly working environment which never made me feel that I am coming from a foreign country with a different cultural background.

With Mr. Arnold Gronau, I gained a good friend and a great team worker who has helped me over the last years and taught me many valuable things about electronics and practical circuit design. For his highly valuable contributions towards the success of the experimental part of this work, I am very thankful.

Special words of gratitude goes to Dr. Frank Bögelsack who gave me valuable advice during my years at the Institute and supported me during the different stages of editing the PhD document.

To Ms. Ingrid Wäger, I say thanks a lot for her support with different matters, especial for helping me to translate and to fill those lengthy official German documents.

Furthermore, I am very grateful to my parents who have always encouraged me throughout all my life and were always there to guide me towards success. Without the support from them, I would have never achieved this goal.

In addition, a very affectionate thanks for my wife and son for their moral support and patience during this PhD work.

Above all, I would like to thank God who made me very successful during my academic life.

Ulm, October 2010

Gurpreet Singh Sangha

Contents

1 Introduction 1

2 Theoretical Analysis of Synthesizers Including Effects of Noise 5
- 2.1 Fundamentals of Phase-Locked Loops and Frequency Synthesizer 5
  - 2.1.1 Phase Detector (PD) . . . 7
  - 2.1.2 Control Filter (CF) . . . 8
  - 2.1.3 Voltage Controller Oscillator (VCO) . . . 9
  - 2.1.4 Frequency Divider . . . 9
- 2.2 Time Domain Analysis of a Second Order Synthesizer . . . 9
- 2.3 Non-ideal Frequency Divider . . . 12
- 2.4 An Improved Linearization Technique . . . 14
- 2.5 Method for Modeling Divider Delay . . . 15
- 2.6 First Order Synthesizer Transfer Function with a Simple Delay . 16
- 2.7 Order and Type of PLL . . . 25
  - 2.7.1 Order of PLL . . . 25
  - 2.7.2 Type of PLL . . . 26
- 2.8 Effects of Sampling . . . 27

3 Noise Analysis and Noise Modeling 29
- 3.1 Phase Noise and Spurious Tone . . . 29
  - 3.1.1 Spurious Signals . . . 29
  - 3.1.2 Phase Noise . . . 30
  - 3.1.3 White Noise . . . 31
  - 3.1.4 Flicker or $1/f$ Noise . . . 32
- 3.2 Noise Modeling . . . 33
  - 3.2.1 Rice's First Noise Model . . . 33
  - 3.2.2 Rice's Second Noise Model . . . 34
- 3.3 Synthesizer Output with Noise . . . 36
  - 3.3.1 Computation of the PLL Output Voltage . . . 41
  - 3.3.2 Average Power Spectrum . . . 48
- 3.4 Normalized Transfer Function of a Synthesizer . . . 51
- 3.5 3 dB Bandwidth for the Second Order PLL and Control Filter Parameter Calculations . . . 52
- 3.6 Noise Bandwidth of a Second Order PLL . . . 53

4 Noise simulations **56**
4.1 Synthesizer Simulation 56
4.1.1 Phase Domain Synthesizer Model 56
4.1.2 Consideration for the Noise Sources 56
4.1.3 Simulation Parameters 58
4.1.4 Simulation Results 58
4.2 Dynamic Behavior of a Synthesizer with Noise 64

5 Experimental Study of Noise **69**
5.1 Test Circuit for Noise Addition and for Studying Effects of DC Noise 69
5.1.1 DC Power Supply Rejection Ratio (PSRR) 70
5.1.2 Low Ripple and Low Noise DC Power Supply 71
5.1.3 Addition of Noise to the System 73
5.2 Frequency Synthesizer Noise Analysis System 79
5.3 Control Filter Design Considerations 84
5.4 Analysis of the Measurement Results and Comparison with Theory 89
5.4.1 Noise Added to the Reference Signal 92
5.4.2 Noise Added to the Phase Detector Output 93
5.4.3 Noise Added to the Control Filter Output 95
5.4.4 Noise Added to the VCO Power Supply 97
5.4.5 Noise Added to the VCO Output in the Feedback Path . 97
5.4.6 Noise Multiplied to the VCO Output 99
5.4.7 Comparing the Noise Floor of a PLL and a Frequency Synthesizer 101

6 Conclusion **103**

A Mathematical Treatments **105**
A.1 Linearization Technique for the Non-ideal Limiter 105
A.2 Synthesizer Transfer Function with Delay, Noise, and Non-ideal Limiter 108
A.3 Active Filter Calculation 116
A.4 Average Power Spectrum of a PLL Including Effects of Noise . . 118

List of Symbols, Indices, and Abbreviations

Symbols

ζ	Damping factor	8
$\theta_{oV}(t)$	Noise free VCO phase angle	19
$\Theta(t)$	Phase angle	10
$\tilde{\Theta}_o$	Initial/Constant value of the phase angle	11
$\Theta_{oV}(s)$	Noise free VCO phase angle in Laplace domain	19
τ_1,τ_2	Filter time constants	8
τ_M	Time delay due to divider	16
ϕ_c	Reference source constant phase offset	13
ϕ_o	VCO constant phase offset	19
$\varphi(t)$	Phase difference	10
φ_∞	Steady state phase difference	12
$\Phi(s)$	Phase difference in Laplace domain	19
$\Delta\psi$	Modulation index	29
$\psi_o(t)$	VCO phase noise	17
$\Psi_o(s)$	VCO phase noise in Laplace domain	19
$\Delta\omega$	Angular frequency step size where $\Delta\omega = {}^{2\pi}/_{T_{\mathrm{ob}}}$	33
$\omega_{3\mathrm{dB}}$	3 dB bandwidth of the PLL	52
ω_c	Reference signal angular frequency	11
ω_m	Spurious tone offset from the carrier	29
ω_n	Natural angular frequency	8
ω_o	VCO output angular frequency	11
ω_s	Sampling angular frequency	27
$\Delta\Omega$	Frequency difference between reference and VCO signals	12
b	Control filter parameter	8
B_L	Noise bandwidth of a PLL	54
C	Capacitance	9
Δf	Noise bandwidth	31

Symbols

$F(s)$	Control filter transfer function	22
$f_d(t)$	Impulse response of delay	16
$F_d(s)$	Transfer function of delay	16
$F_h(s)$	Sample-and-hold function	27
$^1/_f$	Flicker noise	2
$G(s)$	Synthesizer open loop gain	25
$\hat{G}(s)$	Sampled synthesizer open loop gain	27
$G_{\text{samp}}(s)$	Synthesizer gain after sample-and-hold	27
$H(s)$	Synthesizer transfer function	21
$H_e(s)$	Synthesizer error transfer function	26
$< i_n^2 >$	Magnitude square of the RMS noise current	31
K_D	Phase detector gain	15
K_o	VCO gain	11
K_{RM}	Sensitivity of PD to amplitude variations of the reference	15
K_{RN}	Sensitivity of PD to amplitude variations of the VCO	15
L	Inductance	9
M	Reference divider division factor	7
N	Loop divider division factor	7
$n_{CF}(t)$	Noise of the control filter	37
$n_i(t)$	Reference phase noise	17
$n_M(t)$	Noise of the reference divider	37
$n_N(t)$	Noise of the loop divider	37
$n_{PD}(t)$	Noise of the phase detector	37
$n_{VA}(t)$	VCO amplitude fluctuations	17
$n_{vp}(t)$	Phase noise of the VCO	37
R	Resistance	23
$R(t)$	Amplitude fluctuations	10
$R_\psi(\tau)$	Auto-correlation function of phase variation	30
t	Time	10
T_{ob}	Observation time	33
s	Laplace variable	8
$S_\psi(f)$	Spectral density of phase variations	30
u	Voltage Source	5

Symbols

$u_c(t)$	Control filter output voltage	5
$u_d(t)$	Phase detector output voltage	10
$< u_n^2 >$	Magnitude square of the RMS noise voltage	31
$\hat{u}$	Constant amplitude value	17
$< >$	Ensemble average	30
—	Time average	49
$*$	Convolution operator	16

Indices

0	Initial/Constant value	11
c	Control filter output	5
d	Phase detector output	10
i	Input/Reference quantity	12
iM	Phase angle after reference divider	10
iMd	Phase angle after reference divider with delay	18
in	Input/Reference quantity	5
iN	Phase angle after loop divider	10
iNd	Phase angle after loop divider with delay	18
M	Reference divider output	10
Md	Reference divider output with delay	18
N	Loop divider output	10
Nd	Feedback divider output with delay	18
o	VCO output quantity	11

Abbreviations

AGC	Automatic gain control	12
CF	Control filter	5
CMOS	Complementary metal-oxide-semiconductor	33
DC	Direct current	4
LAN	Local area network	1
LP	Lowpass filter	72
Op-Amp	Operational amplifier	70

Abbreviations

PD	Phase detector	5
PFD	Phase frequency detector	7
PI	Perfect integrator	27
PLL	Phase-locked loop	1
PSD	Power spectral density	31
PSRR	Power supply rejection ratio	70
R&S	Rohde & Schwarz	78
RMS	Root mean square	31
RTI	Referred to input	70
RTO	Referred to output	70
SAW	Surface acoustic wave	104
SNR	Signal-to-noise ratio	58
TTL	Transistor-transistor logic	80
VCO	Voltage-controlled oscillator	3
XCO	Crystal-controlled oscillator	3

1 Introduction

The Phase-Looked Loop (PLL) is a device that is used to synchronize the instantaneous phase of a locally generated signal to the instantaneous phase of the received signal. The PLL concept goes back as early as 1930s. Its first application was in the synchronization of the horizontal and vertical scan of television. Later on with the development of integrated technology, PLLs found uses in many other applications [1, 2]. In the recent years, the use of PLLs is widespread into many different areas including radar, telemetry, time and frequency control, cellular phones, cordless phones, wireless LAN, satellite communication, and computers to name a few. The three main areas of interest with respect to the functionality of the PLLs are:

- carrier tracking and synchronization,
- coherent demodulation of analog and digital signals,
- frequency synthesis.

In the first two the phase detector receives a variable input, from which one tries to extract either a carrier or the information that modulates the input signal. In the third the oscillator is coupled to a fixed reference in order to generate an output that transfers the frequency and phase properties of the reference signal.

A frequency synthesizer is a device that can generate a set of output frequencies using as reference a single stable source. Mostly a crystal oscillator is used as the reference source. PLL-based frequency synthesizers offer many advantages due to their ease of integration and low production cost.

There is a wealth of literature available describing the different concepts and applications of PLLs and frequency synthesizers some of the most important ones are [2–21].

The design of a synthesizer including component selection and evaluation is becoming ever more challenging as systems employing synthesizers are demanding higher frequency of operation, higher data rates, and lower operating voltage. As many of the applications are in portable devices, low power dissipation and small size are also required.

The electronic noise is a limiting factor in many applications including wireless communication systems. For example, it limits the transmission range of

communication links via satellite.

One of the critical parameters to consider in the design process of a synthesizer system is the influence of extrinsic and intrinsic electronic noise sources. Intrinsic and extrinsic noise are two of the fundamental types of noise effecting an electronic circuit. Extrinsic noise is due to external sources such as noise from the power supply. Intrinsic noise is generated by the components within the system. The most common types of intrinsic noise is the thermal noise, the shot noise and the flicker noise, also known as $1/f$ noise. In a synthesizer, intrinsic and extrinsic noise sources are responsible for the phase noise affecting the output of the system.

The phase noise is a random modulation of the phase of an oscillator's output due to internal and external noise sources. This random modulation manifests itself in the time domain as jitter, which is the random displacement of clock edges from a nominal position. In the frequency domain, phase noise is seen as a broadening of the oscillator's frequency spectrum due to modulation sidebands. The phase noise behavior must be known for proper loop design. It will impact many critical operating characteristics of the synthesized signal including adjacent channels.

The phase noise of a PLL-based frequency synthesizer can be a key parameter in system design. Being able to model the phase noise and to predict it with accuracy is a desirable engineering goal. Considering the scope of this single circuit, this work is devoted to the research on effect of electronic noise in a PLL-based frequency synthesizer circuit.

This work contains a thorough analysis of a PLL circuit in order to study the effect of electronic noise coming from different intrinsic and extrinsic noise sources. In comparison to the previously done analysis [22–43], a more complete combination of noise sources and better modeling techniques are used.

In addition to external sources like noise and small signal ripple on DC supply, noise from every component in the system is taken into account to study the effect of shot noise, thermal noise, and flicker noise on the system.

A new model for the phase detector is developed that includes not only the influence of the phase noise from the two signals at its input ports, but also the influence of the amplitude fluctuations of these inputs. It will be shown that inside the PLL loop, a part of the amplitude fluctuations is converted into phase noise. In order to demonstrate how the amplitude fluctuations are being converted to phase noise, a new model describing the bandpass limiter and the divider will be shown. This model is more general than the models used in literature for example in [2, 10] where it is mostly considered that the limiter is ideal and thus, the influence of amplitude fluctuations is ignored. The new

model for the bandpass limiter plus the divider will show the influence of the rise time of a signal on the noise that is coupled to the output.

In addition to that, an improved technique for analyzing the noise due to different sources in the system will be demonstrated. Using an improved mathematical noise modeling technique based on Rice's noise models [44], a method is developed that results in the derivation of a very general mathematical model for the output of synthesizers taking into account noise sources at different points in the circuit. A method for calculating the power spectral density for the output of the synthesizer containing the effect of multiple noise sources will be shown. Using the different results from the mathematical considerations, a simulation environment is built to simulate the noise and the dynamic behavior of the system taking into account linear and nonlinear models.

Furthermore, considerations for the effects of delay and sampling on the synthesizer output will be discussed.

Moreover, new results in the noise measurements of frequency synthesizers are shown in this work. Every component in the synthesizer contributes to the total output measured noise curve. Usually, it is not possible to separate the noise sources by just measuring the noise curve at the output of a frequency synthesizer. Here, a new measurement technique with which it is possible to predict the effects of noise due to different devices on the synthesizer output will be presented. In order to accomplish this, a new synthesizer noise analysis system was built with the possibility of adding noise to the output of different devices in the system in order to raise their noise floor above the noise floor of the system. The built synthesizer circuit is optimized to have a low noise floor. Then stronger noise is added at different points in the synthesizer in a way that it would represent noise of a certain device in the system. Not only the influence of additive noise is considered, but also the influence of multiplicative noise on the synthesizer loop.

An improved low noise power supply which helps to lower the noise floor of critical components in the system like XCO and VCO will also be shown.

A part of the work shown here has been published before by the author in [45–48].

Chapter 2 shows the theoretical analysis of the synthesizer. In this chapter a new and more general differential equation of a synthesizer is derived, and a new linear model for the phase detector is developed. A model representing propagation of amplitude fluctuations through a frequency divider will also be demonstrated. In addition to that, the output of the synthesizer including effects of delay will be derived and used to discuss effects of delay and sampling on the synthesizer system.

Chapter 3 contains mathematical noise analysis of a frequency synthesizer. In this chapter Rice's noise models are discussed. Using Rice's model, it will be shown how the output voltage of a synthesizer including effects of different noise sources can be derived. A technique for calculating the power spectral density for the synthesizer output including effects of noise will be shown. Additionally, the noise bandwidth of a PLL will be discussed.

Chapter 4 shows simulation results of a synthesizer system where the influence of different noise sources on the PLL output spectrum will be demonstrated. In addition to that, the dynamic behavior of the system including different noise sources in the loop will be studied through use of phase-plane plots.

Chapter 5 shows the measurement results of a synthesizer with noise. A low noise DC source and a frequency synthesizer noise measurement system will be introduced. This setup will be used to show the influence of component noise on the synthesizer output spectrum. The simulation results from Chapter 4 will be compared with the measurement results.

2 Theoretical Analysis of Synthesizers Including Effects of Phase and Amplitude Variations

In this chapter a theoretical analysis of PLLs and frequency synthesizers will be presented. It provides detailed description into the different concepts of the linear and the non-linear analysis of PLL systems. The results that will be presented here are more general to what is found in the literature. A new differential equation and a novel phase detector model for the synthesizer will be presented. In addition to that consideration for the delay and the sampling effects on the synthesizer will also be taken into account. The noise analysis that will follow is built upon the theoretical analysis presented here.

2.1 Fundamentals of Phase-Locked Loops and Frequency Synthesizer

A Phase-Locked Loop (PLL) is a feedback control circuit. The PLL consists mainly of a small set of building blocks as shown in Fig. 2.1 and listed below:

- a reference source $u_{\text{in}}(t)$,
- a phase detector (PD),
- a loop filter also known as control filter (CF),
- a voltage control oscillator (VCO),
- a feedback path,

The phase-locked loop uses a negative feedback path to lock the output to the phase of the input signal. The phase detector compares the phase of the output signal to the phase of the reference signal. It generates an output voltage u_d that is proportional to the phase error or phase difference of the two signals. This output voltage of the PD passes through the loop filter. The output of the loop filter u_c is passed as an input to the VCO. It allows the output frequency of the VCO to be tuned in the right direction so that the phase error between the VCO signal and the input signal will be constant after the PLL reaches a steady state. This self correcting technique allows the output signal to be in phase with the reference signal. The PLL is said to be in lock condition, when

both signals are synchronized. At this point the phase error between the two signals is zero or constant depending on the type of control filter.

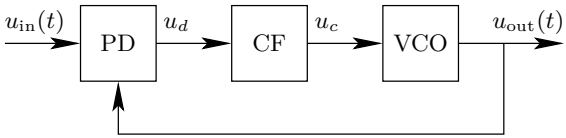

Fig. 2.1: Phase-locked loop block diagram.

For passive control filters there will remain a constant shift between the input phase and the VCO phase. For an active control filter the difference between the two phases can be zero.

The PLL locks onto the input signal, as long as the initial frequency difference between the input and the VCO signal is not too big. This period of frequency acquisition is referred to as pull-in time. Depending on the bandwidth of the PLL, this can be very long or very short. The bandwidth of a PLL is mainly dependent on the characteristics of the phase detector (PD), voltage controlled oscillator (VCO) and on control filter (CF).

One can define different modes of operation of a PLL: acquisition, tracking, and locked or synchronous mode. The acquisition mode refers to the interval during which the loop wanders within its tuning range, searching to follow the input, but still is not locked to it. The tracking mode concerns the function of the PLL when it follows a non constant input, whose variations have to be tracked within the tuning range. Finally, the locked mode refers to the case when PLL has reached steady state and there is a constant phase difference between VCO and input signal.

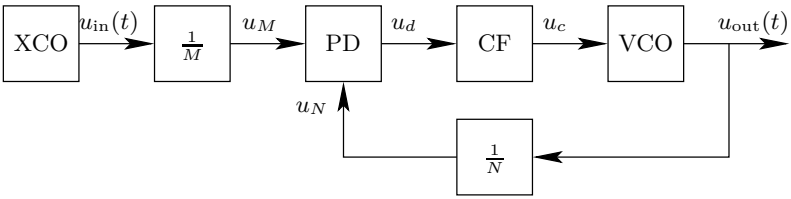

Fig. 2.2: Frequency synthesizer block diagram.

In the case of a synthesizer as shown in Fig. 2.2, the reference frequency is fixed. As a reference source, mostly a crystal-controlled oscillator (XCO) is

used. A reference divider $(1/M)$ follows the reference source. In addition to that, there will be a divider $(1/N)$ in the feedback path.

More complex frequency synthesizers, which employ higher order loops, and multiple phase-locked loops exist and can be considered for theoretical analysis. The mathematical analysis of frequency synthesizers could be very demanding. The theoretical analysis in this work will be limited to second order frequency synthesizer systems. The focus of the next sections would be to develop mathematical models for analyzing phase-locked loops.

In the next subsections a brief introduction into the different fundamental blocks constituting frequency synthesizer will be given.

2.1.1 Phase Detector (PD)

The phase detector (PD) is a device that can produce an output signal that is function of the phase difference between the two harmonic signals at its input ports. There are different types of phase detectors [2, 3, 10].

The type-I phase detector consists of a mixer plus a lowpass filter. The output of this phase detector has a sine wave characteristic. This PD is nearly linear to phase difference between the two input signals over a range of around $(-\pi/4,\pi/4)$. The disadvantage of this phase detector is the small linear range, and the phase detector gain depend on the amplitude of the input signal. The advantage is that it can operate up to very high frequencies.

Replacing the mixer with an EXOR-gate results in a type-II phase detector that has a linear range $(-\pi/2,\pi/2)$.

A type-III phase detector is based on a JK-flip flop and produces a sawtooth characteristic linear to the phase error of the two input signals over a range of $(-\pi,\pi)$.

The most commonly used phase detector in synthesizers is the phase frequency detector (PFD) also known as 3-state phase detector. This type-IV PD consists of two D-flips flops and a reset path. The output of the phase detector is linear to the phase error of the input signals over a range of $(-2\pi,2\pi)$. This phase detector has a large linear range and can be used to detect frequencies when the PLL is out of lock. The disadvantage of this PD is the limited operation frequency and also the *dead zone* problem that may appear depending on the circuit implementation.

Memoryless phase detectors like type-I and type-II have a very limited phase detection range. The presence of memory elements in the phase detector can extend the linear region over several periods depending on the complexity of the phase detector implementation.

As it will be discussed later, the inclusion of digital components into the loop

makes the PLL a sampled system. The continuous description can be used as long as the system bandwidth is much smaller than the sampling frequency.

2.1.2 Control Filter (CF)

The loop filter design is one of the most important parts of the whole synthesizer system and plays a significant role in determining the performance of the loop. The loop filter, which is a lowpass filter inserted between the phase comparator and the VCO input terminal, performs the filtering operation on the error voltage coming out of the phase detector. The main purpose of this filter is to modify the dynamic behavior of the system. It helps to control the PLL bandwidth and thus allows to modify the settling and tracking behavior.

A loop filter introduces poles to the PLL transfer function, which plays a role in determining the bandwidth of the PLL. Note that the order of the PLL is directly proportional to the order of the filter used. When the order of the filter is n, the order of the PLL is n+1.

It is preferable to have a PLL of second order with high loop gain due to the fact that they provide absolute stability [3].

The phase detector output consists of a DC component superimposed with a high frequency component. Usually, an extra lowpass filter is used in front of the control filter in order to filter out the high frequency component which is an undesired part of the input to the VCO. In general, the lower the cutoff frequency of this filter, the more the reference leakage from the phase comparator is suppressed, but care should be taken that this filter does not dominate the control filter behavior. In general, this lowpass filter could be a part of the control filter. The loop filter in this case have the low frequency parts attributing to control filter and higher frequency parts used to attenuate distortion. In practice, higher order loop filters are used in order to increase the attenuation of the spurious signals like carrier leakage and higher frequency harmonics due to non-linear effects.

The control filter could be active or passive. The active control filter is commonly based on an operational amplifier circuit. The lag-lead type of control filter, whose transfer function is given below, is most commonly used:

$$F(s) = \frac{s\tau_2 + 1}{s\tau_1 + b}\,, \tag{2.1.1}$$

with b=0 for active filter and b=1 for passive filter. τ_1 and τ_2 are the filter time constants. As it will be discussed later, this filter has an advantage in that it allows an independent choice of the two important PLL parameters natural angular frequency ω_n and damping factor ζ .

2.1.3 Voltage Controller Oscillator (VCO)

Many different types of VCOs are used in PLLs. Among the important types commonly used are based on the ring oscillator and the LC tuned oscillator [11]. The ring oscillator consists of an odd number of inverter stages connected in feedback. It usually takes less area and has a large tuning range, but has poorer phase noise performance.

The LC oscillators are among the most common types of oscillator used. This resonator consists of an LC network and an amplifier connected to form a feedback system. The LC oscillator type can be designed for a fixed frequency and also for variable frequency operation by using varactor diodes to replace the fixed value of C. The oscillator performance is determined by the quality factor of the LC resonator. The LC oscillator has a smaller tuning range and often takes more chip area due to inductor size, but it can run at a much higher frequency and generally provides a better phase noise performance.

2.1.4 Frequency Divider

The feedback programable frequency divider is an important part of the PLL-based frequency synthesizer circuit [3]. The divider allows to produce a range of output frequencies in a synthesizer system. Based on the divider used, two different types of frequency synthesizers can be defined integer-N and fractional-N.

In the integer-N synthesizer, the used frequency divider is simply a digital counter. The integer frequency division ratio is produced by the counter generating an output pulse every N input pulses. The frequency divider can be thought of as a state machine clocked by the VCO. Every N number of VCO cycles, a rising edge would occur at the divider output.

In fractional-N synthesizers the integer division ratio is alternated between two or more values so that the average division ratio lies somewhere in between. This is commonly referred to as fractional-N averaging. The frequency produced by fractional-N synthesizers will be non-integer multiple of the reference. This allows to use a smaller division ratio N which also means a higher phase detector frequency can be used but at the expense of fractional spurs.

2.2 Time Domain Analysis of a Second Order Synthesizer

In this section the time domain equations of a synthesizer shown in Fig. 2.2 will be described and used to discuss the steady state behavior of a synthesizer. The differential equation relating the phases will be derived taking into account that a first order control filter is being employed. This means the derivations are for a second order synthesizer system.

The signal $u_M(t)$ after the reference divider and the signal $u_N(t)$ after the loop divider can be described in the general form:

$$u_M(t) = f_M(R_M(t), \theta_{iM}(t)) \,, \tag{2.2.1}$$

$$u_N(t) = f_N(R_N(t), \theta_{oN}(t)) \,. \tag{2.2.2}$$

The expressions $R_M(t)$ and $R_N(t)$ describe the amplitude fluctuations of the reference and the voltage control oscillator signal that appear at the phase detector after passing through the dividers. A more elaborated mathematical description of the terms $R_M(t)$ and $R_N(t)$ will follow in the next section.

At the phase detector, the two signals $u_M(t)$ and $u_N(t)$ coming from the reference and the loop divider are compared. A novel model for the output of the phase detector which was derived by the author [45] is:

$$u_d(t) = g(R_M(t), R_N(t), \varphi(t)) \,, \tag{2.2.3}$$

$$\text{with} \quad \varphi(t) = \theta_{iM}(t) - \theta_{oN}(t) \,. \tag{2.2.4}$$

In this model the output voltage $u_d(t)$ of phase detector is described as a function depending not only on the phase difference $\varphi(t)$ between VCO signal phase variations $\theta_{oN}(t)$ and input signal phase variations $\theta_{iM}(t)$, but also on amplitude fluctuations $R_M(t)$ of input signal, as well as of amplitude fluctuations $R_N(t)$ of the VCO signal. The novel model shown in 2.2.3 is thus more complete as compared to models in use in literature for example in [3, 10].

In order to proceed with the analysis of a second order system, a first order control filter can be described mathematical using:

$$\tau_1 \dot{u}_c + b u_c = \tau_2 \dot{u}_d + u_d \,. \tag{2.2.5}$$

In this equation the terms τ_1 and τ_2 represent the filter time constants and the parameter b represents a gain factor. When $\tau_1{=}\tau_2{=}0$ and $b{\neq}0$, then the filter is of order zero. The system will be reduced to a first order synthesizer. Two further cases can be considered where $b{=}0$ representing a second order PLL with an active control filter (first order perfect integrator) and the case with $b{=}1$ representing PLL with a passive control filter. The instantaneous phase at the VCO output can be described by:

$$\Theta_o(t) = \omega_o t + K_o \int_0^t u_c(\tau) \mathrm{d}\tau + \tilde{\Theta}_0 \,, \tag{2.2.6}$$

where the proportionality constant K_o is designated as the oscillator gain with the dimension [rad/Vs]. The instantaneous phase of the VCO can be expressed after the loop divider N as:

$$\Theta_N(t) = \frac{\omega_o}{N}t + \frac{K_o}{N}\int_0^t u_c(\tau)\mathrm{d}\tau + \frac{\tilde{\Theta}_0}{N}\,. \tag{2.2.7}$$

Combining the results from the above discussion, it is possible to derive the second order synthesizer differential equation:

$$\begin{aligned}\tau_1\ddot{\varphi} + \left\{b + \frac{K_o\tau_2}{N}\frac{\partial g(R_M,R_N,\varphi)}{\partial\varphi}\right\}\dot{\varphi} + \frac{K_o}{N}\,g(R_M,R_N,\varphi)\\ + \frac{K_o\tau_2}{N}\frac{\partial g(R_M,R_N,\varphi)}{\partial R_M} + \frac{K_o\tau_2}{N}\frac{\partial g(R_M,R_N,\varphi)}{\partial R_N}\\ = \tau_1\ddot{\Theta}_{iM} + b\dot{\Theta}_{iM} - \frac{b\omega_o}{N}\end{aligned} \tag{2.2.8}$$

This is a nonlinear differential equation for first and second order synthesizers. It is a first order equation when τ_1=0 and a second order equation in all other cases.

The differential equation (2.2.8) differs from what is commonly used due to the introduction of terms that depend on the amplitude fluctuations of the input and VCO signal. The phase detector function is also different than the simple model commonly used. In literature it is usually taken to be dependent only on the phase error between the two phase detector input signals.

In order to understand the steady state properties of a frequency synthesizer, one can look at a very special case of the differential equation (2.2.8). Consider the case where the amplitude of the VCO signal is constant $R_N(t)$=R_{N0} and the VCO frequency is constant and equal to ω_o. The input signal is a sinusoidal with constant amplitude $R_M(t)$=R_{M0} and constant angular frequency ω_c:

$$\begin{aligned}\tau_1\ddot{\varphi} + \left\{b + \frac{K_o\tau_2}{N}\frac{\partial g(R_{M0},R_{N0},\varphi)}{\partial\varphi}\right\}\dot{\varphi} + \frac{K_o}{N}\,g(R_{M0},R_{N0},\varphi)\\ = b\omega_c - \frac{b\omega_o}{N}\,.\end{aligned} \tag{2.2.9}$$

Equation (2.2.9) shows a simplified case which could be used to see if there is a chance of synchronization between the input signal and the VCO signal. If there is a solution for this simplified case, then there is a possibility of getting a solution for the more general case.

For synchronization to be possible, after a sufficiently long time the instantaneous phases of input and VCO signal should differ by at most a constant value. That means $\ddot{\varphi} \to 0$; $\dot{\varphi} \to 0$ and $\varphi \to$ const:=φ_∞ and (2.2.9) reduces to:

$$g(R_{M0}, R_{N0}, \varphi_\infty) = \frac{b}{K_o}(N\omega_c - \omega_o) = \frac{b\Delta\Omega}{K_o}\,, \tag{2.2.10}$$

where $\Delta\Omega$=$N\omega_c$−ω_o describes the initial frequency difference between the input and the VCO signal. Equation (2.2.10) can usually be solved graphically or numerically. It gives a solution for the operating points of a synthesizer. Only if this equation has a solution then there is a possibility (not a guarantee) that the synthesizer will be able to establish a synchronization. The existence of the solution depends on the amplitude value of the input signal. It also depends on the initial angular frequency difference between the input and the VCO signal. In the case where b=0, there will always be a solution. This corresponds to the case with an integrator control filter as mentioned before.

2.3 Non-ideal Frequency Divider

Amplitude noise may originate from different sources within oscillators. For example non-linear or limiting output stages may be sensitive to the power supply, hence directly modulating power supply noise onto the amplitude of the oscillator. An AGC (automatic gain control) circuit can modulate noise onto the signal. Various amplitude limiting mechanisms can similarly degrade the amplitude spectrum.

Usually it is considered that the amplitude of the VCO and the reference signal arriving at the phase detector after the reference and the feedback dividers are constant for example in [2,10]. It is usually assumed that there is a limiting stage for example in front of the divider that limits the amplitude.

The commonly used model for the frequency divider consists of a hard-limiter and a bandpass filter. In this model the amplitude of the signal after the limiter is constant and is equal to $4b/\pi$. b is the maximum amplitude limiting factor. The derivation details for the hard limiter can be found in [49].

A new and superior non-ideal divider model with the block diagram in Fig. 2.3 is derived by the author. This new non-ideal divider consists of a piecewise linear limiter and a frequency divider. The new piecewise linear limiter model represents a real limiter in a frequency divider in a better way. In Section A.1 on page 105 there is a detailed derivation of piecewise linearized characteristic for the non-ideal limiter.

Given is a sinusoidal signal of the form $R(t)\cos(\omega_c t + n_i(t) + \phi_c)$ at the input $u_{\text{in}}(t)$. In this equation $n_i(t)$ is a random process uniformly distributed between

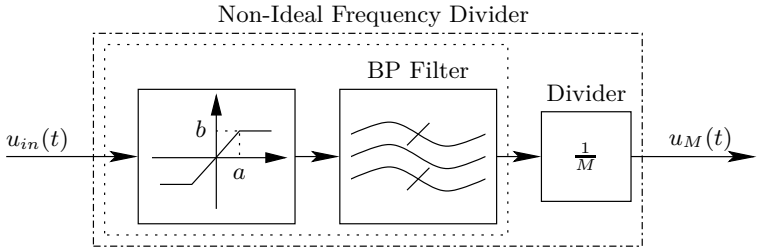

Fig. 2.3: Non-ideal frequency divider where a nonlinear limiter is approached by using piecewise linear characteristic.

$[0, 2\pi)$ describing the phase noise of the input signal and ϕ_c is some constant phase shift. The output signal of this divider can be derived by application of Fourier-series method with respect to the phase while holding the time constant as it is demonstrated in Section A.1. Using the results from A.1, the bandpass divider output signal with its dependency on the input signal amplitude and the phase angle can be expressed as shown in:

$$\begin{aligned} u_M(t) &= R_M(t)\cos(\theta_M(t))\,, \\ &= \left\{ \frac{4b}{\pi}\sin(\theta) + \frac{bR(t)}{a\pi}\left[-\sin(2\theta) + (\pi - 2\theta)\right] \right\} \cdot \\ &\quad \cos\left(\frac{\omega_c}{M}t + \frac{n_i(t)}{M} + \frac{\phi_c}{M} \right)\,, \end{aligned} \tag{2.3.1}$$

with the conduction angle θ=arccos(a/R_L), and R_L being the limiting amplitude value. Parameters a and b describe the x-y-axis amplitude limiting factors.

In contrast to the ideal limiter which suppresses completely the amplitude fluctuations of the input signal, the output signal in this case is dependent on the amplitude variations of the input signal as it would be expected from a real divider. This is due to the fact that a real limiter circuit never has an infinitely short rise time as it is assumed for the ideal limiter. Due to the finite rise time, the output signal is not a perfect square wave. Thus a part of the amplitude fluctuations can couple to the output on the finite rising and falling edge of a real non-ideal square wave signal generated at the output of the limiter. This will be demonstrated later in the measurement in Chapter 5 where amplitude noise will be multiplied to the VCO output.

The model derived in (2.3.1) is more general than that one used in the literature. It shows clearly how a part of the amplitude fluctuations are appearing

at the output of the divider circuit. These amplitude fluctuations are leading to proportional terms at the output of the phase detector and are converted into phase fluctuations inside the synthesizer system. For $a \to 0$ implies the conduction angle $\theta \to \pi/2$, this model gives results that are in agreement with the ideal limiter model, i.e. $R_M(t) = 4b/\pi$. For this particular case the model derived here reduces to the ideal limiter model derived in [49].

2.4 An Improved Linearization Technique

In this section, the linear model describing a PLL-based frequency synthesizer will be derived. Equation (2.2.8) is the nonlinear differential equation for the first and the second order PLL based frequency synthesizer. If it can be ensured that the input signal in (2.2.1) is slowly varying form of a signal of type $f_M(R_{M0}, \omega_c t + \phi_c)$, then the linearization of the phase detector function in the vicinity of the operating point $(R_{M0}, R_{N0}, \varphi_\infty)$ is possible. Here, ϕ_c describes a constant phase shift in the input signal, R_{M0} is the maximum amplitude of input and ω_c is the input signal angular frequency in rad/s.
Performing a first order Taylor series expansion for the output of the phase detector in the vicinity of the operating point gives:

$$\begin{aligned} u_d(t) = g(R_M(t), R_N(t), \varphi(t)) \approx g(R_{M0}, R_{N0}, \varphi_\infty) \\ + \frac{\partial g}{\partial \varphi}\bigg|_{(R_{M0}, R_{N0}, \varphi_\infty)} (\varphi(t) - \varphi_\infty) + \frac{\partial g}{\partial R_M}\bigg|_{(R_{M0}, R_{N0}, \varphi_\infty)} (R_M(t) - R_{M0}) \\ + \frac{\partial g}{\partial R_N}\bigg|_{(R_{M0}, R_{N0}, \varphi_\infty)} (R_N(t) - R_{N0}) \end{aligned} \tag{2.4.1}$$

$$\begin{aligned} u_d(t) \approx \frac{b\Delta\Omega}{K_o} + K_D(\varphi(t) - \varphi_\infty) \\ + K_{RM}(R_M(t) - R_{M0}) + K_{RN}(R_N(t) - R_{N0})\,. \end{aligned} \tag{2.4.2}$$

It was already shown in (2.2.10) that:

$$g(R_{M0}, R_{N0}, \varphi_\infty) = \frac{b\Delta\Omega}{K_o}\,. \tag{2.4.3}$$

From the linearized phase detector output shown in (2.4.2), the following terms can be defined. The well-known phase detector constant also referred to as

phase detector gain in [V/rad]:

$$K_D = \left.\frac{\partial g}{\partial \varphi}\right|_{(R_{M0},R_{N0},\varphi_\infty)} . \tag{2.4.4}$$

Due to this better modeling technique, two new terms are introduced into the linearized phase detector function. The phase detector sensitivity to the input signal amplitude variations is defined as:

$$K_{RM} = \left.\frac{\partial g}{\partial R_M}\right|_{(R_{M0},R_{N0},\varphi_\infty)} , \tag{2.4.5}$$

and the phase detector sensitivity to the VCO signal amplitude variations accordingly is defined as:

$$K_{RN} = \left.\frac{\partial g}{\partial R_N}\right|_{(R_{M0},R_{N0},\varphi_\infty)} . \tag{2.4.6}$$

The new linear model for the phase detector output shows that within the synthesizer bandwidth a part of amplitude fluctuations will be fed as tuning voltage fluctuations to the VCO input and will be converted into phase noise at the output of the synthesizer. This is also evident from the measurement results as it will be shown in the measurement Chapter 5 on page 99.

2.5 Method for Modeling Divider Delay

Due to the discrete nature of the frequency synthesizer, it usually contains a loop delay. The phase detector as well as the divider introduce a certain amount of a delay to the synthesizer system. The presence of the delay restricts the stability region of the PLL. During acquisition stage this delay can be especially critical in systems where the bandwidth is quite large. Root locus techniques could be used to simulate delay effects in the synthesizer system [50]. It is also possible to consider the discrete nature of the synthesizer system and derive a model using Z-transform [51]. As it will be shown later it is also possible to study effects of delay using the phase-plane trajectories.

Figure 2.4 shows a modeling technique for the delay associated with respect to the digital frequency divider. Only a special case of a simple ideal delay affecting the signal is considered. When a signal $u_M(t)$ is applied to a simple time delay element, the resulting output will be a time-shifted version of the input. For a simple delay, it is assumed that the signal does not suffer from any distortion

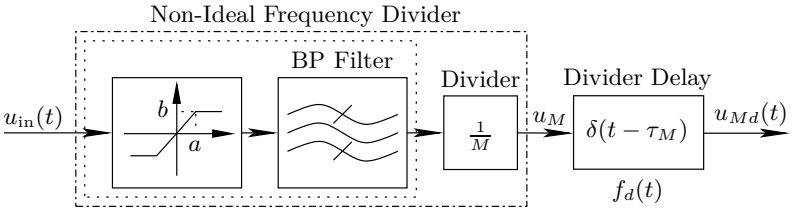

Fig. 2.4: Piecewise linear limiter circuit with delay.

and all the frequencies present in $u_M(t)$ are passed without attenuation. The simple delay has an impulse response of $f_d(t)$=$\delta(t-\tau_M)$. The transfer function of the delay $F_d(s)$ alone can be written down as:

$$F_d(j\omega) = \mathrm{e}^{-\mathrm{j}\omega\tau_M} \,. \tag{2.5.1}$$

This transfer function would change only the phase margin. Depending on how high the delay is, the effect on the phase margin could be significant turning a stable system into an unstable one. In the case of a simple delay element in the system, the output of the divider from (2.3.1) can be rewritten as convolution relation as described below:

$$\begin{aligned} u_{Md}(t) &= u_M(t) * f_d(t)\,, \\ &= R_M(t-\tau_M)\cos(\theta_M(t-\tau_M))\,. \end{aligned} \tag{2.5.2}$$

The Laplace domain expression of 2.5.2 is given as:

$$\begin{aligned} u_{Md}(s) &= u_M(s) f_d(s)\,, \\ &= u_M(s)\mathrm{e}^{-s\tau_M} \,. \end{aligned} \tag{2.5.3}$$

This is the delay theorem of the Laplace transform. It turns a convolution integral into a product relationship. The result is of interest only for functions $u_M(t)$ which are zero for t<0 or more generally for t<τ_M. The delay time τ_M has a fixed value greater than or equal to zero.

2.6 First Order Synthesizer Transfer Function with Consideration of a Simple Delay

In this section a simple first order frequency synthesizer, shown in Fig. 2.5, will be considered in order to demonstrate how the output of the synthesizer in case of delay could be calculated.

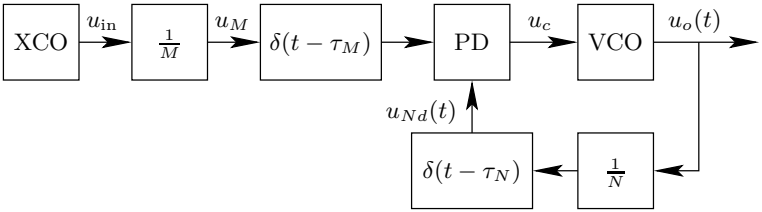

Fig. 2.5: First order synthesizer circuit with a simple delay.

The more elaborated output of a higher order synthesizer with delay and also including effects of different noise sources was also derived as shown in Appendix A.2 on page 108. The reference signal at the synthesizer input is described in general form including effect of amplitude and phase noise:

$$\begin{aligned} u_{\text{in}}(t) &= \hat{u}_{\text{in}}(1+R(t))\cos(\omega_c t + n_i(t) + \phi_c)\,, \\ &= A(t)\cos(\Theta_i(t))\,, \end{aligned} \tag{2.6.1}$$

where $R(t)$ and $n_i(t)$ are random variables representing the amplitude and the phase noise of the reference signal, respectively; ϕ_c is a constant offset. In a similar way the signal coming out of the VCO can be described as:

$$\begin{aligned} u_o(t) &= \hat{u}_o(1+n_{VA}(t))\cos(\omega_o t + \psi_o(t) + \phi_o)\,, \\ &= n_o(t)\cos(\Theta_o(t))\,, \end{aligned} \tag{2.6.2}$$

where $n_{VA}(t)$ describes the amplitude fluctuations and $\psi_o(t)$ represents the phase noise of the VCO. Consider a soft limiter that consists of a piecewise linear limiter and bandpass filter, as described in Section 2.3 on page 12, to be a part of the reference and feedback dividers. The center frequencies for both limiter-bandpass filters are at ω_c and ω_o, respectively. Using previous results, it could be shown that a part of the amplitude fluctuations of the signal will pass through the divider. The reference signal after the bandpass soft limiter plus divider can be described as:

$$\begin{aligned} u_M(t) &= R_M(t)\cos(\Theta_{iM}(t)) = R_M(t)\cos\left(\frac{\Theta_i(t)}{M}\right) \\ &= \left\{\frac{4b}{\pi}\sin(\theta_1) + \frac{A(t)b}{a\pi}\left[-\sin(2\theta_1) + (\pi - 2\theta_1)\right]\right\}\cdot \\ &\quad \cos\left(\frac{\omega_c}{M}t + \frac{n_i(t)}{M} + \frac{\phi_c}{M}\right)\,. \end{aligned} \tag{2.6.3}$$

In a similar way the output of the loop divider and its dependency on the amplitude and the phase of the VCO signal can be expressed as:

$$\begin{aligned} u_N(t) &= R_N(t)\cos(\Theta_{oN}(t)) = R_N(t)\cos\left(\frac{\Theta_o(t)}{N}\right), \\ &= \left\{\frac{4d}{\pi}\sin(\theta_2)+\frac{n_o(t)d}{c\pi}\left[-\sin(2\theta_2)+(\pi-2\theta_2)\right]\right\}\cdot \\ &\quad \cos\left(\frac{\omega_o}{N}t+\frac{\psi_o(t)}{N}+\frac{\phi_o}{N}\right), \end{aligned} \tag{2.6.4}$$

with θ_1 and θ_2 being the conduction angles for the limiters in the reference and the feedback divider, respectively. Parameters a, b, c and d describing corresponding the x-y-axis amplitude limiting factors.

Taking the reference and the feedback divider delays into account, the two input signals to the phase detector can be expressed similar to (2.5.2):

$$u_{Md}(t) = R_M(t-\tau_M)\cos(\theta_{iM}(t-\tau_M)), \tag{2.6.5}$$

$$u_{Nd}(t) = R_N(t-\tau_N)\cos(\theta_{oN}(t-\tau_N)). \tag{2.6.6}$$

In order to facilitate the derivation shown later, the following variables are defined:

$$R_{Md}(t) = R_M(t-\tau_M), \tag{2.6.7}$$

$$R_{Nd}(t) = R_N(t-\tau_N), \tag{2.6.8}$$

$$\theta_{iMd}(t) = \theta_{iM}(t-\tau_M) = \frac{\Theta_i(t-\tau_M)}{M}, \tag{2.6.9}$$

$$\theta_{oNd}(t) = \theta_{oN}(t-\tau_N) = \frac{\Theta_o(t-\tau_N)}{N}. \tag{2.6.10}$$

As it was demonstrated in (2.2.3), the phase detector output is dependent on the amplitude fluctuations of the two input signals as well as the phase difference between them as:

$$u_d(t) = g(R_{Md}(t), R_{Nd}(t), \varphi(t)), \tag{2.6.11}$$

where $\varphi(t)=\theta_{iMd}(t)-\theta_{oNd}(t)$ describes the phase error. The linearized output of the phase detector could be written as in (2.4.2):

$$\begin{aligned} u_d(t) \approx{}& \frac{b\Delta\Omega}{K_o} + K_D(\varphi(t)-\varphi_\infty) \\ &+ K_{RM}(R_{Md}(t)-R_{M0}) + K_{RN}(R_{Nd}(t)-R_{N0}). \end{aligned} \tag{2.6.12}$$

Note: $g(R_{M0}, R_{N0}, \varphi_\infty)$=$b\Delta\Omega/K_o$ with $\Delta\Omega$=$N\omega_c$−ω_o is the equation for the solution of the operating points and was derived in (2.2.10). The corresponding Laplace domain expression for the output of the PD can be expressed as:

$$\begin{aligned} U_d(s) \approx \frac{b\Delta\Omega}{sK_o} + K_D\left(\Phi(s) - \frac{\varphi_\infty}{s}\right) \\ + K_{RM}\left(R_{Md}(s) - \frac{R_{M0}}{s}\right) + K_{RN}\left(R_{Nd}(s) - \frac{R_{N0}}{s}\right) . \end{aligned} \tag{2.6.13}$$

$R_{Md}(s)$ and $R_{Nd}(s)$ are the delayed versions of terms appearing at the output of reference and feedback divider which are proportional to the amplitude fluctuations of the reference and the VCO signal:

$$R_{Md}(s) = R_M(s)\mathrm{e}^{-s\tau_M} , \tag{2.6.14}$$

$$R_{Nd}(s) = R_N(s)\mathrm{e}^{-s\tau_N} . \tag{2.6.15}$$

The instantaneous phase angle of the VCO without taking into account additional phase noise can be expressed as:

$$\theta_{oV}(t) = \omega_o t + K_o \int_0^t u_c(\tau)\mathrm{d}\tau + \phi_o . \tag{2.6.16}$$

The corresponding Laplace domain expression is:

$$\Theta_{oV}(s) = \frac{\omega_o}{s^2} + K_o\frac{U_c(s)}{s} + \frac{\phi_o}{s} . \tag{2.6.17}$$

For first a order PLL there is no control filter in the loop. The control signal is equal to the phase detector output, i.e. $u_c(t)$=$u_d(t)$. Replacing the output of the phase detector from (2.6.13) into the output of the VCO given by (2.6.17) and taking into account the additional phase noise at the output of the VCO $\Theta_o(s)$=$\Theta_{oV}(s) + \Psi_o(s)$ results in:

$$\begin{aligned} \Theta_o(s) = \frac{\omega_o}{s^2} + \frac{b\Delta\Omega}{s^2} - K_D K_o\frac{\varphi_\infty}{s^2} + K_D K_o\frac{\Phi(s)}{s} \\ + \frac{\phi_o}{s} + \frac{K_{RM}K_o}{s}\left(R_{Md}(s) - \frac{R_{M0}}{s}\right) \\ + \frac{K_{RN}K_o}{s}\left(R_{Nd}(s) - \frac{R_{N0}}{s}\right) + \Psi_o(s) . \end{aligned} \tag{2.6.18}$$

Inserting the value of the phase error $\Phi(s)=\Theta_{iMd}(s)-\Theta_{oNd}(s)$ into (2.6.18) gives:

$$\begin{aligned}\Theta_o(s) = &\frac{\omega_o}{s^2} + \frac{b\Delta\Omega}{s^2} - K_D K_o \frac{\varphi_\infty}{s^2} + \frac{\phi_o}{s} \\ &+ \frac{K_D K_o}{s}\Theta_{iMd}(s) - \frac{K_D K_o}{s}\Theta_{oNd}(s) \\ &+ \frac{K_{RM} K_o}{s}\left(R_{Md}(s) - \frac{R_{M0}}{s}\right) \\ &+ \frac{K_{RN} K_o}{s}\left(R_{Nd}(s) - \frac{R_{N0}}{s}\right) + \Psi_o(s)\,.\end{aligned} \tag{2.6.19}$$

$\Theta_{oNd}(s)$ is the instantaneous phase of the VCO after the feedback divider. The loop divider delays the signal and divides it down by N:

$$\Theta_{oNd}(s) = \frac{\Theta_o(s)}{N}\mathrm{e}^{-s\tau_N}\,. \tag{2.6.20}$$

Note that in this calculation no additional noise sources from components within the synthesizer are taken into account. The derivation including noise sources is given in Appendix A.2. Inserting (2.6.20) into (2.6.19) and rearranging terms, the synthesizer output phase could be written as:

$$\begin{aligned}\Theta_o(s) = &\frac{K_D K_o}{s + \frac{K_D K_o}{N}\mathrm{e}^{-s\tau_N}}\Theta_{iMd}(s) \\ &+ \frac{K_{RM} K_o}{s + \frac{K_D K_o}{N}\mathrm{e}^{-s\tau_N}}\left(R_{Md}(s) - \frac{R_{M0}}{s}\right) \\ &+ \frac{K_{RN} K_o}{s + \frac{K_D K_o}{N}\mathrm{e}^{-s\tau_N}}\left(R_{Nd}(s) - \frac{R_{N0}}{s}\right) \\ &+ \frac{1}{s + \frac{K_D K_o}{N}\mathrm{e}^{-s\tau_N}}\Psi_o(s) \\ &+ \frac{\frac{\omega_o}{s} + \frac{b\Delta\Omega}{s} - K_D K_o \frac{\varphi_\infty}{s} + \phi_o}{s + \frac{K_D K_o}{N}\mathrm{e}^{-s\tau_N}}\,.\end{aligned} \tag{2.6.21}$$

Equation (2.6.21) gives a relationship for the output phase of the VCO with respect to the input as well as different noise sources. From this equation it can be seen clearly that a part of the amplitude fluctuations of the input signal and the VCO signal is being converted into phase noise at the synthesizer output. The part that describes the relationship of the VCO output phase $\Theta_o(s)$ and the synthesizer reference phase $\theta_i(s)$ is called the transfer function of the synthesizer.

Equation (2.6.9) can be expressed in Laplace domain. The instantaneous phase of the input signal together with the phase noise term is delayed by τ_M and divided by M:

$$\theta_{iMd}(s) = \theta_{iM}(s)\mathrm{e}^{-s\tau_M}\,, \tag{2.6.22}$$

$$= \frac{\theta_i(s)}{M}\mathrm{e}^{-s\tau_M} = \left(\frac{\omega_c}{Ms^2} + \frac{n_i(s)}{M} + \frac{\phi_c}{Ms}\right)\mathrm{e}^{-s\tau_M}\,. \tag{2.6.23}$$

Inserting (2.6.22) into the expression for the instantaneous output phase for the first order synthesizer (2.6.21) results in:

$$\begin{aligned}\Theta_o(s) = &\frac{K_D K_o}{s + \frac{K_D K_o}{N}\mathrm{e}^{-s\tau_N}}\frac{\theta_i(s)}{M}\mathrm{e}^{-s\tau_M}\\ &+ \frac{K_{RM} K_o}{s + \frac{K_D K_o}{N}\mathrm{e}^{-s\tau_N}}\left(R_{Md}(s) - \frac{R_{M0}}{s}\right)\\ &+ \frac{K_{RN} K_o}{s + \frac{K_D K_o}{N}\mathrm{e}^{-s\tau_N}}\left(R_{Nd}(s) - \frac{R_{N0}}{s}\right)\\ &+ \frac{1}{s + \frac{K_D K_o}{N}\mathrm{e}^{-s\tau_N}}\Psi_o(s)\\ &+ \frac{\frac{\omega_o}{s} + \frac{b\Delta\Omega}{s} - K_D K_o\frac{\varphi_\infty}{s} + \phi_o}{s + \frac{K_D K_o}{N}\mathrm{e}^{-s\tau_N}}\,.\end{aligned} \tag{2.6.24}$$

Equation (2.6.24) is the Laplace domain expression that relates the first order synthesizer output phase to reference phase as well as to the noise from the input and the VCO signal. The transfer function of the first order synthesizer with a simple delay can be derived as:

$$\Theta_o(s) = \frac{\frac{K_o K_D}{N}}{s + \frac{K_o K_D}{N}\mathrm{e}^{-s\tau_N}}\frac{N}{M}\theta_i(s)\mathrm{e}^{-s\tau_M}\,, \tag{2.6.25}$$

$$= H(s)\frac{N}{M}\theta_i(s)\mathrm{e}^{-s\tau_M}\,. \tag{2.6.26}$$

$H(s)$ is the first order system transfer function:

$$H(s) = \frac{\frac{K_o K_D}{N}}{s + \frac{K_o K_D}{N}\mathrm{e}^{-s\tau_N}}\,. \tag{2.6.27}$$

For the case of a second order synthesizer, the transfer function of the system with a simple delay can be derived in Laplace domain as shown in Appendix A.2

on page 108 and it can be written as:

$$H(s) = \frac{\frac{K_o K_D}{N} F(s)}{s + \frac{K_o K_D}{N} F(s) \mathrm{e}^{-s\tau_N}}\,, \tag{2.6.28}$$

with $F(s)$ being a lag-lead control filter with the following transfer function:

$$F(s) = \frac{s\tau_2 + 1}{s\tau_1 + b}\,, \tag{2.6.29}$$

where τ_1,$\tau_2 \geq 0$. The transfer function of a second order synthesizer with delay can be expressed in terms of the control filter $F(s)$:

$$H(s) = \frac{\frac{K_o K_D}{N}(\tau_2 s + 1)}{\tau_1 s^2 + \left(b + \frac{K_o K_D}{N}\tau_2 \mathrm{e}^{-s\tau_N}\right) s + \frac{K_o K_D}{N}\mathrm{e}^{-s\tau_N}}\,. \tag{2.6.30}$$

Including an ideal time delay element in a continuous system is particularly difficult to analyze as it leads to a closed loop characteristic transfer function that is no more algebraic and has an infinite number of solutions. One way to solve this equation is to use the method described in [52]. This method will be applied to first order synthesizer whose transfer function is described in (2.6.27). Equation (2.6.25) can be written as:

$$\Theta_o(s) = \frac{K}{s}\frac{1}{1 + \frac{K}{Ns}\mathrm{e}^{-s\tau_N}}\theta_{iMd}(s)\,, \tag{2.6.31}$$

where $K = K_o K_D$. Performing the division results in the following series solution:

$$\begin{aligned}\Theta_o(s) &= \frac{K}{s}\frac{1}{1 + \frac{K}{Ns}\mathrm{e}^{-s\tau_N}}\theta_{iMd}(s)\,,\\ &= \frac{K}{s}\left\{1 - \frac{K}{Ns}\mathrm{e}^{-s\tau_N} + \frac{K^2}{N^2 s^2}\mathrm{e}^{-2s\tau_N}\right.\\ &\left. - \frac{K^3}{N^3 s^3}\mathrm{e}^{-3s\tau_N} + \cdots\right\}\theta_{iMd}(s)\,.\end{aligned} \tag{2.6.32}$$

The time domain solution is obtained by inverting the series term by term taking into account the delay theorem:

$$\begin{aligned}\Theta_o(t) &= K\theta_{iMd}(t) - \frac{K^2}{N}(t - \tau_N)\theta_{iMd}(t - \tau_N)\\ &+ \frac{K^3}{2!N^2}(t - 2\tau_N)^2\theta_{iMd}(t - 2\tau_N)\\ &+ \frac{K^4}{3!N^3}(t - 3\tau_N)^3\theta_{iMd}(t - 3\tau_N)\\ &+ \cdots\end{aligned} \tag{2.6.33}$$

This is the system impulse response for the case of a simple first order synthesizer. For higher order systems this calculation becomes extremely difficult.

Another method that could be employed for the analysis of the synthesizer with delay is described in [2]. Inside a frequency synthesizer loop all the higher frequencies will be attenuated by the loop filter. For small frequencies and taking into account the fact that usually in a stable system the delay is small i.e. $|s\tau_N| \ll 1$. The delay term can be approximated by using a first order Taylor series approximation as follows:

$$\mathrm{e}^{-s\tau_N} \approx \frac{1}{1+s\tau_N}\,. \tag{2.6.34}$$

This corresponds to a simple one-pole RC lowpass filter with a pole in the left-hand plane. Unfortunately, this method is not very adequate for the analysis of delay in the synthesizer as this simple approximation results in a noticeable degradation of the phase margin for higher frequencies [2].

One approximation method described in [2] that leads to less phase margin degradation and does not give poles in the right half place is the Padé's method which approximates an exponential function as:

$$\mathrm{e}^{-s\tau_N} \approx \lim_{n\to\infty}\left(\frac{1-\frac{s\tau_N}{2n}}{1+\frac{s\tau_N}{2n}}\right)^n\,. \tag{2.6.35}$$

This approximation of the ideal delay is equivalent to cascade of first-order all-pass sections. The modeling error resulting in use of this approximation for different order of n is discussed in details in [2]. For a low approximation error n=3 or higher is desired. This implies that taking an ideal delay into account will transform a first order synthesizer system into a fourth order system. The mathematic calculation becomes quite laborious requiring the solution of a Quartic equation for a first order system and Quintic equation for a second order synthesizer system.
Some alternative approaches of working with delay in the system can also be found in [53–57].

Inclusion of the delay into a synthesizer system is possible and could be easily solved when performing computer simulations, but taking the delay into account when doing mathematical noise analysis brings in extra complexity to the already quite complex topic. Due to this level of complexity further details of this approach would not be elaborated here.

Phase plane plots could be used to study the settling behavior of a synthesizer system. Phase plane is a diagram that plots the phase error $\varphi(t)$ versus the derivative of the phase error $\dot{\varphi}(t)$. The simulation can be performed using Simulink [58]. More details about this simulation method is given in Section 4.2

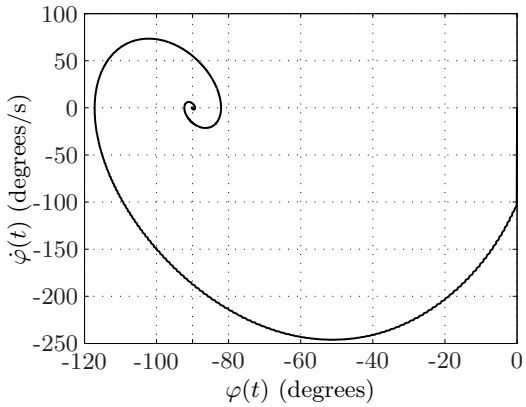

Fig. 2.6: Phase plane trajectory for a second order synthesizer without a delay showing the settling behavior.

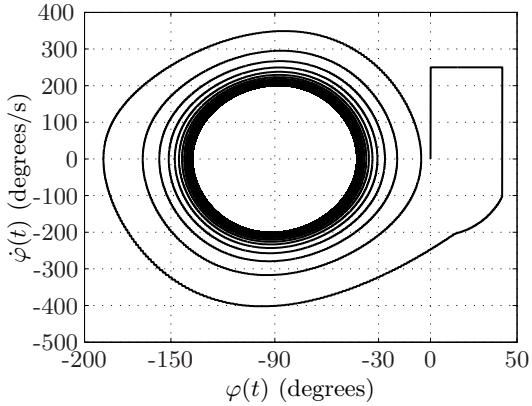

Fig. 2.7: Phase plane trajectory for a second order synthesizer with a large delay in the loop showing that the system becomes unstable.

on page 64. Figures 2.6 and 2.7 show the phase plane trajectories obtained by simulating a second order synthesizer for the case where there is no delay and the case where there is a large delay in the system, respectively.

The system being considered here is a second order synthesizer having a pas-

sive control filter and a type-I phase detector (multiplier plus lowpass filter).The angular frequency of the input signal is chosen to be $50 \cdot 10^3$ rad/sec and the dividers are chosen as M=2 and N=4. Figure 2.6 shows the settling behavior of the synthesizer without delay. As it is expected from a system employing a type-I phase detector, there is a phase shift of 90° between the input and the output.

Figure 2.7 shows that the synthesizer enters into a limit cycle, indicating that large delay could make a synthesizer unstable. All the other parameters of the system are kept constant and the delay is increased until the system loses lock and starts to oscillate as indicated in the phase plane trajectory. The delay effects the phase margin of the system turning a stable system into an unstable one.

2.7 Order and Type of PLL

Considering a special case of the synthesizer transfer function shown in (2.6.28) with no delay and without dividers, i.e. τ_M=τ_N=0 and M=N=1. This leads to the transfer function of second or higher order PLL:

$$H(s) = \frac{\frac{K_o K_D}{s} F(s)}{1 + \frac{K_o K_D}{s} F(s)} = \frac{G(s)}{1 + G(s)}\,, \tag{2.7.1}$$

where $G(s)$ is the open loop gain:

$$G(s) = \frac{K_o K_D}{s} F(s)\,. \tag{2.7.2}$$

2.7.1 Order of PLL

Considering the case where $F(s)$=1, (2.7.1) reduces to:

$$H(s) = \frac{K_o K_D}{s + K_o K_D}\,. \tag{2.7.3}$$

Since the largest power of s in the denominator is 1, this PLL is designated as of first-order. Generally, there is a control filter in the loop having a transfer functions $F(s)$ that can be written as a ratio of two polynomials in s. The denominator polynomial of $H(s)$ is of higher order in s leading to PLL of second order, third order, and so on according to the degree of the polynomial in the denominator of (2.7.1). The order of the PLL is 1+control filter order.

2.7.2 Type of PLL

When the steady state error in a PLL system is of high interest, the number of poles in the transfer function $G(s)$, that is to say the number of integrators in the loop, is important. The number of integrators define the type of PLL. Every PLL has one integrator connected with the VCO so a PLL in general is called of type-I. The error transfer function for a PLL can be defined from (2.7.1) as:

$$H_e(s) = 1 - H(s) = \frac{1}{1 + G(s)}\,. \tag{2.7.4}$$

The error transfer function relates the input phase $\Theta_i(s)$ to the phase error $\varphi(s)$ between the input phase and the VCO phase $\Theta_o(s)$:

$$\varphi(s) = \frac{1}{1 + G(s)}\Theta_i(s)\,. \tag{2.7.5}$$

The open loop gain $G(s)$ can be written as a ratio of two polynomials:

$$G(s) = \frac{A(s)}{s^n B(s)}\,, \tag{2.7.6}$$

then the phase error could be expressed as:

$$\varphi(s) = \frac{s^n B(s)}{A(s) + s^n B(s)}\Theta_i(s)\,. \tag{2.7.7}$$

Every PLL has one integrator from the VCO, which implies that $n \geq 1$ in the above equation. In order to study the steady state behavior of phase error, the following limit can be taken:

$$\lim_{t\to\infty} \varphi(t) = \lim_{s\to 0}\left[\frac{s^{n+1} B(s)}{A(s) + s^n B(s)}\Theta_i(s)\right]\,. \tag{2.7.8}$$

Using (2.7.8), it is possible to show the steady state behavior of the phase error depending on different types of input signals: phase step, frequency step and frequency ramp.

In the case of a phase step with $\Theta_i(s) = {}^{\Delta\Theta}/_{s}$, it can be shown that the final value of phase error is zero in all PLLs.

For the frequency step with $\Theta_i(s) = {}^{\Delta\omega}/_{s^2}$, all type-I (passive filter) PLLs of the second order (n=1) would result in a steady state phase error:

$$\lim_{t\to\infty} \varphi(t) = \lim_{s\to 0}\left[\frac{s^2 B(s)}{A(s) + sB(s)}\,\frac{\Delta\omega}{s^2}\right] = \frac{\Delta\omega}{K_o K_D F(0)}\,. \tag{2.7.9}$$

Equation (2.7.9) leads to a zero phase error only when $F(0) \to \infty$. Which means a control filter with infinite DC gain is needed. That is to say a first order PI-filter (perfect integrator) has to be used as the control filter of the PLL. This is a second order PLL of type-II where there are two integrators in the loop, one from VCO and other from the control filter.

In the same manner it can be shown that a PLL of type-III (third order PLL) having a PI-filter of second order is needed in order to eliminate frequency ramp $\Theta_i(s) = {}^{\beta}/_{s^3}$.

2.8 Effects of Sampling

Systems that use all-digital approaches for synthesizer must be analyzed using Z-transforms. Frequency synthesizers in general are analog systems that contain digital components like phase detectors and loop dividers. They can be analyzed by continuous and pseudo-continuous models. Continuous representation of discrete processes is exclusively determined by system percentage bandwidth. Continuous and pseudo-continuous models can be used, if the system bandwidth is much smaller than the sampling rate. The modeling inaccuracies will increase when system bandwidth is larger than 10% of the sampling frequency [2]. Sampling effects can adversely affect PLL stability, settling time, and phase noise performance.

Pseudo-continuous models can be derived from the original open loop transfer function of the synthesizer as shown in [2, 3]. Consider that the open loop time response $g(t)$ is subjected to sample-and-hold function so that the Laplace transform of the open loop transfer function of the synthesizer becomes:

$$G_{\text{samp}}(s) = F_h(s)\hat{G}(s)\,, \tag{2.8.1}$$

where $F_h(s)$ is the sample-and-hold function of duration T as described:

$$F_h(s) = \frac{1 - \mathrm{e}^{-sT}}{s}\,, \tag{2.8.2}$$

and $\hat{G}(s)$ is a function of the sampling frequency $\omega_s = {}^{2\pi}/_{T}$ as:

$$\hat{G}(s) = \frac{1}{T} \sum_{n=-\infty}^{+\infty} G(s - \mathrm{j}n\omega_s)\,. \tag{2.8.3}$$

With results from (2.8.2) and (2.8.3), the open loop transfer function can be written as:

$$G_{\text{samp}}(s) = \frac{1 - \mathrm{e}^{-sT}}{s} \cdot \frac{1}{T} \sum_{n=-\infty}^{+\infty} G(s - \mathrm{j}n\omega_s)\,. \tag{2.8.4}$$

Consider that in the synthesizer system the higher frequency terms will be filtered out by the loop filter:

$$G_{\text{samp}}(s) \approx \frac{1 - \mathrm{e}^{-sT}}{s} \cdot \frac{1}{T} G(s)\,. \tag{2.8.5}$$

Considering that inside the control loop the frequencies are very small so that $|sT| \ll 1$ which results in:

$$G_{\text{samp}}(s) \approx \frac{\sinh(\frac{sT}{2})}{\frac{sT}{2}} G(s) \mathrm{e}^{-\frac{sT}{2}}\,, \tag{2.8.6}$$

$$\approx G(s) \mathrm{e}^{-\frac{sT}{2}}\,. \tag{2.8.7}$$

The simplified results obtained above are similar to what was found by considering effects of the delay in the system. This implies that in order to consider the effects of sampling on the synthesizer system, similar analysis techniques are required as were presented for the delay analysis in Section 2.5 on page 15.

3 Noise Analysis and Noise Modeling

3.1 Phase Noise and Spurious Tone

The random fluctuations of amplitude and phase of a frequency generator are the limiting factors in many applications. These fluctuations are designated as electronic noise. In general the output voltage must be assumed to have the form:

$$u(t) = \hat{u}(1 + R(t)) \sin(\omega_o t + \psi(t)) \,. \tag{3.1.1}$$

In this equation $R(t)$ represents the amplitude fluctuations and $\psi(t)$ the phase fluctuations. Ideally, the spectrum of an oscillator signal should be infinitesimally narrow, but due to noise there is an extensive spread of energy around the desired frequency.

As it was mentioned before, in most of the literature on synthesizers the amplitude fluctuations are neglected [3, 11]. It is usually assumed that the amplitude fluctuations can be removed or greatly alleviated by a limiter or an automatic amplitude control circuit. In this work the amplitude fluctuations are taken into account. As it was shown in Section 2.3 on page 12, a part of the amplitude fluctuations propagates through the limiter circuit and are converted into phase fluctuations inside a synthesizer loop.

The phase term $\psi(t)$ describes distortion and can be subdivided into two terms representing the periodic variation and the random variation which can mathematically be expressed as:

$$\psi(t) = \Delta\psi \sin(\omega_m t) + \phi(t) \,. \tag{3.1.2}$$

The first term in 3.1.2 represents the periodic variation and it describes a spurious tone at an offset angular frequency of ω_m from the carrier angular frequency ω_o.

3.1.1 Spurious Signals

Assume for the following consideration that the amplitude fluctuations $R(t)$ and the phase fluctuations $\phi(t)$ are negligible. The magnitude of the spurious tone can be derived as:

$$u(t) = \hat{u} \sin(\omega_o t + \Delta\psi \sin(\omega_m t))$$

$$= \hat{u}\left\{\sin(\omega_o t)\cos(\Delta\psi\sin(\omega_m t)) + \cos(\omega_o t)\sin(\Delta\psi\sin(\omega_m t))\right\} . \quad (3.1.3)$$

Considering a small phase modulation implies that $\Delta\psi \ll \pi/2$. The following approximations are valid:

$$\cos(\Delta\psi\sin(\omega_m t)) \approx 1 , \quad (3.1.4)$$

$$\sin(\Delta\psi\sin(\omega_m t)) \approx \Delta\psi\sin(\omega_m t) . \quad (3.1.5)$$

Taking the above results into account, (3.1.3) yields:

$$\begin{aligned} u(t) &\approx \hat{u}\left\{\sin(\omega_o t) + \Delta\psi\sin(\omega_m t)\cos(\omega_o t)\right\} \\ &= \hat{u}\left\{\sin(\omega_o t) - \frac{\Delta\psi}{2}\sin((\omega_o - \omega_m)t) + \frac{\Delta\psi}{2}\sin((\omega_o + \omega_m)t)\right\} . \end{aligned} \quad (3.1.6)$$

Equation (3.1.6) shows that the two spurious tones at $\omega_o - \omega_m$ and $\omega_o + \omega_m$ are both below the carrier by $-20\log(\Delta\psi/2)$ dB.

In frequency synthesizers the discrete spurious signals observed at the output of phase detector can be due to different sources: leakage of the reference signal and its harmonics; signals that are superimposed onto reference or the VCO like for example ripple on the DC supply; different mixing products due to nonlinearities in the system. The phase detector can produce some spurs by itself due to its own nonlinear characteristics.

Experimental results showing effects of the DC supply ripple on the XCO output leading to spurs are shown in Section 5.1.2 on page 71.

3.1.2 Phase Noise

The second term in $\psi(t)$ shown in (3.1.2) represents the random phase fluctuations which produces phase noise. The spectral density of the phase variation is:

$$S_\psi(f) = \int_{-\infty}^{+\infty} R_\psi(\tau) e^{-\mathrm{j}2\pi f\tau} \mathrm{d}\tau , \quad (3.1.7)$$

with $R_\psi(\tau)$ being the auto-correlation function of the random phase variation $\psi(t)$. It can be expressed in terms of the expected value of the random variable $\psi(t)$ with a shifted version of it:

$$R_\psi(\tau) = \langle \psi(t)\psi(t+\tau) \rangle , \quad (3.1.8)$$

where $< >$ denotes ensemble average over processes with identical statistical properties.

The noise at the output of a frequency synthesizer is due to different physical effects. The types of noise that is taken into consideration in this work are:

- white noise with a constant power spectral density $S(f)$=const,
- flicker noise also called $1/f$ noise with a power spectral density $S(f)\sim 1/f$.

3.1.3 White Noise

Typical representatives of white noise are the thermal noise of resistors and the shot noise in electronic devices.

3.1.3.1 Thermal noise

Thermal noise is caused by fluctuations (random motion) of charge carriers within a conductor. The short current pulses generated by collisions of a large number of electrons in a conductor result in noiseless conductor being connected in series with a noise generator with a RMS noise voltage u_n. It is usually measured under the condition that no external field is applied to the conductor. Because the motion of charge carriers increase with temperature so does the magnitude of the thermal noise. Thermal noise is due to the quantum nature of charge carriers. More details on thermal noise can be found in [3, 59]. The magnitude square of the RMS noise voltage could be expressed as:

$$< u_n^2 > = 4kTR\Delta f\,, \tag{3.1.9}$$

where k is Boltzmann's constant, T is the absolute temperature, R is the resistance of the conductor, Δf is the noise bandwidth. Similarly, with the assistance of the Thevenin theorem the square of the RMS value of the noise current i_n flowing into the conductance G=$1/R$ can be expressed as follows:

$$< i_n^2 > = 4kTG\Delta f\,. \tag{3.1.10}$$

As can be seen from (3.1.9) and (3.1.10), power contained in the thermal noise signal is directly proportional to temperature and bandwidth. These relations also show the importance of using low resistance components when possible in a system.

Statistically speaking, the random thermal noise signal can be represented by a Gaussian distribution also referred to as normal distribution. The corresponding power spectral density (PSD) in 1 Hz bandwidth for both voltage and

current noise can be arrived at after dividing the relations (3.1.9) and (3.1.10) by the frequency bandwidth Δf:

$$S_{u,n}(f) = 4kTR\,, \tag{3.1.11}$$

$$S_{i,n}(f) = 4kTG\,. \tag{3.1.12}$$

Thermal noise power density is constant throughout the frequency spectrum at room temperature up to a frequency f<600GHz as discussed in [59].

3.1.3.2 Shot Noise

Shot noise is important in electronics, telecommunication, and fundamental physics. It consists of random fluctuations of the average electric current, which are caused by the fact that the current is carried by discrete charges (electrons) that give rise to detectable statistical fluctuations in a measurement. The output current is composed of random arrivals of a large number of particles leading to rise of the observed random fluctuations around the average DC value which gives a spectrum of white noise type. The strength of this noise increases for growing magnitude of the average current flowing through the device. The spectral power density of shot noise can be derived as shown in [3, 60] and is given as:

$$S_{i,n}(f) = 2qI\,, \tag{3.1.13}$$

where I is the mean or average current and q=$1.6 \cdot 10^{-19}$ C is the electron or hole charge. Equation (3.1.13) is valid generally whenever the current consists of independent random events, each carrying a charge q. It is applicable for example to p-n junction diodes, bipolar transistors, metal-semiconductor diodes, etc. wherever charges are carried across potential barriers [60].

Shot noise is to be distinguished from current fluctuations in equilibrium, which happen without any applied voltage and without any average current flowing. These equilibrium current fluctuations are known as Johnson-Nyquist noise or thermal noise.

3.1.4 Flicker or $1/f$ Noise

The name flicker noise comes from the days of vacuum-tubes were a flicker type of fluctuations was observed in the anode current. It is a type of noise that is not yet completely understood though it is already known since more than 80 years [3, 60]. There is no single theory that can fit all the observed cases. It is not only a type of electronic noise but a fluctuations phenomenon that is also observed in fields of physics, biology and other sciences. Its spectral density is

inversely proportional to frequency i.e. $1/f$ from which its name is derived. In a more general way the spectrum should be described as $1/f^{\alpha}$ where α has a value in the range of 1.

Theoretically, the spectrum of the flicker noise goes to infinity as the frequency goes to zero. $1/f$ phenomenon is found to be true at frequencies as low as a few cycles per day [60, 61]. The slow change with time is typical for $1/f$ noise.

Many CMOS op-amps has a relatively high $1/f$ noise corner frequency. For example, in OPA301 the voltage noise has a $1/f$ corner frequency higher than 100 kHz [62] [62]. Such an op-amp can be used to build a $1/f$ noise source.

It is important to note that the $1/f$ noise also follows a normal distribution as will be shown in the next section.

3.2 Noise Modeling

A good mathematical noise modeling technique is required in order to model noise at different points in the PLL systems when performing theoretical analysis and doing simulations. There are many different modeling techniques found in literature such as [63]. Two of the important modeling techniques are so called Rice's noise models [44]. It is very critical to pick up the right model for analysis, otherwise it may lead to unnecessary complications in the system analysis.

3.2.1 Rice's First Noise Model

S.O. Rice [44] has developed two different models to describe the measured noise mathematically. The first model is well known and widely used. It describes a band limited noise signal having a maximum bandwidth of BW as:

$$u(t) = \sum_{n=1}^{N} V_n \cos(n\Delta\omega t + \varphi_n)\,, \tag{3.2.1}$$

$$= \sum_{n=1}^{N} \left(A_n \cos(n\Delta\omega t) + B_n \sin(n\Delta\omega t)\right)\,. \tag{3.2.2}$$

The maximum noise bandwidth is defined as $BW = N\,\Delta\omega/2\pi$. $\Delta\omega = 2\pi/T_{\mathrm{ob}}$ is the angular frequency step size. T_{ob} is the observation time. The longer the observation time is the better the approximation will be.

In this model both V_n and φ_n are random variables with V_n following a Rayleigh distribution and φ_n being uniformly distributed in the interval $[0, 2\pi)$. This is equivalent to saying that parameters A_n and B_n are approximately fitting Gaussian curves. Due to the Gaussian nature of these distributions the mathematical analysis becomes complex.

3.2.2 Rice's Second Noise Model

The not so well-known Rice's second model which is the heart of the noise analysis that was presented by the author in [45] and is also employed in this work. The other way of approaching the measured band limited noise can be described as:

$$u(t) = \sum_{n=1}^{N} A_n \cos(n\Delta\omega t + \varphi_n)\,. \tag{3.2.3}$$

In this model parameters A_n are deterministic and φ_n are random variables, uniformly distributed in the interval $[0, 2\pi)$. Due to the uniform distributions of φ_n terms, this model is mathematically simpler than the first model, and by the virtue of the central limit theorem it leads to the same results as the first model [44, 49]. The central limit theorem [49] describes conditions under which the mean of an arbitrary finite distribution will be approximately normally distributed provided that the number of observations for calculating the mean is large enough.

More details on the applications of Rice's second model in RF and Microwave engineering can be found in [64].

The accuracy of Rice's second model increases as the number of sum terms increases. Figure 3.1 (a) and (b) demonstrates this fact by comparing the uniform distribution obtained by using Rice's second model for a value of N equal to 10000 and 50000, respectively. The horizontal axis in Fig. 3.1 is divided into 50 bins in the interval $(-180^\circ, 180^\circ)$.

In order to demonstrate the strength of Rice's second model, an example involving calculation of the PLL output spectrum will be illustrated later in Section 3.3.2. The advantages of Rice's second model becomes obvious when calculating the average power spectrum by applying the autocorrelation method represented in (3.1.8). Considering the ensemble average calculations $\langle u(t)u(t+\tau)\rangle$, it can be observed that for Rice's second model ensemble average is needed to be done only with respect to one random variable φ_n which follows uniform distribution. Where as, for the first model it is necessary to do ensemble average with respect to random variables V_n and φ_n having Rayleigh and uniformly distribution, respectively.

Rice's second model can be used to generate different types of noise sources. For white noise for example all the A_n terms would be equal and constant. This constant value can be calculated according to the signal to noise ratio needed using the following equation relating the signal and noise power:

$$\text{Power Ratio} = 10\log\left(\frac{\hat{u}^2}{\sum_{n=1}^{N} A_n^2}\right) = 10\log\left(\frac{\hat{u}^2}{nA_n^2}\right)\,, \tag{3.2.4}$$

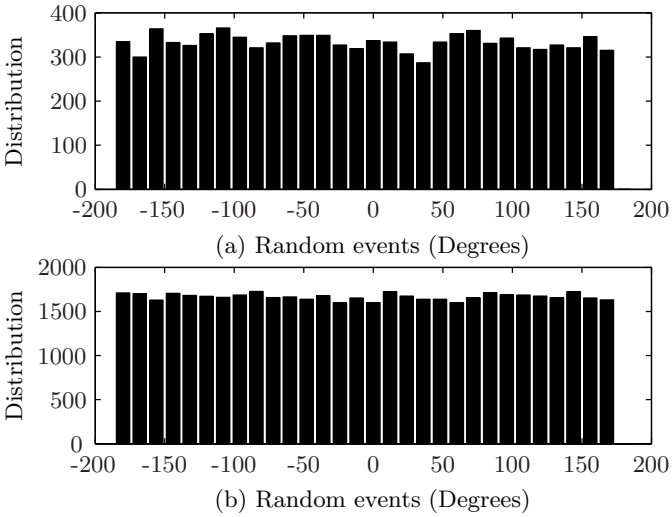

Fig. 3.1: Histogram of Rice's second model showing that increasing the number of sum terms leads to a better accuracy.

where $\hat{u}^2/2R$ represents the useful signal average power.

Figure 3.2 (a) shows the white noise source generated using the Rice's second model. The generated noise sample is of length 100 sec and is generated by using $N{=}5 \cdot 10^5$ sum terms with a $T_{\text{ob}}{=}1000$ sec. Figure 3.2 (b) shows the corresponding distribution function. As it is expected, the white noise generated by the Rice's second model follows a Gaussian distribution with mean of zero since there is no DC component. It should be noted that in thermal noise the standard deviation and the RMS value are equal, since the mean is zero.

In a similar manner, $1/f$ noise can be generated by modifying the amplitude terms in Rice's second model to get $A_n/\sqrt{n}$. By modeling the amplitude terms in this way, it can be observed that the noise spectral components will go down by $1/f$. Fig. 3.3 (a) shows the $1/f$ noise source generated using the Rice's second model. The generated noise sample is of length 500 sec and is generated by using $N{=}5 \cdot 10^5$ sum terms with $T_{\text{ob}}{=}1000$ sec. Fig. 3.3 (b) shows the corresponding distribution function. Similar to the white noise, the $1/f$ noise follows a Gaussian distribution. Note that the mean value of $1/f$ noise in Fig. 3.3 is not zero due to taking a limited observation time. $1/f$ noise is very slowly varying over time

so a much longer observation time is necessary. In general noise generation by employing Rice's model in Matlab [58] takes lot of time and CPU power.

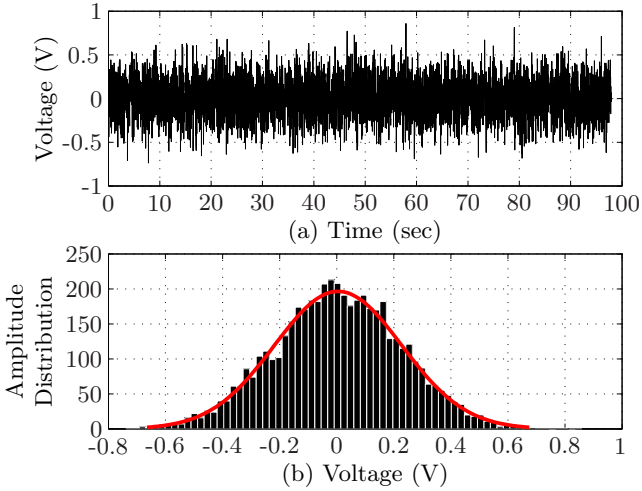

Fig. 3.2: Diagram (a) shows a white noise voltage generated by using Rice's second model. Diagram (b) shows the corresponding histogram indicating the Gaussian distribution for the generated white noise.

3.3 Synthesizer Output with Noise

For a good design of a PLL based frequency synthesizer, the investigation of the effect of electronic noise is an important factor to be considered and analyzed. Electronic noise can result in random modulation of the phase of an oscillator's output due to a variety of internal and external noise sources.

In this section a detailed noise analysis methodology for a PLL-based frequency synthesizer will be elaborated. Fig. 3.4 represents a phase model of the frequency synthesizer that is used to derive the output signal containing effect of different noise sources. As illustrated in this diagram a very complex combination of noise sources is considered here:

- At the input, the amplitude fluctuations $R(t)$ and the phase noise $n_i(t)$ of the reference signal are taken into account. The reference signal amplitude

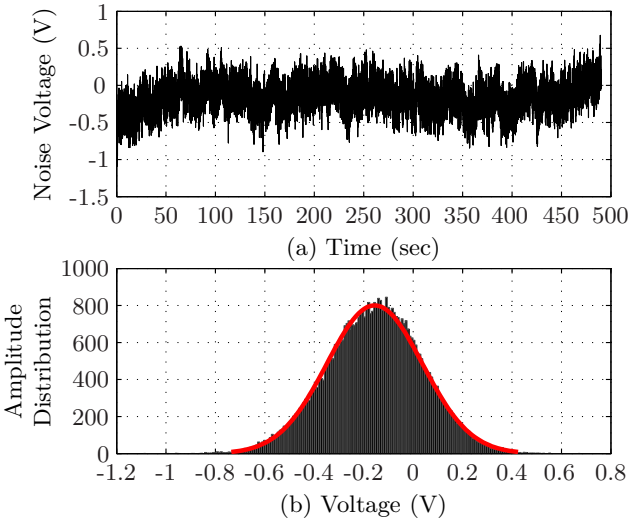

Fig. 3.3: Diagram (a) shows a $1/f$ noise voltage generated by using Rice's second model. Diagram (b) shows the corresponding histogram indicating the Gaussian distribution for the generated $1/f$ noise.

fluctuations $R(t)$ result in a proportional term $R_M(t)$ in the phase detector function $u_d(t)$ after the divider M. Additionally, noise source $n_M(t)$ of the divider M is also considered. The noise sources at the reference side are taken to be white and are converted into components affecting amplitude and phase of the synthesizer. More details to this will be given later.

- The two noise sources $n_{PD}(t)$, $n_{CF}(t)$ represent the noise of the phase detector and the control filter, respectively. These sources are taken to be a superposition of $1/f$ and white noise.
- The VCO noise can be divided into amplitude and phase components $n_{vA}(t)$ and $n_{vp}(t)$, respectively. VCO amplitude fluctuations $n_{vA}(t)$ result in a proportional term $R_N(t)$ in the phase detector function $u_d(t)$ after the feedback divider. Noise after the VCO is also taken to be a superposition of $1/f$ and white noise.
- An additional noise source $n_N(t)$ is taken at the output of loop divider N to represent noise due to the divider.

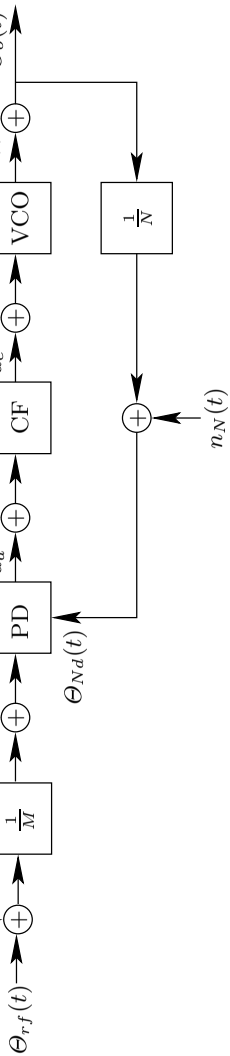

Fig. 3.4: Phase model of a frequency synthesizer including noise coming from different components.

The nonlinear differential equation of this synthesizer system is described in (2.2.8) on page 11. The analysis of such an equation without linearization is usually mathematically very complex. A novel linearization approach was presented in Section 2.4 on page 14.

Using this approach, expression for the synthesizer output voltage and output average power are derived containing effect of all noise sources for the synthesizer model shown in Fig. 3.4. These are rather complex and lengthy formulas that involve high amount of advanced mathematics and will not be shown here.

In order to demonstrate the methodology for doing the theoretical analysis of a synthesizer system containing different noise sources, a simpler example considering only one single noise source in the system will be shown here.

In Appendix A.2 on page 108 the Laplace transform for the instantaneous output phase angle for a second order synthesizer containing effect of all noise sources, and also considering a delay associated with the divider in the system was derived. Consider the case where there is no delay in the system as shown in Fig. 3.4. Applying the techniques discussed in the Appendix, the output phase angle of this synthesizer can be derived as shown in (3.3.1).

Note that in the second order synthesizer shown in Fig. 3.4 the reference and feedback dividers are non-ideal. The output of the dividers can be derived as shown in Section 2.3 on page 12. This divider model represent a real divider in a better way. In contrary to the ideal divider model, a part of the amplitude fluctuations of the reference and the VCO signal propagates through the divider.

The different terms can be identified in the instantaneous output phase (3.3.1) of the synthesizer:

- Term **(1)** shows the output of the synthesizer in relation to the reference and the phase noise of the reference. The reference noise is reduced by $1/M$ of the reference divider.
- Terms **(2)** and **(3)** show how the amplitude fluctuations of the reference and the VCO are converted into phase noise inside the loop.
- Terms **(4)** and **(8)** show effect of the reference and feedback divider on the phase noise of the synthesizer.
- Terms **(5)**, **(6)** and **(7)** represent the effects of phase detector, control filter, and VCO phase noise on the synthesizer, respectively.
- Terms **(9)** to **(12)** do not represent any noise behavior. In the steady state, terms **(9)** to **(11)** lead to a constant offset phase angle and term **(12)** goes to zero.

$$
\begin{aligned}
\Theta_o(s) = & \frac{K_D K_o(s\tau_2+1)}{\tau_1 s^2+\left(b+\frac{K_D K_o \tau_2}{N}\right)s+\frac{K_D K_o}{N}}\left(\frac{\Theta_{rf}(s)}{M}+\frac{n_i(s)}{M}\right) && \textbf{(1)}\\
& + \frac{K_o K_{RM}(s\tau_2+1)}{\tau_1 s^2+\left(b+\frac{K_D K_o \tau_2}{N}\right)s+\frac{K_D K_o}{N}}\left(R_M(s)-\frac{R_{M0}}{s}\right) && \textbf{(2)}\\
& + \frac{K_o K_{RN}(s\tau_2+1)}{\tau_1 s^2+\left(b+\frac{K_D K_o \tau_2}{N}\right)s+\frac{K_D K_o}{N}}\left(R_N(s)-\frac{R_{N0}}{s}\right) && \textbf{(3)}\\
& + \frac{K_D K_o(s\tau_2+1)}{\tau_1 s^2+\left(b+\frac{K_D K_o \tau_2}{N}\right)s+\frac{K_D K_o}{N}} n_M(s) && \textbf{(4)}\\
& + \frac{K_o(s\tau_2+1)}{\tau_1 s^2+\left(b+\frac{K_D K_o \tau_2}{N}\right)s+\frac{K_D K_o}{N}} n_{PD}(s) && \textbf{(5)}\\
& + \frac{K_o(s\tau_1+b)}{\tau_1 s^2+\left(b+\frac{K_D K_o \tau_2}{N}\right)s+\frac{K_D K_o}{N}} n_{CF}(s) && \textbf{(6)}\\
& + \frac{s(s\tau_1+b)}{\tau_1 s^2+\left(b+\frac{K_D K_o \tau_2}{N}\right)s+\frac{K_D K_o}{N}} n_{vp}(s) && \textbf{(7)}\\
& - \frac{K_D K_o(s\tau_2+1)}{\tau_1 s^2+\left(b+\frac{K_D K_o \tau_2}{N}\right)s+\frac{K_D K_o}{N}} n_N(s) && \textbf{(8)}\\
& + \frac{(s\tau_2+1)}{\tau_1 s^2+\left(b+\frac{K_D K_o \tau_2}{N}\right)s+\frac{K_D K_o}{N}} \frac{b\Delta\Omega}{s} && \textbf{(9)}\\
& - \frac{K_D K_o(s\tau_2+1)}{\tau_1 s^2+\left(b+\frac{K_D K_o \tau_2}{N}\right)s+\frac{K_D K_o}{N}} \frac{\varphi_\infty}{s} && \textbf{(10)}\\
& + \frac{(s\tau_1+b)}{\tau_1 s^2+\left(b+\frac{K_D K_o \tau_2}{N}\right)s+\frac{K_D K_o}{N}} \frac{\omega_o}{s} && \textbf{(11)}\\
& + \frac{(s\tau_1+b)}{\tau_1 s^2+\left(b+\frac{K_D K_o \tau_2}{N}\right)s+\frac{K_D K_o}{N}} \phi_o && \textbf{(12)} \quad (3.3.1)
\end{aligned}
$$

A more detailed discussion about the characteristic transfer function between the synthesizer output phase angle and the different noise sources will be presented later.

3.3.1 Computation of the PLL Output Voltage

A synthesizer output signal containing effects of all the noise sources was derived. The calculations are very complex and lengthy so that they cannot be presented here. In order to explain the technique of calculating a synthesizer output voltage and power spectral density, a simple example of a second order PLL, shown in Fig. 3.5, that has a single noise source in front of the loop filter, will be demonstrated. Except for phase detector, all other components in the PLL circuit are considered to be noise-free. It is assumed also that the amplitude fluctuations of the reference and VCO are negligible in this case. In this particular case, the instantaneous output phase of the PLL from (3.3.1) reduces to:

$$\begin{aligned}\Theta_o(s) = &\frac{K_D K_o(s\tau_2+1)}{\tau_1 s^2 + (b + K_D K_o \tau_2)\, s + K_D K_o}\Theta_i(s) \\ &+ \frac{K_o(s\tau_2+1)}{\tau_1 s^2 + (b + K_D K_o \tau_2)\, s + K_D K_o} n_{PD}(s) \\ &+ \frac{(b\Delta\Omega - K_D K_o \varphi_\infty)(s\tau_2+1)}{s\,(\tau_1 s^2 + (b + K_D K_o \tau_2)\, s + K_D K_o)} \\ &+ \frac{(\omega_o + s\phi_o)(s\tau_1+b)}{s\,(\tau_1 s^2 + (b + K_D K_o \tau_2)\, s + K_D K_o)}\,.\end{aligned} \tag{3.3.2}$$

where $\Delta\Omega$=ω_c-ω_o. In order to model the noise source mathematically, Rice's second model introduced by 3.2.3 will be used:

$$n_{PD}(t) = \sum_{n=1}^{N} A_n \cos(n\Delta\omega t + \varphi_n)\,. \tag{3.3.3}$$

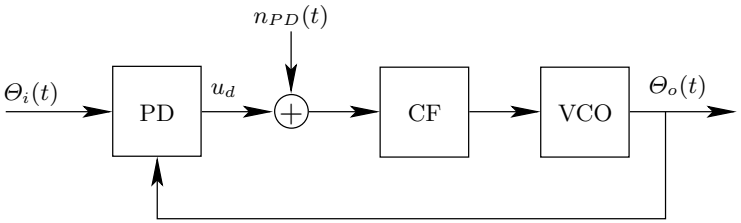

Fig. 3.5: Phase model of a PLL including noise in front of the control filter.

The corresponding expression for the noise source in the Laplace domain is:

$$n_{PD}(s) = \sum_{n=1}^{N} A_n \left(\frac{s\cos(\varphi_n)}{s^2 + (n\Delta\omega)^2} - \frac{(n\Delta\omega)\sin(\varphi_n)}{s^2 + (n\Delta\omega)^2} \right) . \tag{3.3.4}$$

In order to obtain a time domain expression for the PLL output phase, a solution of (3.3.2) will be demonstrated. Performing the inverse Laplace transform will lead to transient terms as well as to a steady state solution. The transient terms will describe a point in time where the PLL has not yet been stabilized and has not reached the lock condition.

Considering the PLL to be in lock state implies that all transient terms has disappeared. In the following analysis only steady state solutions will be shown. Inserting the expression for the input phase angle

$$\Theta_i(s) = \frac{\omega_c}{s^2} + \frac{\phi_c}{s} ,$$

and the noise source $n_{PD}(s)$ into (3.3.2) and taking the inverse Laplace transform, the solution can be obtained. Equation (3.3.2) consists of a linear combination of many terms. The problem can be subdivided into parts and each part can be converted into time domain separately. The inverse Laplace transform can be preformed with the aid of Maple [65].

As shown in (3.3.3), the noise source consists of a linear combination of harmonic terms. To perform the inverse Laplace transform, the nth sum term can be considered alone. The time domain expression for the instantaneous phase angle of PLL in terms of the noise is:

$$\begin{aligned} \Theta_o(t) = {} & \omega_c t + \phi_c \\ & + K_o \sum_{n=1}^{N} C(n)X(n)A_n \cos(n\Delta\omega t + \varphi_n) \\ & + K_o \sum_{n=1}^{N} C(n)Y(n)A_n \sin(n\Delta\omega t + \varphi_n) \\ & + \frac{b\omega_c}{K_o K_D} - \varphi_\infty . \end{aligned} \tag{3.3.5}$$

The terms A_n and φ_n from Rice's second model represent the deterministic amplitude and random phase of the noise source, respectively. The different variable in the above equation are described as:

$$M_n = n\Delta\omega ,$$

$$X(n) = b\tau_2 M_n^2 - \tau_1 M_n^2 + K_o K_D \tau_2^2 M_n^2 + K_o K_D \,,$$
$$Y(n) = bM_n + \tau_1 \tau_2 M_n^3 \,,$$

$$C(n) = \frac{1}{b^2 M_n^2 + 2bK_o K_D \tau_2 M_n^2 + K_o^2 K_D^2 \tau_2^2 M_n^2 + \tau_1^2 M_n^4 - 2K_o K_D \tau_1 M_n^2 + K_o^2 K_D^2} \,.$$

Expanding $\cos(n\Delta\omega t + \varphi_n)$ and $\sin(n\Delta\omega t + \varphi_n)$ terms and rearranging the result gives:

$$\begin{aligned} \Theta_o(t) &= \omega_c t + \phi_c \\ &+ K_o \sum_{n=1}^{N} A_n C(n) \left\{ X(n)\cos(\varphi_n) + Y(n)\sin(\varphi_n) \right\} \cos(n\Delta\omega t) \\ &+ K_o \sum_{n=1}^{N} A_n C(n) \left\{ Y(n)\cos(\varphi_n) - X(n)\sin(\varphi_n) \right\} \sin(n\Delta\omega t) \\ &+ \frac{b\omega_c}{K_o K_D} - \varphi_\infty \,. \end{aligned} \tag{3.3.6}$$

In order to facilitate further calculation, (3.3.6) is rewritten in a more compact way:

$$\begin{aligned} \Theta_o(t) &= \omega_c t + \Phi_{\text{const}} \\ &+ \sum_{n=1}^{N} \left\{ D_n \cos(n\Delta\omega t) + E_n \sin(n\Delta\omega t) \right\} \,, \end{aligned} \tag{3.3.7}$$

with

$$D_n = K_o A_n C(n) \left\{ X(n)\cos(\varphi_n) + Y(n)\sin(\varphi_n) \right\} \,, \tag{3.3.8}$$

$$E_n = K_o A_n C(n) \left\{ Y(n)\cos(\varphi_n) - X(n)\sin(\varphi_n) \right\} \,, \tag{3.3.9}$$

$$\Phi_{\text{const}} = \frac{b\omega_c}{K_o K_D} - \varphi_\infty + \phi_c \,. \tag{3.3.10}$$

In (3.3.7) the terms D_n and E_n are random variables because they are functions of φ_n. φ_n terms are from the Rice's second model and represent random variables uniformly distributed in the interval $[0, 2\pi)$. In order to facilitate the solution, the limits for the sum terms from (3.3.7) are extended to be $-\infty$ to $+\infty$. When designing the noise source, it should be kept in mind that the amplitude terms A_n are zero outside the frequency range defining the bandwidth of this source:

$$\Theta_o(t) = \omega_c t + \Phi_{\text{const}}$$

$$+ \sum_{n=-\infty}^{+\infty} \{D_n \cos(n\Delta\omega t) + E_n \sin(n\Delta\omega t)\} \,. \tag{3.3.11}$$

The voltage at the output of a PLL can be written in terms of the output instantaneous phase angle $\Theta_o(t)$ from (3.3.11), assuming that the VCO exhibits no amplitude fluctuations and has a constant amplitude $\hat{u}_o$:

$$\begin{aligned} u_o(t) &= \hat{u}_o \cos(\Theta_o(t)) \,, \\ &= \hat{u}_o \cos\Bigg(\omega_c t + \Phi_{\text{const}} + \sum_{n=-\infty}^{+\infty} D_n \cos(n\Delta\omega t) \\ &\qquad + \sum_{n=-\infty}^{+\infty} E_n \sin(n\Delta\omega t)\Bigg) \,. \end{aligned} \tag{3.3.12}$$

Note that the PLL was taken to be in lock state. This is evident from (3.3.12), since in the phase expression for the output of PLL it is valid that $\omega_o = \omega_c$. The above equation can be written in a different way for the case where the spectrum is spread and concentrated around a center frequency ω_c. The center frequency of the spectrum can be defined as:

$$\omega_c = L\Delta\omega \,, \tag{3.3.13}$$

where L is an integer number and $\Delta\omega = {}^{2\pi}/_{T_{\text{ob}}}$ is the frequency step size which is inversely proportional to the observation time as it was discussed before. The relationship between indices n and L can be written as:

$$m = n - L \quad \Rightarrow \quad n = m + L \,. \tag{3.3.14}$$

Replacing (3.3.13) and (3.3.14) into equation of the output phase angle of the VCO from (3.3.11) results in:

$$\begin{aligned} \Theta_o(t) &= \omega_c t + \Phi_{\text{const}} \\ &\quad + \sum_{m=-\infty}^{+\infty} \{D_{m+L} \cos(\omega_c t + m\Delta\omega t) \\ &\qquad + E_{m+L} \sin(\omega_c t + m\Delta\omega t)\} \,. \end{aligned} \tag{3.3.15}$$

Equation (3.3.15) can be expanded to obtain:

$$\begin{aligned} \Theta_o(t) &= \omega_c t + \Phi_{\text{const}} \\ &\quad + \sum_{m=-\infty}^{+\infty} \{D_{m+L} \cos(m\Delta\omega t) + E_{m+L} \sin(m\Delta\omega t)\} \cos(\omega_c t) \end{aligned}$$

$$+\sum_{m=-\infty}^{+\infty}\{E_{m+L}\cos(m\Delta\omega t)-D_{m+L}\sin(m\Delta\omega t)\}\sin(\omega_c t)\,. \tag{3.3.16}$$

In order to write the above equation in a compact form, the following variables $V(t)$ and $W(t)$ are introduced:

$$V(t)=\sum_{m=-\infty}^{+\infty}\{D_{m+L}\cos(m\Delta\omega t)+E_{m+L}\sin(m\Delta\omega t)\}\,, \tag{3.3.17}$$

$$W(t)=\sum_{m=-\infty}^{+\infty}\{E_{m+L}\cos(m\Delta\omega t)-D_{m+L}\sin(m\Delta\omega t)\}\,, \tag{3.3.18}$$

$$\Rightarrow \Theta_0(t)=\omega_c t+\Phi_{\text{const}}+V(t)\cos(\omega_c t)+W(t)\sin(\omega_c t)\,. \tag{3.3.19}$$

The output phase angle $\Theta_o(t)$ from (3.3.19) can be inserted into the expression for the output voltage of PLL given in (3.3.12). The resulting equation can be expanded to obtain:

$$\begin{aligned}u_o(t)=\hat{u}_o\{&\cos\left(V(t)\cos(\omega_c t)\right)\cos\left(W(t)\sin(\omega_c t)\right)\cos(\omega_c t+\Phi_{\text{const}})\\&-\sin\left(V(t)\sin(\omega_c t)\right)\sin\left(W(t)\sin(\omega_c t)\right)\cos(\omega_c t+\Phi_{\text{const}})\\&-\sin\left(V(t)\cos(\omega_c t)\right)\cos\left(W(t)\sin(\omega_c t)\right)\sin(\omega_c t+\Phi_{\text{const}})\\&-\cos\left(V(t)\cos(\omega_c t)\right)\sin\left(W(t)\sin(\omega_c t)\right)\sin(\omega_c t+\Phi_{\text{const}})\}\,.\end{aligned} \tag{3.3.20}$$

The obtained result in (3.3.20) contains effects of a single noise source on the output voltage of a PLL. This expression shows the complexity involved especially when analyzing the results to compute the output spectrum.

In what follows, a method will be developed in order to find an approximation for the output of the PLL. Bessel functions can be used in order to approximate the output voltage of a PLL. Terms in (3.3.20) can be expanded with the help of Bessel functions of first kind [66] to obtain:

$$\cos\left(V(t)\cos(\omega_o t)\right)=J_0(V(t))+2\sum_{k=1}^{+\infty}(-1)^k J_{2k}(V(t))\cos(2k\omega_c t)\,, \tag{3.3.21}$$

$$\cos\left(W(t)\sin(\omega_o t)\right)=J_0(W(t))+2\sum_{k=1}^{+\infty}J_{2k}(W(t))\cos(2k\omega_c t)\,, \tag{3.3.22}$$

$$\sin\left(V(t)\cos(\omega_o t)\right)=2\sum_{k=0}^{+\infty}(-1)^k J_{2k+1}(V(t))\cos((2k+1)\omega_c t)\,, \tag{3.3.23}$$

$$\sin\left(W(t)\sin(\omega_o t)\right) = 2\sum_{k=0}^{+\infty} J_{2k+1}\big(W(t)\big)\sin((2k+1)\omega_c t)\,, \tag{3.3.24}$$

with

$$J_\nu(X) = \left(\frac{X}{2}\right)^\nu \sum_{k=0}^{+\infty} \frac{\left(-\frac{1}{4}X^2\right)^k}{k!\Gamma(\nu+k+1)}\,, \tag{3.3.25}$$

where $\Gamma(n)$ is the gamma function. In case where n is a positive integer this results in the factorial expression $\Gamma(n)=(n-1)!$.

In (3.3.20) the terms $V(t)$ and $W(t)$ are function of the variables D_{m+L} and E_{m+L} which in turn contain expressions coming from the Rice's second model of the form $A_n\cos(\varphi_n)$. A_n represent noise amplitudes which are very small quantities in the case where a stable PLL in lock condition is being considered. It can be assumed that A_n^p will be negligibly small quantities when $p\geq 2$. Based on the above discussion (3.3.21) to (3.3.24) can be approximated for the case where $k\leq 1$:

$$\cos\left(V(t)\cos(\omega_o t)\right) \approx J_0\big(V(t)\big) - 2J_2\big(V(t)\big)\cos(2\omega_c t)\,, \tag{3.3.26}$$

$$\cos\left(W(t)\sin(\omega_o t)\right) \approx J_0\big(W(t)\big) + 2J_2\big(W(t)\big)\cos(2\omega_c t)\,, \tag{3.3.27}$$

$$\sin\left(V(t)\cos(\omega_o t)\right) \approx 2J_1\big(V(t)\big)\cos(\omega_c t) - 2J_3\big(V(t)\big)\cos(3\omega_c t)\,, \tag{3.3.28}$$

$$\sin\left(W(t)\sin(\omega_o t)\right) \approx 2J_1\big(W(t)\big)\sin(\omega_c t) + 2J_3\big(W(t)\big)\sin(3\omega_c t)\,. \tag{3.3.29}$$

In a similar way, equation (3.3.25) can be approximated for $k\leq 1$ as follows:

$$J_\nu(X) \approx \left(\frac{X}{2}\right)^\nu - \frac{1}{4}\frac{1}{2^\nu}\frac{X^{\nu+2}}{(\nu+1)!}\,. \tag{3.3.30}$$

The Bessel functions J_0 to J_3 could be approximated for $X \ll 1$ as:

$$J_0(X) \approx 1 - \frac{X^2}{4}\,, \tag{3.3.31}$$

$$J_1(X) \approx \frac{X}{2} - \frac{X^3}{16}\,, \tag{3.3.32}$$

$$J_2(X) \approx \frac{X^2}{4} - \frac{X^4}{96}\,, \tag{3.3.33}$$

$$J_3(X) \approx \frac{X^3}{8} - \frac{X^5}{768}\,. \tag{3.3.34}$$

For the same reason as mentioned before, the terms in the above expressions which have a power greater than 3 will be neglected. Inserting the Bessel functions J_0 to J_3 into (3.3.21) to (3.3.24) results in:

$$\cos\left(V(t)\cos(\omega_o t)\right) \approx 1 - \frac{V(t)^2}{4} - \frac{V(t)^2}{4}\cos(2\omega_c t)\,, \tag{3.3.35}$$

$$\cos\left(W(t)\sin(\omega_o t)\right) \approx 1 - \frac{W(t)^2}{4} + \frac{W(t)^2}{4}\cos(2\omega_c t)\,, \tag{3.3.36}$$

$$\sin\left(V(t)\cos(\omega_o t)\right) \approx \left(V(t) - \frac{V(t)^3}{8}\right)\cos(\omega_c t) - \frac{V(t)^3}{24}\cos(3\omega_c t)\,, \tag{3.3.37}$$

$$\sin\left(W(t)\sin(\omega_o t)\right) \approx \left(W(t) - \frac{W(t)^3}{8}\right)\sin(\omega_c t) + \frac{W(t)^3}{24}\sin(3\omega_c t)\,. \tag{3.3.38}$$

The above four equations i.e. (3.3.35) to (3.3.38) are inserted into the expression for the output voltage of the PLL shown in (3.3.20). The resulting equation can be expanded and approximated by neglecting all the higher harmonics, because they are not of interest, and they are considered to suppressed within the PLL bandwidth. At the same time the amplitude terms $V(t)$ and $W(t)$ which are proportional to amplitudes of the noise source are negligibly small for higher values of k. The intermediate steps are very lengthy and would not be shown here. The final result of the calculation considering only the output voltage signal at the center frequency ω_c while ignoring the higher harmonics is:

$$\begin{aligned}
u_o(t) = \hat{u}_o \Bigg\{ & \Bigg[\left(1 - \frac{3V(t)^2}{8} - \frac{W(t)^2}{8} + \frac{V(t)^2 W(t)^2}{32}\right)\cos(\Phi_{\text{const}}) \\
& - \left(\frac{V(t)W(t)}{4} - \frac{V(t)W(t)^3}{48} - \frac{V(t)^3 W(t)}{48} \right. \\
& \qquad \left. + \frac{V(t)^3 W(t)^3}{768}\right)\sin(\Phi_{\text{const}}) \Bigg] \cos(\omega_c t) \\
& + \Bigg[\left(1 - \frac{3V(t)^2}{8} - \frac{W(t)^2}{8} + \frac{V(t)^2 W(t)^2}{32}\right)\sin(\Phi_{\text{const}}) \\
& + \left(\frac{V(t)W(t)}{4} - \frac{V(t)W(t)^3}{48} - \frac{V(t)^3 W(t)}{48} \right. \\
& \qquad \left. + \frac{V(t)^3 W(t)^3}{768}\right)\cos(\Phi_{\text{const}}) \Bigg] \sin(\omega_c t) \Bigg\}\,.
\end{aligned} \tag{3.3.39}$$

The output of the PLL with a single noise source has the form:

$$u_o(t) = \tilde{u}_1(t)\cos(\omega_c t) + \tilde{u}_2(t)\sin(\omega_c t)\,. \tag{3.3.40}$$

The functions $\tilde{u}_1(t)$ and $\tilde{u}_2(t)$ are random processes. From (3.3.39) it can be seen that they are functions of the noise source $n_{PD}(t)$ in front of the control filter through the terms $A_n \cos(\varphi_n)$. This dependency can be seen by looking at the expressions for $W(t)$ and $V(t)$ in (3.3.17) and (3.3.18). $W(t)$ and $V(t)$ depend on D_n and E_n, shown in (3.3.8) and (3.3.9), which are functions of the PD noise terms $A_n \cos(\varphi_n)$.

Using the results from (3.3.39), the output average power spectral density for a PLL including effects of a single noise source in front of the control filter are derived. These are also very complex and lengthy calculations and would not be shown here. In order to demonstrate the methodology, calculation for the power spectral density of a simple signal containing effects of electronic noise will be demonstrated.

3.3.2 Average Power Spectrum

In order to demonstrate the methodology for calculating the average output power spectral density employing Rice's second model for describing noise, a simple example of a signal containing noise in the amplitude is taken. Consider an input signal that has only amplitude modulation noise as shown in:

$$u_{\mathrm{in}}(t) = \hat{u}_{\mathrm{in}}(1 + R(t)) \cos(\omega_c t + \phi_c)\,. \tag{3.3.41}$$

Using Rice's second model from (3.2.2), the noise source modulating the amplitude in the above equation could be expressed as:

$$\begin{aligned} u_{\mathrm{in}}(t) =& \hat{u}_{\mathrm{in}} \left(1 + \sum_{n=-N}^{n=N} \frac{A_n}{\hat{u}_{\mathrm{in}}} \cos(n\Delta\omega t + \varphi_n) \right) \cos(\omega_c t + \phi_c)\,, \\ =& \underbrace{\hat{u}_{\mathrm{in}} \cos(\omega_c t + \phi_c)}_{u_{\mathrm{s,i}}(t)} + \underbrace{\cos(\omega_c t + \phi_c) \sum_{n=-N}^{n=N} A_n \cos(n\Delta\omega t + \varphi_n)}_{u_{\mathrm{N,i}}(t)}\,. \end{aligned} \tag{3.3.42}$$

In the above equation $u_{\mathrm{s,i}}(t)$ is the useful signal and $u_{\mathrm{N,i}}(t)$ describes the additional noise. In Rice's second description of noise the amplitude terms A_n are deterministic and the phases φ_n are equally distributed in the interval $[0, 2\pi)$. The density function for the random variable φ_n is:

$$p(\varphi_n) = \begin{cases} \frac{1}{2\pi} & \text{for} \quad \varphi_n \in [0, 2\pi)\,, \\ 0 & \text{elsewhere}\,. \end{cases} \tag{3.3.43}$$

The average power of the useful signal $u_{\mathrm{s,i}}(t)$ can be calculated as:

$$\begin{aligned} P_s &= \frac{1}{R}\overline{(u_{\mathrm{s,i}}(t))^2}\,, \\ &= \frac{1}{R}\lim_{T\to\infty}\frac{1}{2T}\int_{-T}^{T}(u_{\mathrm{s,i}}(t))^2\mathrm{d}\tau\,, \\ &= \frac{1}{R}\lim_{T\to\infty}\frac{1}{2T}\int_{-T}^{T}(\hat{u}_{\mathrm{in}}\cos(\omega_c\tau+\phi_c))^2\mathrm{d}\tau\,, \\ &= \frac{\hat{u}_{\mathrm{in}}^2}{R}\lim_{T\to\infty}\frac{1}{4T}\int_{-T}^{T}(1+\cos(2\omega_c\tau+\phi_c))\mathrm{d}\tau\,, \\ &= \frac{\hat{u}_{\mathrm{in}}^2}{2R}\,. \end{aligned} \tag{3.3.44}$$

The average power of the noise signal $u_{\mathrm{N,i}}(t)$ can be calculated as:

$$P_N = \frac{1}{R}\overline{\langle u_{\mathrm{N,i}}(t)^2\rangle}\,. \tag{3.3.45}$$

This represents taking the ensemble and time average of noise signal $u_{\mathrm{N,i}}(t)$. The average noise power calculation involves taking time average as well as average over the family of functions (ensemble average) since the process is not ergodic. Taking the average over family of functions for the noise signal $u_{\mathrm{N,i}}(t)$ from (3.3.42) leads to:

$$\begin{aligned} \left\langle u_{\mathrm{N,i}}(t)^2\right\rangle = \Bigg\langle &\cos(\omega_c t+\phi_c)^2\cdot \\ &\sum_{n=-N}^{n=N}\sum_{k=-N}^{n=N}A_nA_k\cos(n\Delta\omega t+\varphi_n)\cos(k\Delta\omega t+\varphi_k)\Bigg\rangle\,. \end{aligned} \tag{3.3.46}$$

In the above equation the terms $\cos(\omega_c t+\phi_c)^2$, A_n, and A_k are deterministic and φ_n and φ_k are random variables. This expression could be rewritten as:

$$\begin{aligned} \left\langle u_{\mathrm{N,i}}(t)^2\right\rangle = &\cos(\omega_c t+\phi_c)^2\cdot \\ &\sum_{n=-N}^{n=N}\sum_{k=-N}^{n=N}A_nA_k\left\langle\cos(n\Delta\omega t+\varphi_n)\cos(k\Delta\omega t+\varphi_k)\right\rangle\,, \end{aligned}$$

$$= \cos(\omega_c t + \phi_c)^2 \cdot \sum_{n=-N}^{n=N} \sum_{k=-N}^{n=N} \frac{A_n A_k}{2} \langle \cos((n-k)\Delta\omega t + \varphi_n - \varphi_k) \rangle + \langle \cos((n+k)\Delta\omega t + \varphi_n + \varphi_k) \rangle \,, \quad (3.3.47)$$

φ_n and φ_k are statistically independent and equally distributed in the interval $[0, 2\pi)$. Considering the cosine terms separately it follows:

$$\langle \cos((n-k)\,\Delta\omega t + \varphi_n - \varphi_k) \rangle = \int_{-\infty}^{+\infty} \int_{-\infty}^{+\infty} \cos((n-k)\Delta\omega t + \varphi_n - \varphi_k) p(\varphi_n) p(\varphi_k) \mathrm{d}\varphi_n \mathrm{d}\varphi_k \,. \quad (3.3.48)$$

After inserting the probability density function it result in:

$$\langle \cos() \rangle = \frac{1}{(2\pi)^2} \int_0^{2\pi} \int_0^{2\pi} \cos((n-k)\Delta\omega t + \varphi_n - \varphi_k) \mathrm{d}\varphi_n \mathrm{d}\varphi_k \,. \quad (3.3.49)$$

Two different cases $n{=}k$ and $n{\neq}k$ have to be distinguished:

$$\langle \cos() \rangle = \begin{cases} \frac{1}{(2\pi)^2} \int_0^{2\pi} \int_0^{2\pi} \cos((n-k)\Delta\omega t + \varphi_n - \varphi_k) \mathrm{d}\varphi_n \mathrm{d}\varphi_k & \text{for} \quad n \neq k \,, \\ \frac{1}{(2\pi)^2} \int_0^{2\pi} \int_0^{2\pi} 1 \mathrm{d}\varphi_n \mathrm{d}\varphi_k & \text{for} \quad n = k \,. \end{cases}$$

Performing integration with respect to φ_n it follows

$$\langle \cos() \rangle = \begin{cases} \frac{1}{(2\pi)^2} \int_0^{2\pi} \left[\sin((n-k)\Delta\omega t + \varphi_n - \varphi_k) \right]_{\varphi=0}^{2\pi} \mathrm{d}\varphi_k = 0 & \text{for} \quad n \neq k \,, \\ \frac{1}{2\pi} \int_0^{2\pi} 1 \mathrm{d}\varphi_k = 1 & \text{for} \quad n = k \,. \end{cases}$$

The same calculations method can also be applied to the other ensemble average resulting in:

$$\langle \cos((n+k)\Delta\omega t + \varphi_n + \varphi_k) \rangle = 0 \qquad \forall \quad n, k \,. \quad (3.3.50)$$

Taking into account the obtained results, it leads to the following description for the ensemble average of noise signal:

$$\left\langle u_{\mathrm{N,i}}(t)^2 \right\rangle = \cos(\omega_c t + \phi_c)^2 \sum_{n=-N}^{n=N} \frac{A_n^2}{2} \,. \quad (3.3.51)$$

If the process is not ergodic as it will be the case in a PLL noise analysis, then not only ensemble but also time average is needed to be calculated before an average value of the power can be found. As it can be seen from (3.3.51), the ensemble average of the noise signal is still dependent on time. Taking the time average results in:

$$P_N = \frac{1}{R}\overline{\langle u_{\mathrm{N,i}}(t)^2\rangle} = \frac{1}{R}\overline{\cos(\omega_c t+\phi_c)^2}\sum_{n=-N}^{n=N}\frac{A_n^2}{2}\,,$$
$$= \frac{1}{2R}\overline{(1+\cos(2\omega_c t+\phi_c))}\sum_{n=-N}^{n=N}\frac{A_n^2}{2} = \sum_{n=-N}^{n=N}\frac{A_n^2}{4R}\,. \tag{3.3.52}$$

A methodology for calculating the average output power of a synthesizer taking into account noise coming from different sources within the synthesizer as well as external sources has been demonstrated. As it can be seen from these calculation, Rice's second model makes it much easier to consider the statistical nature of the noise sources. Rather than dealing with more complex noise models involving taking ensemble average of Gaussian or Rayleigh distributions, this model makes the calculation simpler. With this mathematical noise modeling technique, one has to deal with noise components that have uniform distribution. By the virtue of the central limit theorem [49], it can be proved that Rice's first and second models lead to the same result.

The author has also looked at the synthesizer containing effects of all noise sources including a non-ideal limiter model discussed in Section 2.3. Because that involves very complex and lengthy derivation, this topic will not be discussed any further here. To indicate the complexity involved Appendix A.4 on page 118 shows results for a simplified case of a synthesizer with noise.

Some of the material consulted by the author during the process of these derivations include [67–72].

3.4 Normalized Transfer Function of a Synthesizer

The transfer function of a second order synthesizer that was derived in the previous section can also be described in the normalized form in agreement with the theory of servomechanism; that is to say in terms of the natural angular frequency ω_n and the damping factor ζ as:

$$H(s) = \frac{\frac{K_D K_o}{\tau_1 N}(s\tau_2+1)}{s^2+\left(\frac{b}{\tau_1}+\frac{K_D K_o}{\tau_1 N}\tau_2\right)s+\frac{K_D K_o}{\tau_1 N}}\,, \tag{3.4.1}$$

$$= \frac{\left(2\zeta\omega_n - \frac{bN}{K_D K_o}\omega_n^2\right) s + \omega_n^2}{s^2 + 2\zeta\omega_n s + \omega_n^2}\,, \tag{3.4.2}$$

where (3.4.3)

$$\omega_n = \sqrt{\frac{K_D K_o}{\tau_1 N}}\,, \tag{3.4.4}$$

$$\zeta = \frac{\omega_n}{2}\left(\tau_2 + \frac{bN}{K_D K_o}\right)\,. \tag{3.4.5}$$

The natural angular frequency ω_n and the damping factor ζ depend on the divider factor N. The well-known formulas for a PLL can be used for the synthesizer if the influence of the divider is modeled by the phase detector constant $\tilde{K}_D = {}^{K_D}/_N$ or by an N-dependent oscillator constant $\tilde{K}_o = {}^{K_o}/_N$.

The calculations here are based on a phase lag-lead control filter. The advantage of this type of filter is that it provides a freedom of independent choice of natural angular frequency ω_n and damping factor ζ, but with a price of reduced slope of the transfer function $H(s)$ in the stop band and a reduced phase margin [3].

3.5 3 dB Bandwidth for the Second Order PLL and Control Filter Parameter Calculations

The 3 dB bandwidth of the second order PLL can be calculated from the transfer function in (3.4.2) by considering two different choices of filters; active filters and passive filters [7, 11]. For a second order type-I system, that is to say a second order PLL that employs a first order passive control filter, the 3 dB bandwidth is:

$$\omega_{3\mathrm{dB}} = \omega_n\sqrt{(1-2\zeta^2) + \sqrt{(1-2\zeta^2)^2 + 1}}\,. \tag{3.5.1}$$

For a second order PLL of type-II that uses a first order perfect integrator as a loop filer, the 3 dB bandwidth is defined to be:

$$\omega_{3\mathrm{dB}} = \omega_n\sqrt{(1+2\zeta^2) + \sqrt{(1+2\zeta^2)^2 + 1}}\,. \tag{3.5.2}$$

It was mentioned before in Section 2.8 that the 3 dB bandwidth of PLLs should be less than 10% of the sampling rate, which means 10% of the frequency at the front of the phase detector.

After selecting the 3 dB bandwidth as less than or equal to 10% of the sampling frequency, the natural angular frequency ω_n can be calculated by using

the equations relating $\omega_{3\mathrm{dB}}$ and ω_n. For fast settling, usually a value of the damping factor $\zeta = 1/\sqrt{2}$ is chosen.

Using these results, the parameters of the control filter τ_1 and τ_2 can be calculated from (3.4.4) and (3.4.5) as:

$$\tau_1 = \frac{K_D K_o}{N\omega_n^2}\,, \tag{3.5.3}$$

$$\tau_2 = \frac{2\zeta}{\omega_n} - \frac{bN}{K_D K_o}\,. \tag{3.5.4}$$

3.6 Noise Bandwidth of a Second Order PLL

In PLLs and frequency synthesizers the relative instantaneous phase of the VCO signal is a lowpass filtered version of the relative instantaneous phase of the input signal. The noise bandwidth that is usually defined for a lowpass filter can be taken to describe the noise behavior at the PLL output.

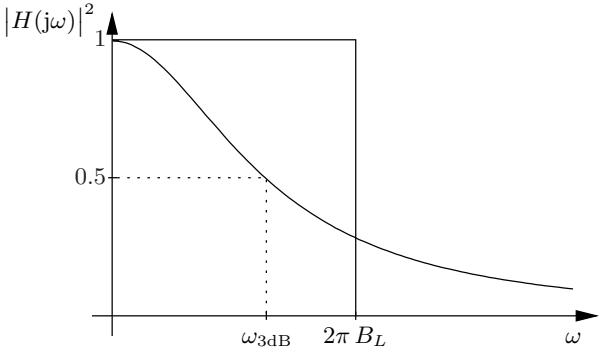

Fig. 3.6: Comparison of brick-wall lowpass filter to real world filter showing the definition of the noise bandwidth B_L.

In order to define the noise bandwidth of a lowpass filter, consider the absolute value of the transfer characteristics shown in Fig. 3.6 for a normal lowpass filter and a brick-wall filter. Consider that the lowpass filter is fed with white noise. The power of the signal produced at the output will be finite and is measured to be P_N.

Consider a ficticious brick-wall filter whose absolute transfer function has the same value at zero frequency point as the other lowpass filter. The brick-wall

filter is fed with the same white noise as the other lowpass filter. The bandwidth B_L of the brick-wall filter is varied until the output noise power is also P_N as it was for the original filter. In this case the B_L is called the noise bandwidth of the original lowpass filter. By comparing the equations for the noise power of the original filter and the brick-wall filter, a relation for the noise bandwidth of the original lowpass filter can be computed [3] in terms of the filter transfer function $H(\mathrm{j}\omega)$:

$$B_L = \frac{1}{2} \int_{-\infty}^{+\infty} \frac{|H(\mathrm{j} \cdot 2\pi f)|^2}{|H(0)|^2} \mathrm{d}f \,. \tag{3.6.1}$$

Similar to any lowpass filer, the noise bandwidth of a PLL or a synthesizer can be described by applying the definition to the transfer function of the synthesizer from (3.4.2). It can be shown that for a second order PLL the noise bandwidth is given by:

$$B_L = \frac{\omega_n \zeta}{2} \left(1 + \frac{1}{4\zeta^2}\right) . \tag{3.6.2}$$

From the above equation, it can be proved that a minimum noise bandwidth for a second order synthesizer is achieved when ζ=0.5. For the purpose of achieving a faster settling behavior, a value of $\zeta = {}^1/_{\sqrt{2}}$ is used.

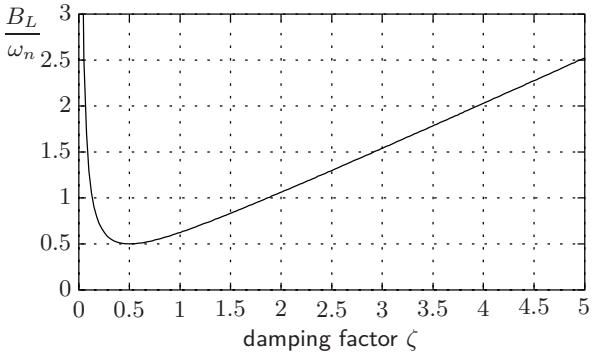

Fig. 3.7: Noise bandwidth B_L for a second order PLL versus damping factor ζ.

Figure 3.7 gives a curve of the noise bandwidth for a second order PLL. This curve is obtained by using (3.6.2) to plot normalized the noise bandwidth B_L

versus the damping factor ζ. As is can be seen from the graph, there is only an increase of 6% in noise bandwidth when the optimum value of $\zeta = 1/\sqrt{2}$ is chosen. When designing PLLs, this compromise is often done in order to have a better settling behavior.

4 Noise Simulations in Frequency Synthesizers

4.1 Synthesizer Simulation

All the simulation models were developed using combination of Matlab code and Simulink block sets [58,73,74]. Simulink has a very big library of blocks for performing different tasks. It has blocks that generate noise, other blocks for VCO, phase detector, etc., but these blocks were not used. Most of these block sets do not provide the possibility to see their internal structure. In order to build a synthesizer system based on the theoretical analysis results obtained in the previous chapters, only the basic building blocks from Simulink were used; for example adders, multipliers, integrators, transfer functions, etc.

4.1.1 Phase Domain Synthesizer Model

For the simulations, a phase domain model of a frequency synthesizer similar to what is shown in block diagram in Fig. 3.4 on page 38 was implemented. The instantaneous output phase $\Theta_o(t)$ of the synthesizer is passed through a sinusoidal signal generator block. The resulting signal is multiplied by the amplitude of the VCO to get the output signal:

$$u_o(t) = \hat{u}_o(1 + n_{VA}(t)) \cos(\Theta_o(t)) \,. \tag{4.1.1}$$

As it was explained in Sections 2.3 and 2.4, the effect of amplitude fluctuations of the VCO and the reference signal are taken into account as proportional terms that effect the phase detector output.

Linear and non-linear models of the phase detector were implemented. By using of phase plane trajectories as it would be discussed in a later section, the non-linear model provides more information on the settling behavior for the synthesizer with noise.

4.1.2 Consideration for the Noise Sources

The noise sources considered in the simulations are white noise and $1/f$ noise sources; the sources are generated by implementing Rice's second model in Matlab. In order to produce multiple uncorrelated noise sources, a different seed is provided to the random number generator in Matlab. Different noise

sources are used for different points in the circuit where all are generated in a similar way.

In order to be able to compare results from different simulations run at different times, it is better to generate noise sources beforehand and to use always the same noise source for the same point in the circuit. Furthermore, since the noise generation routines require a lot of time and CPU power, it is better to generate them at one point and save the data into files. A program is written that will automatically load the noise sources from files into the Simulink work space at the start of the simulation.

The same combination of noise sources that was discussed in Section 3.3 on page 36 is used for the simulations also. In the simulations, the noise after the reference oscillator is considered to be additive white noise. A bandpass reference signal can be described as consisting of two terms that represent the useful signal $u_s(t)$ and additional bandpass noise $u_n(t)$ where noise is modeled by using Rice's second model:

$$\begin{aligned} u_i(t) &= u_s(t) + u_n(t)\,, \\ &= \hat{u}_s \cos(\omega_c t + \phi_c) + \sum_{n=-N}^{n=N} A_n \cos(\omega_c t + n\Delta\omega t + \varphi_n + \phi_c)\,, \end{aligned} \tag{4.1.2}$$

where coefficients A_n are deterministic and the terms φ_n are random variables uniformly distributed in the interval $(0, 2\pi]$. Because a phase model of the synthesizer is being considered for simulation, the noise should be split into terms that effect the phase and the amplitude separately. The phase noise part will be added to the reference source phase and the amplitude noise part will appear as a proportional term at the output of the phase detector as explained in Section 2.4. The expression for reference signal plus noise from (4.1.2) can be rewritten to divide the noise into terms affecting the amplitude and phase of the useful signal as shown here:

$$u_i(t) = R(t)\cos(\omega_c t + \psi_R(t) + \phi_c)\,. \tag{4.1.3}$$

A detailed description for the amplitude term $R(t)$ and the phase term $\psi_R(t)$ is given later in Section 5.1.3.1 through (5.1.9) and (5.1.10) on page 77.

In a similar way, the additive bandpass noise at VCO can also be described by dividing it into terms effecting the amplitude and the phase. The amplitude noise term of the VCO will also lead to a proportional term at the phase detector output.

Inside the loop, the noise sources are taken to be a combination of $1/f$ noise and white noise. The baseband signal inside the loop will be affected by $1/f$ noise in addition to thermal and shot noise coming from different components.

The $^1/_f$ noise source affects the lower frequency part of the spectrum up to some kHz range whereas the white noise dominates at higher frequencies.

In the loop, that is to say in the path between the phase detector and the VCO, noise sources are not needed to be split into phase and amplitude terms. The output of the phase detector is a voltage or a current signal as shown in the phase model of the synthesizer given in Fig. 3.4. This implies that the baseband voltage or current noise sources can be added directly.

4.1.3 Simulation Parameters

The angular frequency of the reference signal is chosen to be ω=$50 \cdot 10^3$ rad/s. For a fast settling, the damping factor is given as ζ=$^1/_{\sqrt{2}}$. The reference and the feedback dividers are M=2 and N=4, respectively. The VCO and the phase detector gain are chosen to be K_o=$\pi \cdot 10^3$ rad/Vs and K_D=0.5 V/rad, respectively.

As mentioned in Section 2.8, to avoid sampling effects the synthesizer bandwidth is taken to be 10% of frequency at the phase detector. Section 3.5 shows the relationships between synthesizer bandwidth and the natural angular frequency ω_n for a second order synthesizer employing an active or passive filter. Using these results the value of ω_n is calculated.

For active and passive filters the parameters of a lag-lead filter τ_1 and τ_2 are calculated by using (3.5.3) and (3.5.4) taking into account the given specifications.

All the random noise sources in this simulation are designed for SNR of 10 dB in a similar way to what is described in (3.2.4).

In order to study the effect of noise on the output, simulations are performed for each noise source separately. Combinations of different noise sources are also considered. For the simulations, both linear and nonlinear phase detector models are taken. In the steady state, both models offer similar results. Only the most important simulation results from the non-linear model will be given here. The same model is used in Section 4.2 to show effects of noise on the dynamic behavior of the system.

4.1.4 Simulation Results

The diagrams for the relative output power of a synthesizer with noise at different points in the circuit will be discussed. As it is expected from theoretical results, simulations show how the noise at different points in the circuit affects the output of the synthesizer. The simulation results also fit very well to the measurements that will be discussed in Chapter 5.

A comparison between the measured, simulated and theory will follow also in Chapter 5. In this section the simulation results will be presented without comparing them to what is expected from theory.

Note that a one-to-one comparison of the measured and simulated results is not done in this work. To accomplish that, models for the physical component need to be developed, noise and distortion from the physical components need to be extracted and to be modeled into the simulator. This was not done here. Simulations that are based on the mathematical models are presented here. They fit very well in terms of the expected spectral shape with the measurements that are shown in Chapter 5. In this work, the two main expected types of noise in a synthesizer system, white and $1/f$, are generated using Rice's second model. The simulation system that was built is flexible. It is also possible to use physically measured noise of components, if it is extracted from a synthesizer circuit.

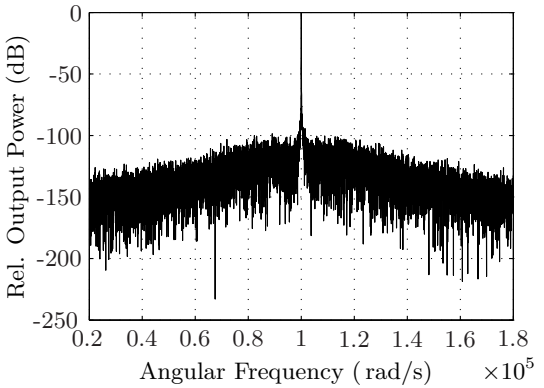

Fig. 4.1: Semi-log spectrum shows that the bandpass noise from the reference source forms a lowpass characteristic on the synthesizer output.

Figure 4.1 shows the simulation results with a bandpass white noise added after the reference source at the noise insertion point $n_i(t)$ shown in Fig. 3.4 on page 38. The white noise source is divided into phase and amplitude components. The curve shows effect of phase noise. The amplitude noise will be discussed later. The reference phase noise causes a flatting of the output spectrum around the center frequency. As expected, a bandpass reference noise results in a lowpass characteristic at the output.

Figure 4.2 shows simulation results where a baseband white voltage noise source is inserted after the phase detector at the noise insertion point $n_{PD}(t)$ in Fig. 3.4. It will be shown in Chapter 5 that the noise source placed after the phase detector produces a lowpass characteristic on the synthesizer output. Similar to reference noise, the noise source after the phase detector that falls within the bandwidth of the synthesizer will pass through the system retaining its spectral form.

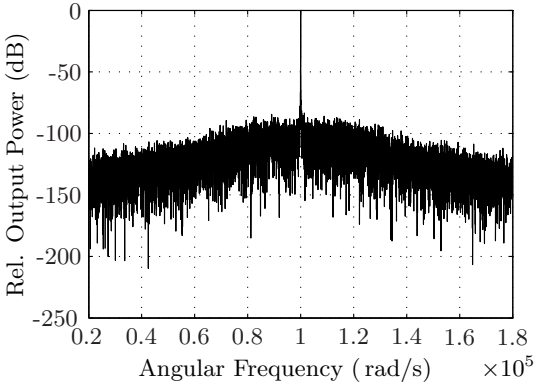

Fig. 4.2: Semi-log spectrum shows that the baseband noise from the phase detector forms a lowpass characteristic on the synthesizer output.

In the case a synthesizer with a prescaler M after reference and with a loop divider N is being considered, the noise source at the phase detector having the same power as the noise source at reference will have different impact on the system. Taking the instantaneous output phase angle of the synthesizer in (3.3.1) into account, it can be shown that the reference noise will be scaled by factor N/M before it appears at the output whereas the noise from the phase detector will be scaled by factor N/K_D. This implies that the prescaler can help to decrease the phase noise level of the reference signal.

Figures 4.3 and 4.4 show the relative output power in logarithmic form for the case where baseband white voltage noise is inserted after the control filter at the noise insertion point $n_{CF}(t)$ shown in Fig. 3.4. Using (3.3.1), it can be proved that a noise source after the control filter results in either a lowpass or a bandpass characteristic response at the synthesizer output depending the on filter transfer function as will be demonstrated in Chapter 5.

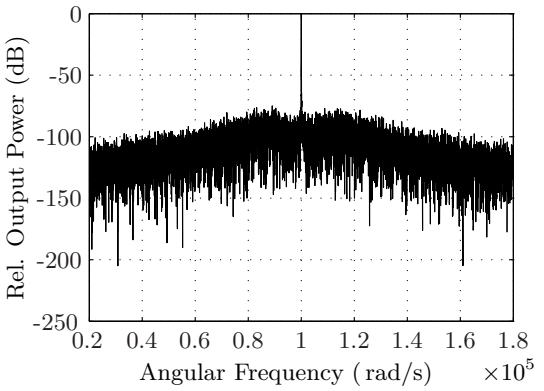

Fig. 4.3: Semi-log spectrum shows that the baseband noise from the passive control filter forms a lowpass characteristic on the synthesizer output.

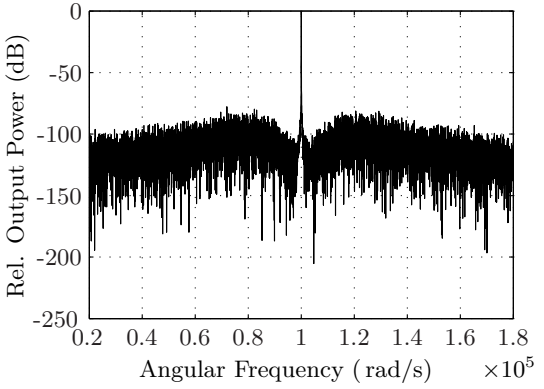

Fig. 4.4: Semi-log spectrum shows that the baseband noise from the active control filter forms a bandpass characteristic on the synthesizer output.

With a passive control filter in the loop, Fig. 4.3 shows that the output spectrum of the synthesizer will form a lowpass characteristic for a baseband noise source at the control filter output. From the synthesizer output spectrum, it can be seen that with this particular passive control filter there is a small amount of overshoot in the response. With an active control filter, Fig. 4.4 shows that the response of the synthesizer to the baseband noise source has a bandpass characteristic.

It was observed during the simulations, that the noise source in front of the VCO (control filter noise) could be critical to the stability of the system as it can lead to strong phase noise modulation in the output spectrum, especially in the cases where the gain K_o of the VCO is relatively high.

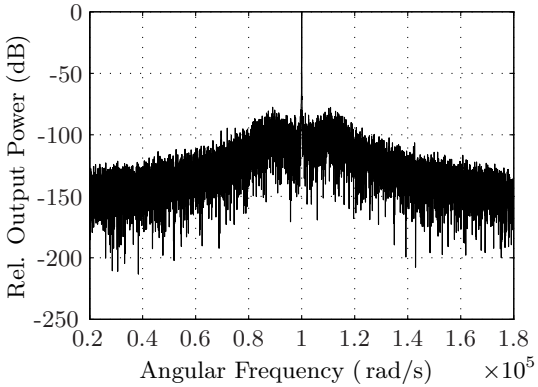

Fig. 4.5: Semi-log spectrum shows that the bandpass noise from VCO forms a highpass characteristic on the synthesizer output.

Figure 4.5 shows the effect of the bandpass phase noise source $n_{vp}(t)$ inserted after the VCO as shown in Fig. 3.4. As it was explained before, the bandpass noise at the output of the VCO is divided into amplitude $n_{VA}(t)$ and phase $n_{vp}(t)$ components. Using (3.3.1), it can be proved that the response of the synthesizer to noise inserted after the VCO is of highpass type. Moving from a point near to the center frequency outwards to the edge of the synthesizer bandwidth region, it can be observed that the noise of the VCO will be suppressed the most near the carrier and the least at the edge of the synthesizer bandwidth. Note that outside the bandwidth, the synthesizer spectrum will follow the spectral shape of an open loop VCO.

Figure 4.6 shows the effect of amplitude fluctuations of the VCO on the output of a synthesizer. Amplitude fluctuations can play a significant role in the output spectra forming. It was shown before in Section 2.4 that amplitude fluctuations of the VCO can be considered as a proportional term affecting the amplitude of the phase detector output signal. The output of the phase detector is passed through the loop filter and is fed as a control signal to the VCO. In this manner, the VCO amplitude fluctuations are fed back to the VCO and result in being converted into phase noise. The effect of amplitude fluctuations on the phase noise performance of a synthesizer system is usually smaller than the effect of other noise sources. Usually, in a synthesizer system only a small amount of amplitude variations are appearing at the output of the phase detector.

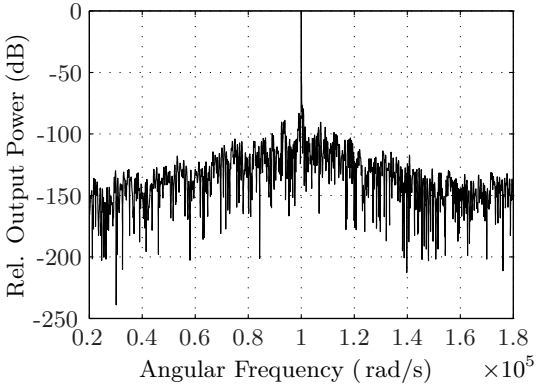

Fig. 4.6: Semi-log spectrum shows that the VCO amplitude fluctuations forms a lowpass characteristic on the synthesizer output.

Using (3.3.1), it can be shown that the amplitude noise will result in a lowpass characteristic at the output. The amplitude noise transfer function related to the synthesizer output phase is the same as the synthesizer transfer function scaled by factor K_{RN}/K_D.
The amplitude fluctuations of the reference were also considered in the simulations, but the results are not shown here since fluctuations will also lead to similar results.

Figure 4.7 shows that a bandpass white noise $n_N(t)$ added to the divider output as shown in Fig. 3.4 leads to a lowpass characteristic at the output of

a synthesizer. The response of the system is similar to the case where noise is added at the reference side except for a constant factor $-N$ in front of the transfer function instead of the factor $^N/_M$. This is expected as a synthesizer phase response to a signal in front of the phase detector results in a lowpass characteristic.

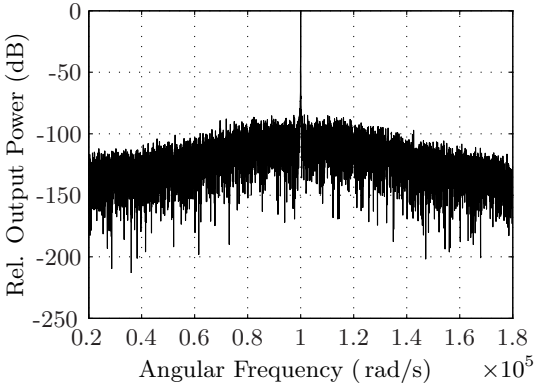

Fig. 4.7: Semi-log spectrum shows that the bandpass noise from the feedback divider forms a lowpass characteristic on the synthesizer output.

4.2 Dynamic Behavior of a Synthesizer with Noise

The behavior of a PLL might not be described by a linear model when it is far from lock, for example during switching transients, and when responding to large input signals. Important parameters such as settling time, switching speed and capture range are often dominated by non-linear behavior.

Phase plane analysis is one of the most important techniques for studying the behavior of nonlinear systems, since in many cases it is not possible to derive an explicit analytical solution of a nonlinear equation. The phase plane is a two-dimensional geometric representation of the trajectories or all possible states of a dynamic system. Phase plane plot provides an extremely useful way of visualizing and understanding the qualitative features of solution. Phase plane for a two-state variable system consists of curves of one state variable versus the other state variable. In the case of a synthesizer system, it is a plot of

solution developed in time domain showing phase errors at the output of the phase detector $\varphi(t)$ versus the derivative of the phase error $\dot{\varphi}(t)$. For more details on the derivation of phase plane plots consult [5].

In the previous section, simulation results for the behavior of a synthesizer with respect to noise was presented. In this section, the nonlinear aspects of a synthesizer with noise will be described. With the noise present at different points in the loop, the locking behavior can be best demonstrated by observing the phase plane trajectories. Simulations are performed in Simulink using the nonlinear model of a synthesizer. As mentioned before, this model does not use any of the standard VCO or PLL models found in Simulink.
The same noise sources and the same simulation setup that were used for the noise simulations in the previous section are also considered here. The phase plane trajectories show how the PLL settling behavior is modified when a noise source at one of the points shown in Fig. 3.4 is introduced. Only few example phase plane curves will be shown in this work.

The settling behavior of the synthesizer without noise was presented before and is repeated here in Fig. 4.8 for ease of comparison.

Figures 4.9 and 4.10 show that the same baseband noise source added after passive and active control filter have different impact on the settling behavior of the synthesizer. This is expected from the phase noise measurement curves in a previous section where it was shown that a noise source after the passive filter results in a lowpass output characteristic and a noise source after an active filter results in bandpass output characteristic. The phase plane curves show that the phase noise components are leading to some random phase deviations which are causing the synthesizer to have some regular transitions to outside the settling point (operating point). The noise here is not strong enough to cause the synthesizer to lose lock.

Figures 4.11 and 4.12 show how the VCO phase noise and amplitude fluctuations effect the settling behavior of a synthesizer system, respectively. The amplitude fluctuations of the VCO which are usually ignored are taken into account in this work. As expected, the phase plane trajectories show that the effect of amplitude fluctuations is weaker than the other phase noise sources. The output of the VCO usually does not have high amplitude fluctuations. The simulation as well as the measurement results in Chapter 5 show that the phase noise performance of the synthesizer could degrade if the amplitude fluctuations get stronger.

Figure 4.13 shows that with increasing noise level, there is a possibility that system will experience a cycle slip. This curve is produced by adding even stronger amount of noise to the output of a passive control filter in a synthesizer system. The noise is causing the system to skip one cycle which means that the

phase plane trajectories jump to the settling point separated by 360° from the original one.

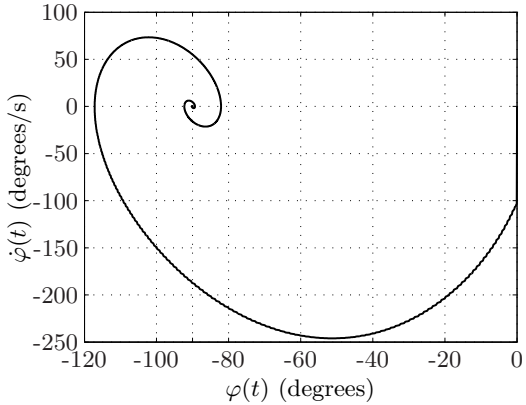

Fig. 4.8: Phase plane trajectory for a second order synthesizer without noise and delay showing the settling behavior.

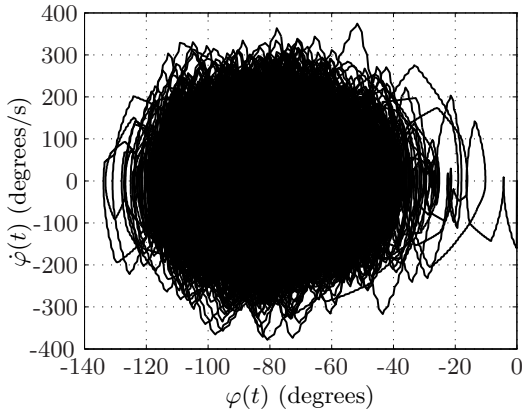

Fig. 4.9: Phase plane plot showing effects of noise from passive control filter on a second order synthesizer.

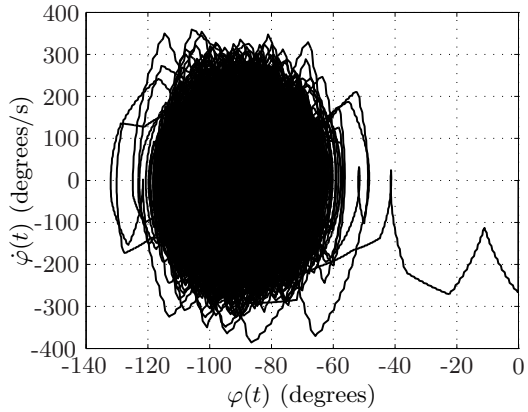

Fig. 4.10: Phase plane plot showing effects of noise from active control filter on a second order synthesizer.

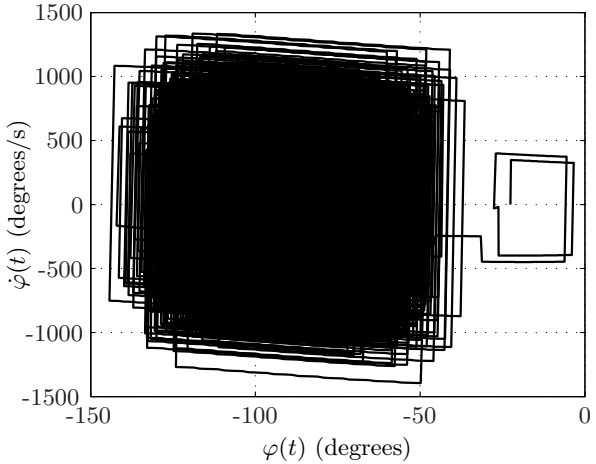

Fig. 4.11: Phase plane plot showing effects of VCO phase noise on a second order synthesizer.

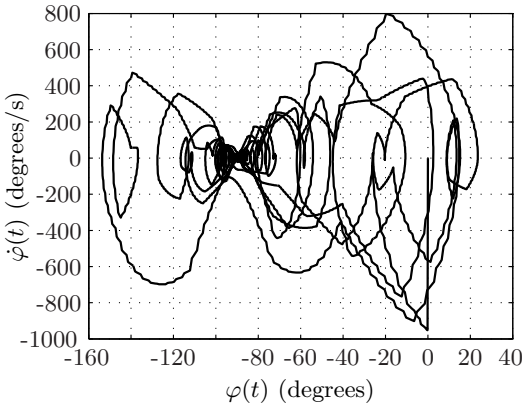

Fig. 4.12: Phase plane plot showing effects of VCO amplitude noise on a second order synthesizer.

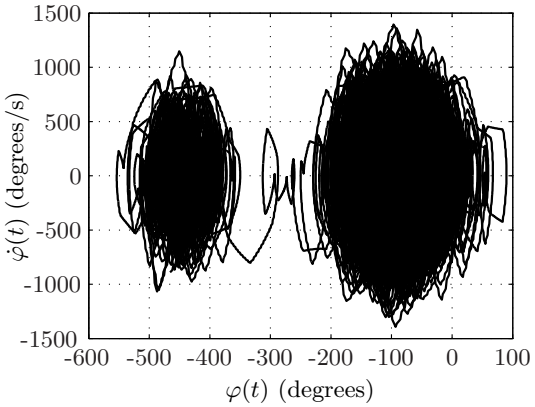

Fig. 4.13: Phase plane plot showing the possibility of getting a cycle slip when electronic noise is too strong in a synthesizer system.

5 Experimental Study of Noise in a Frequency Synthesizer

By just measuring the output spectrum of a frequency synthesizer, it is not possible to separate the effects of different noise sources on the system. A methodology was searched for that will help in characterizing the effect of noise coming from different components in a synthesizer on the total output noise. Different investigations were done in order to find a method to accomplish this task. The idea was to insert additional noise after different components in the system in order to raise the noise floor of this particular component above the noise floor of the system [75]. By applying this method, it is possible to study how certain types of noise coming from some particular components will effect the output of the system.

Furthermore, investigations were also done to reduce distortions and the noise floor of a synthesizer circuit. System noise floor reduction is an important task for having a synthesizer system with low noise floor at the output. This plays also an important role in the investigation of effects of component noise on the system. If the noise floor of the system is too high, adding weak electronic noise at different points in the system will only show a minor or no effect as the noise source could lie below the system noise floor.

5.1 Test Circuit for Noise Addition and for Studying Effects of DC Source Noise on Components

In the beginning, a simple test circuit whose block diagram is shown in Fig. 5.1 was constructed. This test circuit has two purposes. The first is to consider how noise could be added to XCOs, buffers and other components in the synthesizer circuit which produce output signals having rectangular shape with fast rise time. This investigation will help in exploring how noise of these devices contribute to the total output noise of a synthesizer. The second purpose of this circuit is to explore the effects of power supply noise on the components in a synthesizer.

From Fig. 5.1, it can be seen that a low noise voltage regulator is used to feed a crystal oscillator either directly or through a special circuit consisting of a

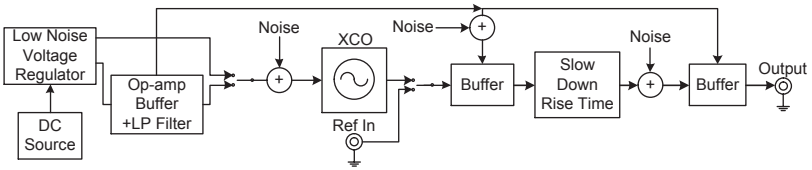

Fig. 5.1: Block diagram of a circuit used to add bandpass noise to signals with fast rise time and to show the effect of supply noise on the XCO and the buffer.

lowpass filter combined with an op-amp voltage follower that will be discussed shortly. Additional noise or distortion can be added to the XCO power supply in order to study effects of power supply noise on the reference. The output of the XCO is passed through a buffer. After the buffer, comes a circuit that is used to slow down the rise time. This circuit converts a digital signal to an analog signal. It is used to study effects of noise onto the buffer stages in a synthesizer system. It also helps to explore the possibility of adding noise to digital signals. After this stage, there is another buffer that is used to make the rise time faster. It helps to convert analog signals to square wave signals again after the noise is added to it in the previous stage.

5.1.1 DC Power Supply Rejection Ratio (PSRR)

The power supply rejection ratio (PSRR) is a term used in amplifiers (especially op-amps) and voltage regulators to describe how well a circuit can reject ripple coming from the input power supply at various frequencies [76]. If a change of ΔV_{in} Volts in the supply produces an output voltage change of ΔV_{out} Volts, then the PSRR on that supply referred to the output (RTO) in decibels can be written as dimensionless ratio:

$$\text{PSRR} = 20 \log \left(\frac{\Delta V_{\text{in}}}{\Delta V_{\text{out}}} \right) \text{dB} \ . \tag{5.1.1}$$

An ideal op-amp would have an infinite PSRR [77]. The PSRR can be expressed either as referred to the input (RTI) or the output (RTO). Dividing the RTO value by the amplifier gain gives the RTI value. The PSRR is usually given in the data sheet expressed as a positive or negative value in dB, depending on whether it is defined as the power supply change divided by the output voltage change, or vice versa. When the amplifier has dual power supplies, the PSRR is usually given separately for each. This provides useful information for amplifiers

that can be used in either dual or single-supply applications. The PSRR is a function of ripple or noise frequency as shown in Fig. 5.2 taken from the data sheet of the op-amp AD8061 [78].

5.1.2 Low Ripple and Low Noise DC Power Supply

In this work, low drop linear regulators where used to supply the circuit. In most cases, the used regulator was of low noise type like Micrel MIC5209 [79], but the noise of these regulators is still high in the applications where ultra low noise performance is needed; for example power supply of the XCO and the VCO.

Usually, the regulators are used in conjunction with *LC* filters in order to suppress ripple and noise. This *LC* filter works well for frequencies higher than approximately 50 to 100 kHz. Using *LC* filters to suppress frequencies lower than this can become impractical due to the size of the required *L* and *C* components. In the lower frequency range, usually an active filtering technique would be required.

In order to suppress noise and distortion from the regulator even further down

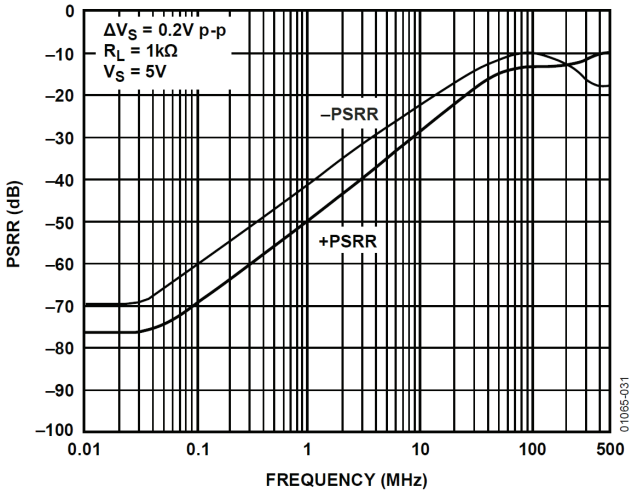

Fig. 5.2: PSRR versus frequency delta for operational amplifier AD8061 taken from the data sheet [78].

in frequencies, a special DC filtering technique shown in Fig. 5.3 was employed. This filter consists of two stages, a lowpass filter and an op-amp buffer amplifier (voltage follower). This circuit results in increased rejection to the variations and the noise in the power supply voltage. The *RC* filter in front of the op-amp has a very low cutoff frequency and helps to clean out the reference DC signal to the op-amp by suppressing distortion and noise. The op-amp itself has a high power supply rejection ratio (PSRR) and a better noise performance than the regulator. These together leads to a better suppression of power supply small signal variations and to a better noise rejection.

Note that the ripple on the power supply could lead to spurs at the output of the XCO as it would be shown later.

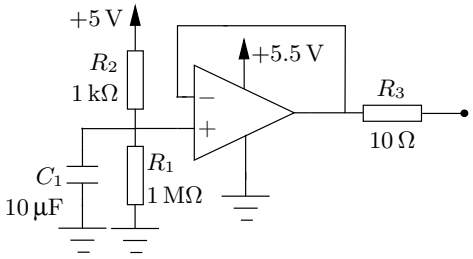

Fig. 5.3: Lowpass filter followed by an op-amp voltage follower to generate a low ripple and low noise power supply.

The filter shown in Fig. 5.3 is used in the DC path of the XCO. A commercial, of the shelf 10 MHz, crystal oscillator is used. As it can be seen from the block diagram in Fig. 5.1, the XCO could be supplied directly from low noise regulator output or over the lowpass buffer filter (LP–buffer) cleaned supply from Fig. 5.3. Using the Rohde&Schwarz FSUP [80], phase noise measurement were done for the XCO output considering both supply paths. As it can be seen from the single side band spectrum (SSB spectrum) in Fig. 5.4, the LP–buffer combination results in a better phase noise performance. The phase noise of the XCO is around 16 dB lower at 1 kHz offset from the carrier in the case of using this improved power supply shown in Fig. 5.3.

Note that the improvement in the performance depends on the XCO. To be more specific, it depends on how good is the XCO internal suppression for noise and PSRR. Some of the commercial XCOs saw less improvement using this LP–buffer circuit than the others.

The principle shown here could be employed to supply power for the whole PLL circuit, but there is a limitation to this approach. The op-amp's output

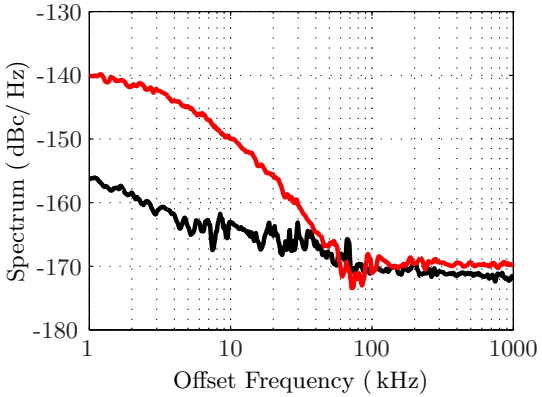

Fig. 5.4: SSB spectrum shows effects of the XCO DC source filtering.

voltage drop increases as the amount of current drawn from it goes higher. This means that this circuit can not be used in its existing form to supply the complete PLL. A number of improvements can be implemented to address this limitation. First of all, an op-amp that can supply higher amount of current like the AD8616 [81] can be used and this was done in the built-up synthesizer system. It can drive up to 50 mA with an output voltage drop of approximately 250 mV. Because of the limited supply current, multiple circuits built similar to Fig. 5.3 are used to supply different subparts of the synthesizer system. This solution was implemented in the synthesizer system that would be discussed later.

Another circuit that can be used for this purpose is shown in Fig. 5.5. It is based on similar principle, but to derive higher current a P-N junction transistor is used after the op-amp.

5.1.3 Addition of Noise to the System

In order to study effects of noise on the system, the test circuit with block diagram in Fig. 5.1 was built. This block diagram shows three different noise addition points. Two noise addition points are on the power supply of the XCO and the RF buffer, the third point is after the RF buffer. Different techniques were used in order to add noise according to the noise addition point. The noise in the baseband is added by using an op-amp adder circuit similar to that one

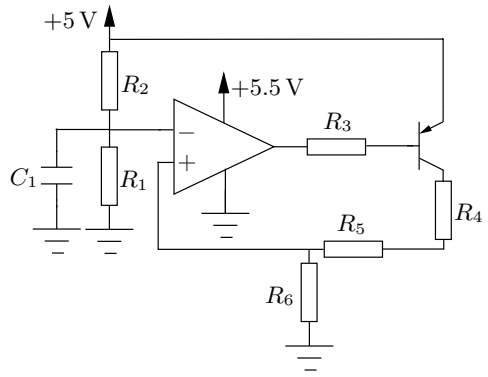

Fig. 5.5: Low noise power supply that can drive larger current loads.

shown in Fig. 5.6. In this diagram $u_s(t)$ is the signal voltage and $u_n(t)$ is the added noise voltage.

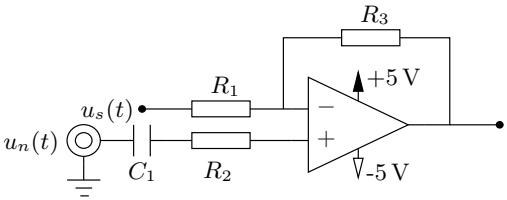

Fig. 5.6: Noise addition using an operational amplifier.

To add noise to a signal that has a very fast rise time like a square wave, a circuit shown in Fig. 5.7 is employed. The purpose of this circuit is to turn a digital signal into an analog one. The working principle of this circuit is shown in the next section.

5.1.3.1 Adding Noise to Square Wave Signals

Consider the Fourier series expansion of a square wave:

$$u_s(t) = \frac{4}{\pi} \sum_{k=1}^{\infty} \frac{(\sin(2k-1)\omega_c t)}{2k-1}\,, \tag{5.1.2}$$

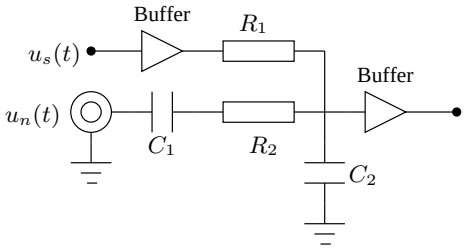

Fig. 5.7: Noise added to digital signal by slowing down the rise time.

$$= \frac{4}{\pi}\left(\sin(\omega_c t) + \frac{1}{3}\sin(3\omega_c t) + \frac{1}{5}\sin(5\omega_c t) + \cdots\right).$$

Slowing down the rise time means that a lowpass filter is used in order to filter out the higher harmonics of a square wave. Figure 5.8 shows a circuit where the lowpass cutoff frequency can be changed. In this circuit, tabbing in additional capacitors results in moving the cutoff frequency to lower values but which are higher than the fundamental frequency of the signal. Hence allowing further filtering of the higher frequencies. Figure 5.9 shows that decreasing the cutoff frequency of the lowpass filter makes a square wave signal approaches a sine wave.

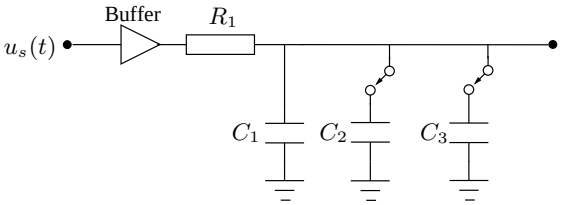

Fig. 5.8: The corner frequency of the lowpass filter used to filter out the higher harmonics of a square wave can be varied.

In order to see how noise is being coupled into the system by slowing down the rise time, a lowpass filter is considered to have a low enough cutoff frequency so that only the fundamental signal remains. A bandpass signal $u_i(t)$ can be expressed as consisting of a useful signal part plus bandpass noise:

$$u_i(t) = u_s(t) + u_n(t)\,, \tag{5.1.3}$$

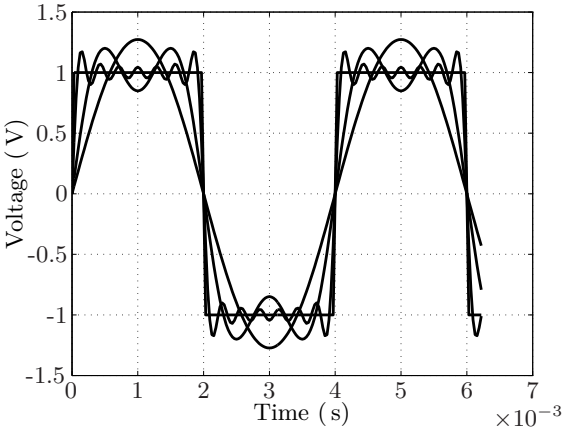

Fig. 5.9: The four curves show that as the higher harmonics of a square wave are filter out, it's rise time is slowing down. If all the harmonics are filtered out, then only the fundamental sine wave will remain which has the slowest rise time compared to all the other curves.

$$= \hat{u}_s \cos(\omega_c t + \psi(t) + \phi_c) + \sum_{n=-N}^{n=N} A_n \cos(\omega_c t + n\Delta\omega t + \varphi_n + \phi_c)\,, \quad (5.1.4)$$

where the noise is described using Rice's second model. This expression can be expanded to obtain the following:

$$u_i(t) = u_1(t)\cos(\omega_c t + \phi_c) - u_2(t)\sin(\omega_c t + \phi_c)\,, \quad (5.1.5)$$

with

$$u_1(t) = \hat{u}_s \cos(\psi(t)) + \sum_{n=-N}^{n=N} A_n \cos(n\Delta\omega t + \varphi_n)\,, \quad (5.1.6)$$

$$u_2(t) = \hat{u}_s \sin(\psi(t)) + \sum_{n=-N}^{n=N} A_n \sin(n\Delta\omega t + \varphi_n)\,. \quad (5.1.7)$$

The signal in (5.1.5) can be combined to obtain an amplitude and a phase term:

$$u_i(t) = R(t)\cos(\omega_c t + \psi_R(t) + \phi_c)\,, \quad (5.1.8)$$

with

$$R(t) = \sqrt{u_1^2(t) + u_2^2(t)}\,, \tag{5.1.9}$$

$$\tan\psi_R(t) = \frac{u_2(t)}{u_1(t)}\,, \tag{5.1.10}$$

$$\dot{\psi}_R(t) = \frac{u_1(t)\dot{u}_2(t) - u_2(t)\dot{u}_1(t)}{R^2(t)}\,. \tag{5.1.11}$$

This shows that the additive bandpass noise can be divided into two terms affecting the amplitude and the phase of a useful signal.

Note that the derivation here is based on [82], where it is explained that when the terms $u_1(t)$ and $u_2(t)$ vary with time, then $\psi_R(t)$ has to be described in a general form shown in (5.1.11) rather than considering it to be:

$$\psi_R(t) = \arctan\frac{u_2(t)}{u_1(t)}\,. \tag{5.1.12}$$

It is is explained in [82], that an arctan function does not describe clearly transitions of $\psi_R(t)$ to values outside the interval $(-\pi/2, \pi/2)$. When the terms $u_1(t)$ and $u_2(t)$ are time dependent, there is a possibility that $\psi_R(t)$ can go to values outside this interval.

Figure 5.7 shows another buffer being used after the noise addition stage. The purpose of the second buffer is to make the signal square wave again. Usually, in a synthesizer system employing a 3-state phase detector, it is required that the two input signals to the phase detector should have square wave form with a fast rise time. It was discussed in Section 2.3 and in Appendix A.1 that a real limiter (buffer) has a finite rise time. When the rise time is finite, a part of the amplitude noise will couple to the output. In addition to that, it was also shown in the same sections that phase noise in the input signal will always pass through the limiter without being suppressed independent of whether an ideal or non-ideal limiter is being considered.

The above discussion implies that using a circuit similar to Fig. 5.7 will result in both amplitude and phase noise being coupled into a system where the output signal has a square wave shape.

5.1.3.2 Effect of Spurs and Noise on the System

To investigate effects of noise on a limiter buffer, the test system shown in Fig. 5.1 is used. In this system there are two buffer at the output of the XCO which are separated by a noise addition point lying between them. The noise

addition point is a combination of circuits from Fig. 5.7 and 5.8. It consists of a lowpass filter and a noise coupling circuitry.

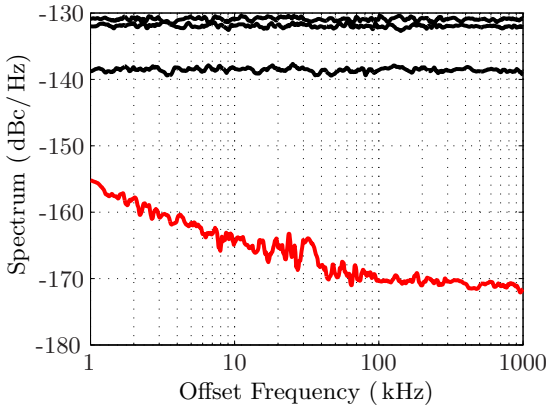

Fig. 5.10: The red curve shows the phase noise SSB spectrum at the output of the second buffer without additional noise. The black curves show that the amount of phase noise at the output of a buffer increases as rise time is slowed down.

Figure 5.10 shows SSB phase noise spectrum measured at the output of the second buffer as the capacitors C_2 and C_3 are tabbed in. The red curve shows measured phase noise taken from the output of the second buffer when no noise is added after the first buffer. As discussed in the previous section, lowering the cutoff frequency of the lowpass filter filters out the higher harmonics of a square wave and thus converting it into an analog signal. If there is an additive noise source in front of a buffer then the output phase noise level will increase. A part of the amplitude fluctuations will also be present in the output signal, but they were not measured. R&S FSUP [80] is able to do phase noise measurements only.

It was shown in Fig. 5.4 that noise on the DC power supply of the XCO will increase the noise floor of the output signal.

Consider now a case where there is a small ripple at the DC power supply of an XCO. Any ripple that couples to the DC supply will show some effect on the output signal. The ripple can come from the input power source that drives the regulator. Due to the limited PSRR of the regulator and the difficulty in filtering ripple especially when it lies at relatively low frequencies, a part of

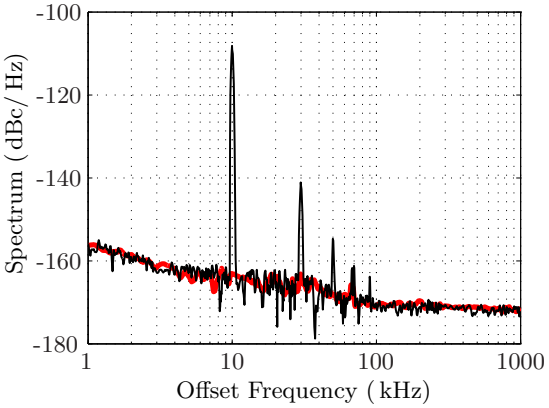

Fig. 5.11: SSB spectrum with 10 kHz triangular wave at 20 mVp-p added to the XCO power supply. The red curves shows the phase noise curve of the XCO without any ripple on DC supply.

the ripple can propagate to the output and can be fed to the components being supplied by the regulator. Power and ground couplings on a system board could also lead to ripple. Especially, the switching currents of output drivers of high-speed digital circuits can generate a significant amount of distortion in power and ground supply systems.

In this test, a 10 kHz at 20 mVp-p triangular signal is added to the power supply of an XCO using a circuit similar to Fig. 5.6. Figure 5.11 shows the measured SSB phase noise spectrum where the red curve is the output without any ripple on the power supply. The black curve shows that a ripple on the power supply would lead to spurs on the output of an XCO. The power supply ripple produces a spur at 10 kHz plus some additional harmonics. Note that the XCO was fed from a low noise DC power supply similar to that in Fig. 5.3. The ripple signal was added after the low noise power supply.

A very similar behavior is also observed if there is a ripple or noise on the power supply of a buffer.

5.2 Frequency Synthesizer Noise Analysis System

To study effects of noise on a frequency synthesizer, a new experimental setup shown in Fig. 5.12 was built. On the reference side of this setup an external

clock generator can be used through Ref In and a bandpass noise can be added to it. The resulting signal is passed through a high speed comparator that converts it into a square wave as required for the phase detector.

This is a less attractive approach, because usually signal generators have a higher amount of phase noise. The preferred approach is to use a crystal oscillator whose low noise power supply is provided through a DC filtering approach as demonstrated in Fig. 5.3. Using this method, it is also possible to investigate the effects of baseband DC supply noise as it was discussed in the previous sections.

After the reference, there is another bandpass noise addition point representing the noise of the reference. It is implemented by slowing down the rise time similar to what was shown in Fig. 5.7. The signal is then passed either directly to the phase detector or through the divider depending on whether PLL or synthesizer is being studied.

The output of the phase detector is filtered to eliminate higher frequencies. Baseband noise is added to the output of the phase detector before passing it to the control filter. After the control filter, there is another baseband noise addition point representing the additional noise coming from the control filter. It is added directly in front of the VCO.

Different VCOs exist, some producing a square wave signal and others produce a sinusoidal signal at their output. This signal is fed back either through a bandpass filter, or fed directly to the divider, bypassing the bandpass filter stage. The VCO signal passed through a bandpass filter is converted to an analog signal which facilitates in coupling noise. The amplitude noise (multiplicative baseband noise) is coupled through an amplitude modulator circuit implemented using a double-balanced mixer based on Mini-Circuits TUF-3 [83]. The additive bandpass noise is coupled using a configuration similar to Fig. 5.6, but by replacing the op-amp by a fast TTL/CMOS comparator, ADCMP601 [84]. The comparator works both as a noise adder and also converts the resulting signal into a square wave.

On the direct path from the VCO to the divider, additive noise can also be couple by slowing down the rise time. The signal after the VCO, goes either to the phase detector or to the loop divider depending on whether a PLL or a synthesizer are being considered.

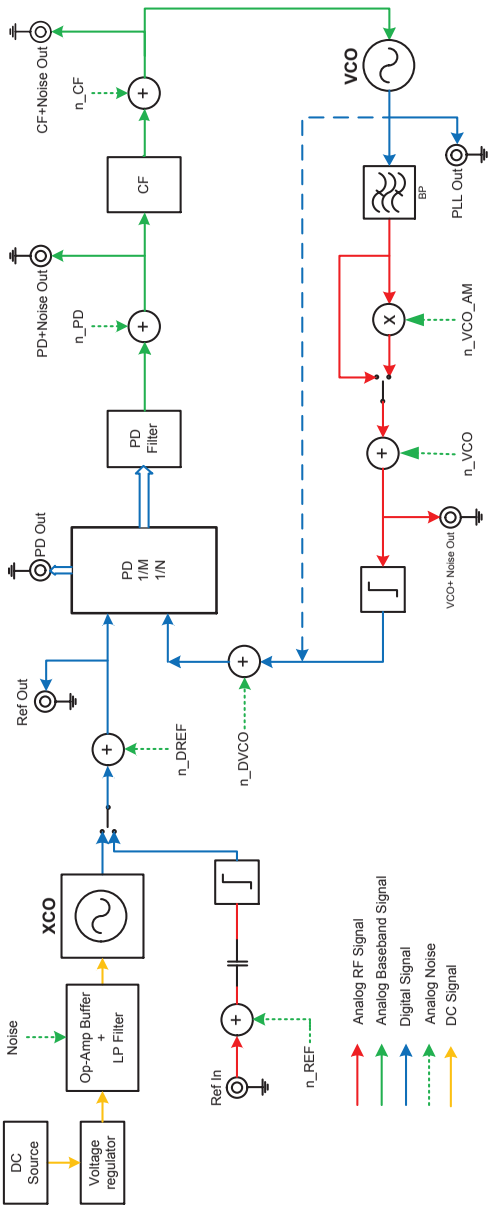

Fig. 5.12: Overview of the system used to experimentally study noise in a frequency synthesizer.

Figure 5.13 shows a photograph of the system that was constructed to study effects of noise. It is a very flexible system where five separate adapter boards are used for XCO, phase detector, control filter, VCO, and reference/feedback dividers. Using this technique, it is possible to build a large number of different integer-N and fractional-N setups.

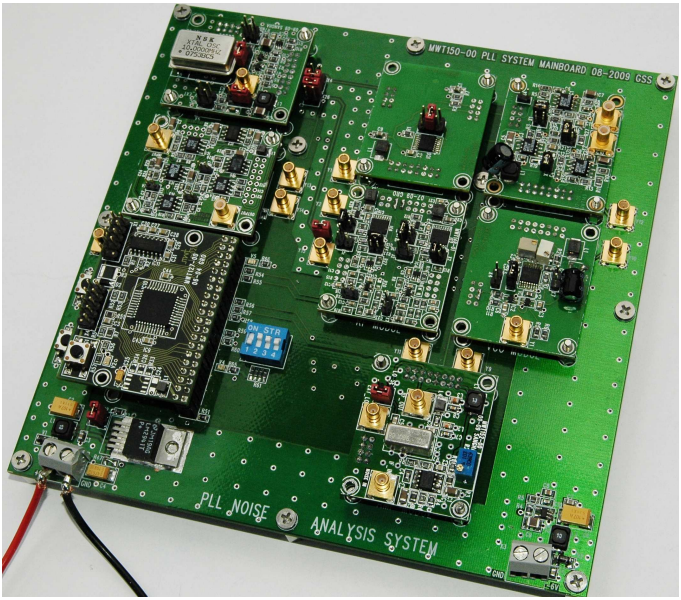

Fig. 5.13: Frequency synthesizer noise analysis system.

It facilitates in comparing the effects of using different control filters, dividers, phase detector, VCOs, and XCOs on the system noise behavior. There are three more plug-in board places, which are occupied by the multiplicative noise generator, $1/f$ noise source and a controller board that helps to program a synthesizer on the fly.

The multilayered main-board was constructed with paying special attention to routing of different signals and supply lines in order to minimize effect of coupling and noise. This setup was operated up to a frequency of around 100 MHz. It was not tested at higher frequencies. The RF signals from different adapter boards are routed either through coaxial cables or through board-to-board connectors.

The positive supply is designed around a low voltage drop regulator that can supply up to 1 A of current. Using this as a reference, low noise supply based on lowpass plus voltage follower circuit similar to what was discussed in Section 5.1.2 on page 71 is built locally for each of the adapter boards.

Two different PLL and synthesizer setups were developed running either at 10 MHz or at 65 MHz. The 10 MHz setup is based on the CMOS PLL chip SN74LV4046A from Texas Instruments [85]. This chip contains a VCO as well as three different types of phase detectors; an XOR PD a 3-state PD, and a PD based on RS Flip-Flop. As the PD and the VCO are built on separate adapter boards, two chips are used; one for VCO and the other for PD. Both active and passive control filters are implemented. Measurements are done using XOR and 3-state PD, as well as both active and passive filters. The results that will be shown here are only for the 3-state PD. There are four different PLL setups running at 10 MHz as shown below:

- with active filter without dividers,
- with passive filter without divider,
- with active filter employing a reference and a feedback divider with a fixed division ratio of 16,
- with passive filter employing a reference and a feedback divider with a fixed division ratio of 16.

This setup has the advantage that it gives access to all the different points in a PLL where noise can be added, but disadvantage is due to the fixed divider ratio.

A new setup running at 65 MHz was developed in order to further investigate effects of noise, and to have a possibility to use flexible divider ratios. In this setup the phase detector is implemented using Analog Devices ADF4002 chip [86]. This is a frequency synthesizer chip that could also operate as a standalone phase frequency detector (PFD) by setting the reference and feedback divider ratio to one. The VCO is implemented using a Maxim MAX2605 chip [87], and it is operated around a center frequency of 65 MHz.

With this setup, it is also possible to investigate effects of noise on both integer-N and fractional-N synthesizers. As mentioned before, the feedback and the reference dividers are implemented on the same adapter board. They are implemented on a separate board than the phase detector. The main difference between integer-N and fractional-N synthesizers is due to the feedback divider. The reference divider is a prescalar which is implemented in a similar way for the two synthesizers. Two different dividers sets, integer-N and fractional-N, each containing one reference and one feedback divider are implemented. The reference and the feedback divider are located on the same chip.

For the integer-N divider an Analog Devices ADF4002 [86] is used and for the $\Sigma-\Delta$ based fractional-N synthesizer an Analog Devices ADF4156 [88] is used. Note that both of these chips are pin compatible which facilitates the board design.

These newer boards give the flexibility of using variable dividers and possibility to compare fractional-N and integer-N synthesizer noise behaviors.

Due to the time constrains towards the end of my PhD contract, no detailed comparative, theoretical and practical, study of the noise behavior due to an integer-N and a fractional-N was possible.

5.3 Control Filter Design Considerations

It is preferable to use PLLs of a second order (first order control filter) with high loop gain due to the fact that they provide absolute stability [2]. In practice, higher order loop filter are used in order to increase the attenuation of the spurious signals like the carrier leakage and higher frequency harmonics due to non-linear effects [3]. Additional lowpass filter stages (higher frequency poles) would usually be added to the control filter forming a second or even third order loop filter. Higher order loop filters are rarely used because the phase margin is reduced with more poles [6]. Additional lowpass filter stages can be important, especially where the reference signal frequency is low, which can very often be the case in integer-N synthesizers. However, care should be taken that the behavior of the control filter shall dominate over that of the additional lowpass filter stages, so that the synthesizer can be approximated as a second order system. The cutoff frequencies of the lowpass filters should be much higher than the 3 dB cutoff frequency of the control filter.

Design considerations with respect to different parameters of a synthesizer natural angular frequency ω_n, damping factor ζ, and cutoff frequency of the additional lowpass filters ω_{LP} is discussed below:

- If the divider ratio is changed, the PLL should settle quickly to the new output frequency
  $\Longrightarrow$ choose $\zeta = 1/\sqrt{2}$ for fast settling
  $\Longrightarrow$ ω_n should be large
- The noise bandwidth of the PLL is proportional to ω_n
  $\Longrightarrow$ a good noise behavior is obtained for a small ω_n
- In the phase detector a lowpass filter is required to suppress higher frequency spectral components, as they deteriorate the spectrum of the VCO by modulation sidebands.

$\Longrightarrow$ The lower the cutoff frequency ω_{LP} of the lowpass the better the suppression. But it should also be considered that $\omega_{\mathrm{LP}} \gg \omega_n$, otherwise the influence of the lowpass on the PLL can not be neglected and the order of the PLL is raised.
$\Longrightarrow$ ω_{LP} should be small and hence ω_n should be small.

This discussion shows that in general there are contrary requirements when designing a synthesizer system. A trade-off between the different aspects is usually necessary.

In practice, one can encounter additional poles in the circuit due to some leakage impedances and time delay. The time delay is especially important to consider in modern digital systems. In most cases, the undesired poles will lie further away from the poles of the control filter so that the dominant behavior can still be taken to be of a second order system with a slightly reduction in damping factor ζ and phase margin. The stray elements can also lead to the reduction of the pull-in range of the system [3].

The calculation of the filter parameter was discussed in Section 3.5. It was also mentioned that the bandwidth of the PLL is usually taken to less than 10% of the sampling rate.

In this work a flexible control filter structure was built that not only allows to add noise before and after the control filter, but also allows to easily change from a PLL with an active filter to a PLL with a passive filter.

Figures 5.14 and 5.15 show the two parts of the schematics of the control filter used in this work. Both active and passive filters are constructed on the same PCB with the possibility to select one at a time. The operational amplifier TS922 [89] is a placeholder. In the actual circuit a faster op-amp from Analog Devices ADA4841-2 [90] which also has a better noise behavior is used.

Part I of the schematic in Fig. 5.14 shows the input to the control filter DIG_OUT_SIG_1. After the input there is a first order *RC* lowpass filter to filter out the higher frequency components of the PD signal. The baseband noise in front of the control filter is added through the BNC connector Y1. IC1-A acts as a buffer stage. IC1-B is used to add noise to the signal coming from the phase detector. Jumper X1 allows to select whether a PLL with an active or a passive filter is being considered. The combination of R15,R17 and C11 in the top branch forms a passive control filter. The active filter is built around IC3-A. Note that the resistor R21 is a placeholder and is not used in the actual control filter. R21 can be soldered if one needs to control the DC gain of the active control filter. Appendix A.3 shows the parameter calculation method and the Bode diagram for the active filter. The influence of R21 is also discussed there.

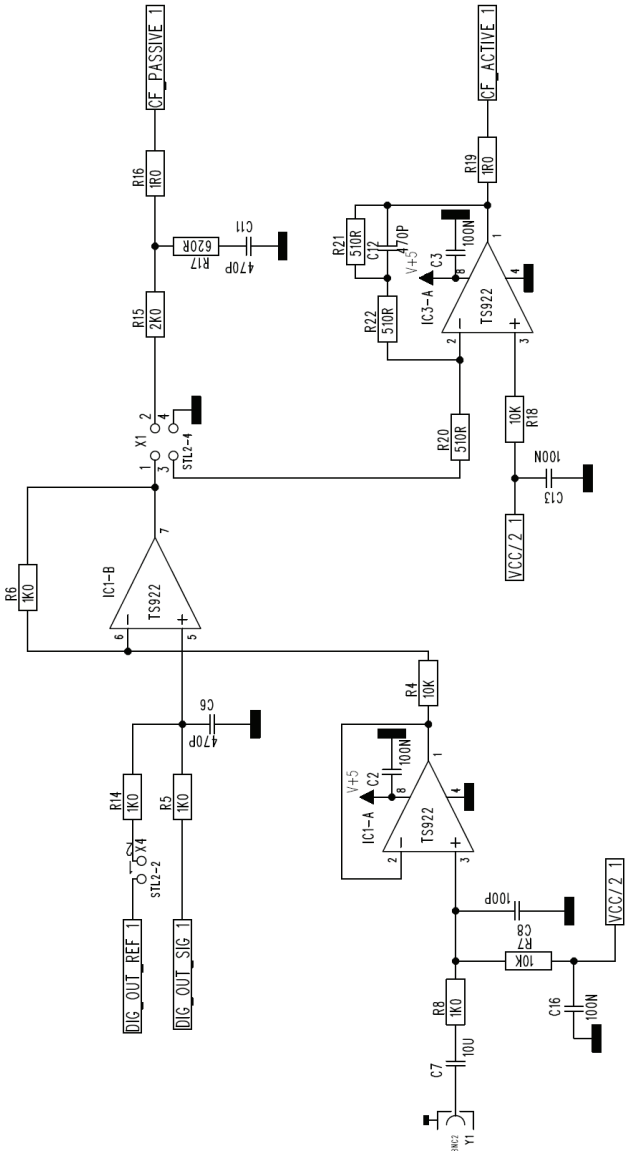

Fig. 5.14: Part I of the control filter schematic.

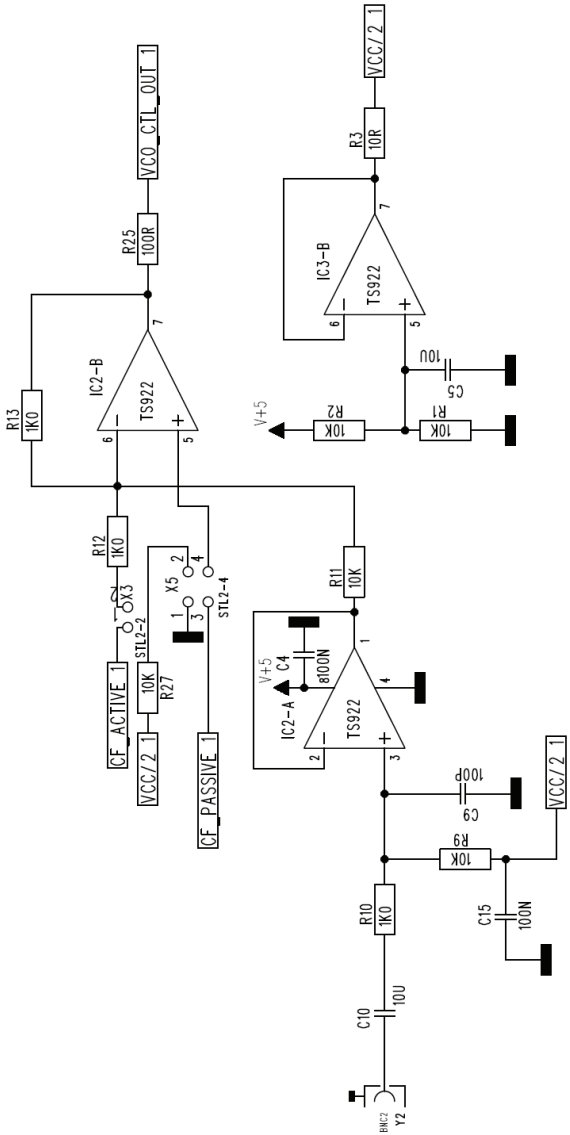

Fig. 5.15: Part II of the control filter schematic.

Part II of the schematic in Fig. 5.15 shows the output stage of the control filter. As discussed before, noise is added before and after the control filter. This schematic shows the noise addition at the output of the control filter. The baseband noise after the control filter is added through the BNC connector Y2. IC2-A acts as a buffer stage. IC2-B adds noise to the output of either an active or a passive control filter. X3 and X5 shown in Fig. 5.15 and X1 shown in Fig. 5.14 allow to select between a PLL with an active or PLL with a passive filter. IC3-B is used to generate a low noise reference voltage of half the supply which is needed in other parts of the circuit.

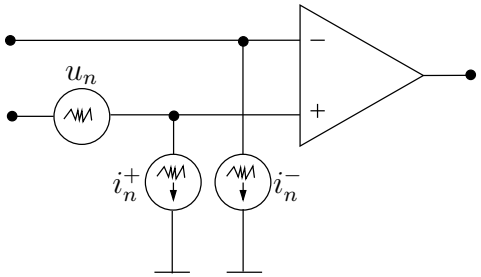

Fig. 5.16: Current and voltage noise sources of an operational amplifier.

Care should be taken when selecting components for building a control filter in order to lower the influence of noise. To reduce the thermal noise unnecessarily high resistor values should be avoided. It is crucial to select low noise amplifiers for the design of active control filters. Operational amplifier data sheets usually specify RMS values for current and voltage noise referred to the input using a standard op-amp noise model. Figure 5.16 shows the standard noise model for an op-amp which consists of two uncorrelated current noise sources and one voltage noise source connected to the op-amp inputs. The voltage noise source can be thought of as a time-varying input offset voltage component and the current noise sources as time-varying bias current components. Using the RMS noise values from the data sheet, [91] shows a method to determine the worst case peak-to-peak output noise of an op-amp for the most simple circuits taking into account the statistical properties of thermal, shot, and $^1/_f$ noise.

Total intrinsic noise of an active control filter whose circuit is shown in Fig. A.3 can be considered to be a sum of the following five components:

- thermal noise of feedback resistive network,
- voltage and current noise of the op-amp, which can be subdivided into

two components each:

- low frequency component (flicker or 1/f noise),
- broadband component (white noise).

5.4 Analysis of the Measurement Results and Comparison with Theory

In this section, noise measurement results of a PLL employing both active and passive control filters will be shown. Measurements are done for a system running at 10 MHz with and without dividers. Only the most important results for the 10 MHz system will be demonstrated.

A different set of active and passive control filters are designed for the case with dividers and the case without dividers. The active and passive filters are optimized using LTspice [92] in order to get a similar response. The value of the damping factor $\zeta = 1/\sqrt{2}$ is chosen. The natural frequency is set to be $f_n = 100\,\text{kHz}$ in the case where the PLL is running at 10 MHz without dividers in the loop. For the case where there are fixed dividers with division ratio of 16 in the feedback and reference path, the natural frequency is set to be $f_n = 30\,\text{kHz}$.

For the setup built around the SN74LV4046A CMOS PLL chip, the VCO tuning characteristic and sensitivity are measured using a tunable low noise DC supply from the R&S FSUP. From this measurement, the gain of the VCO was found to be $K_o = 4.57 \cdot 10^6\,\text{rad/Vs}$. The gain of the 3-state phase detector $K_D = 0.6\,\text{V/rad}$ was found by measuring the phase detector output characteristic curve with the help of a mechanical 360° phase shifter.

The measurements were done using the synthesizer system whose photograph is shown in Fig. 5.13. This system is built with optimizations to reduce distortion and coupling on the main-board as well as power supply noise. This plays a vital rule in reducing the noise floor of the system, which is important to be able to add weak external noise sources. Otherwise, the noise floor of the source could lie below the system noise floor.

The state of the art noise measurement device, R&S FSUP Signal Source Analyzer [80], was used for the phase noise measurements.

Figure 5.17 shows the phase noise measurement results for the case where PLL is operated without dividers and without any additional noise sources. The x-axis in this graph shows that the measurement performed from an offset frequency of 1 kHz to 1 MHz from the center. The y-axis gives the single side band (SSB) spectrum of phase noise measured in dBc/ Hz.

The black curves show free running VCO. The red curve shows the phase noise of the system when an active control filter is used. The blue curve gives

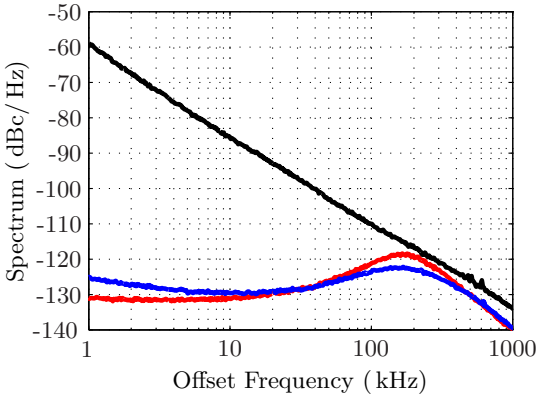

Fig. 5.17: SSB spectrum showing the free running VCO versus the PLL output. The black curve is for the free running VCO, the blue curve is the PLL with a passive filter and red curve is for the PLL with an active filter.

the phase noise behavior of the PLL with a passive control filter in the loop. Inside the loop bandwidth of the two PLLs, the noise of the VCO is reduced. Outside the PLL bandwidth, the phase noise curves of the PLLs follow closely the curve of the free running VCO. As a reference, an XCO employing a low noise DC power supply was used. The SSB phase noise spectrum for this XCO with a low noise supply is shown by the black curve in Fig. 5.4.

It can be observed that near to the center frequency, the active filter, due to its very high DC gain, is able to suppress noise better than the passive filter. The phase noise response of the passive filter shown by the blue curve indicates that from an offset frequency of 1 kHz to around 5 kHz, the curve is going down approximately by $1/\sqrt{f}$. The measurements done on the XCO alone in Fig. 5.4 shows that the XCO's internal noise has $1/\sqrt{f}$ behavior in this region. As expected, the PLL acts as a lowpass filter with respect to the reference phase noise. The noise of the reference attains its spectral shape at the output of the PLL system. Note that the PLL with active filter also exhibits similar behavior but the corner frequency for the $1/\sqrt{f}$ noise behavior lies below the 1 kHz offset point.

Figure 5.18 shows the phase noise plot for the same PLL with the active filter, whose output without additional noise was shown in Fig. 5.17. The curve in red is the SSB output phase noise spectrum without additional noise. The curves

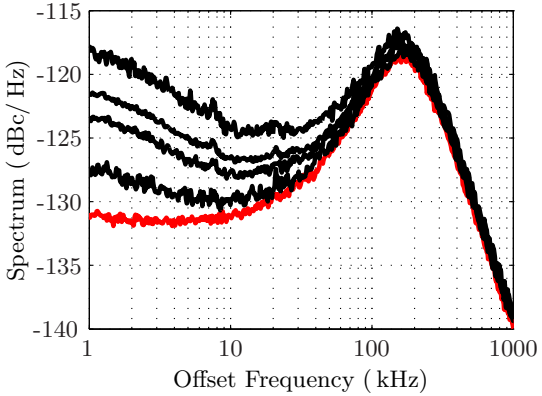

Fig. 5.18: SSB spectrum showing the effect of baseband filtered white noise added to XCO low noise power supply. The red curve is the system phase noise spectrum without additional noise. The black curves shows the phase noise response of the PLL when noise on the power supply is increased in steps.

in black show the SSB output spectrum where lowpass filtered white noise with cutoff of 1.28 MHz is inserted to the XCO power supply. The low noise power supply discussed before is used for the XCO. The noise is added after the low noise supply. A white noise signal is generated with the help of Tektronix AFG3102 Dual Channel Arbitrary/Function Generator [93]. This device has a built-in wide band white noise source that can produce a flat spectrum up to around 100 MHz. The noise level was varied starting from 1 V peak-to-peak up to 4 V peak-to-peak in steps of 1 V.

The curves show the importance of low noise supply for system components like XCOs, VCOs, PDs, and dividers. The higher the noise of the power supply, the more phase noise will appear on the output of the PLL. As discussed before, the XCO is internally generating $1/\sqrt{f}$ noise. Increasing power of white noise coupled to the DC source, increases the level of the $1/\sqrt{f}$ noise produced by XCO at its output. It was mentioned in the discussion about Fig. 5.17, that due to the high DC gain of an active filter the $1/\sqrt{f}$ cutoff is located further towards the center frequency than in the case of a passive filter. From Fig. 5.18 it becomes evident that as the XCO supply noise increases, the active filter will not be able to keep the noise at same level as before. The XCO $1/\sqrt{f}$ noise cutoff frequency

will cover a larger band as the noise floor of the XCO is higher due to stronger DC noise.

In the next sections experimental results of noise insertion inside the PLL will be shown. A comparative study of the simulations and the measurements will be performed also.

5.4.1 Noise Added to the Reference Signal

Figure 5.19 shows the SSB phase noise spectrum for a PLL with an active control filter in the loop. The red curve is used as reference and shows the SSB phase noise spectrum for the same PLL without additional noise. The black curves show the response of the system when additional noise is added to the noise addition point n_DREF after the XCO as shown in Fig. 5.12. The output of the XCO is a rectangular signal. A circuit similar to the one that was discussed in Fig. 5.7 on page 75 is used in order to add noise by filtering out the higher harmonics and thus slowing down the rise time of the signal. Bandpass white noise with a center frequency at 10.7 MHz and extending from around 9.5 MHz to around 11.5 MHz is added to the output of the XCO. The noise level is increased in steps of 200 mV starting from a peak-to-peak value of 200 mV up to 800 mV. The black curves in Fig. 5.19 show that increasing the white noise level shifts the noise floor of the system in the upward direction.

In order to interpret the results, (3.3.1) on page 40 can be used in order to find a transfer function relating a PLL output phase angle with the phase noise source $n_i(t)$ added after the reference signal:

$$\Theta_o(s) = \frac{K_D K_o(s\tau_2 + 1)}{\tau_1 s^2 + (b + K_D K_o \tau_2)\, s + K_D K_o} n_i(s)\,. \tag{5.4.1}$$

This is a transfer function of a second order lowpass filter relating the PLL output phase angle to the reference phase noise. Figure 5.19 shows that a bandpass noise at the reference source forms a lowpass characteristic on the synthesizer output. In this equation the factor b defines the type of control filter. With b=0 gives a PLL with an active control filter, and b=1 indicates a PLL with a passive loop filter. It can be seen that the response of the system does not change if an active or a passive filter is used.

In Fig. 4.1 on page 59, a simulation curve was shown were a bandpass noise source was added after the reference source. Comparing the simulated curve with the measurements in Fig. 5.19 show that the theoretical and practical results agree. Both results show that the response of the system to a bandpass noise after the XCO gives a lowpass characteristic curve at the output.

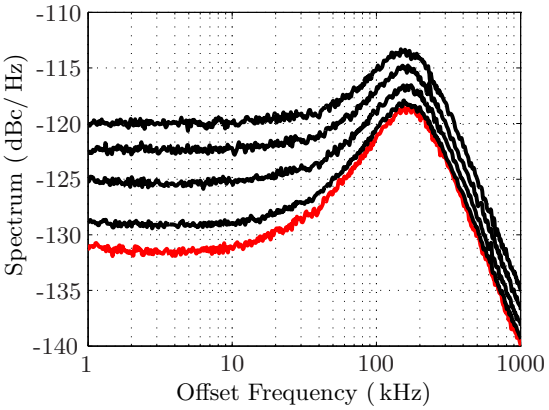

Fig. 5.19: SSB spectrum with bandpass white noise added after the XCO in a PLL using an active control filter. The red curve gives the phase noise response without additional noise. The black curves show that system noise floor goes higher as strong noise is added.

5.4.2 Noise Added to the Phase Detector Output

Fig. 5.20 gives the SSB phase noise measurement spectrum for a PLL with an active control filter, where baseband white noise is added after the phase detector at noise addition point n_PD shown in Fig. 5.12 on page 81. At the output of the phase detector, a lowpass filter is placed before the control filter in order to filter out the high frequencies. For the 10 MHz system, the cutoff frequency of this filter is placed at around 5 MHz. Noise is added between the lowpass filter and the control filter using an op-amp noise adder circuit similar to that in Fig. 5.6.

The red curve in Fig. 5.20 is the phase noise response of the PLL with active filter without additional noise. The black curves shows the system phase noise response as noise is increased. The white noise source is passed through a lowpass filter having a cutoff frequency at 1.28 MHz. The noise level is increased in steps of 200 mV starting at a peak-to-peak value of 200 mV and up to 800 mV. The PLL output noise floor goes higher as strong noise is added after the phase detector. Using (3.3.1), a transfer function relating the PLL output phase with

the noise source $n_{PD}(s)$ added after the phase detector can be derived:

$$\Theta_o(s) = \frac{K_o(s\tau_2 + 1)}{\tau_1 s^2 + (b + K_D K_o \tau_2)\, s + K_D K_o} n_{PD}(s)\,. \tag{5.4.2}$$

This is a transfer function of a second order lowpass filter. Similar to the case where bandpass noise was added after the XCO as shown in (5.4.1), this transfer function shows that the baseband noise source added after the phase detector results also in a lowpass phase response from the PLL. The only difference in response is the absence of the phase detector gain factor K_D from (5.4.2) compared to (5.4.1). Again the transfer function is independent of whether an active or a passive filter is used in the synthesizer.

Comparing the measurement results from Fig. 5.20 with simulation results in Fig. 4.2 shows that the theoretical and measurement results agree. The noise added after the phase detector in both cases forms a lowpass characteristic with respect to the synthesizer output.

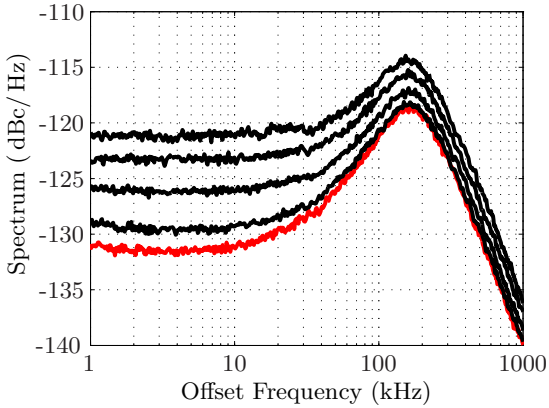

Fig. 5.20: SSB phase spectrum with baseband white noise added after the PD where an active control filter is used. The red curve is the case where no additional noise is added. The black curves show that the noise floor of the system goes higher as stronger noise is added to the PD.

5.4.3 Noise Added to the Control Filter Output

In order to analyzed the influence of noise from a control filter on the output of a PLL, (3.3.1) can be used to derive a transfer function relating the noise source $n_{CF}(s)$ to the PLL output phase angle:

$$\Theta_o(s) = \frac{K_o(s\tau_1 + b)}{\tau_1 s^2 + (b + K_D K_o \tau_2)\, s + K_D K_o} n_{CF}(s)\,. \tag{5.4.3}$$

The transfer function depends on the control filter parameter b. For the case where b=1, the transfer function is that of a second order lowpass filter. For the case where b=0, the transfer function is that of a second order bandpass filter. This implies that depending on whether an active or a passive control filter is used in the loop, the noise source in front of the VCO will either result in a bandpass or a lowpass characteristic at the output of a PLL.

The measurement results for both PLLs containing an active and a passive control filter will be shown next. In both cased, a baseband white noise source filtered with a lowpass filter having a cutoff frequency of 1.28 MHz is added after the control filter at noise addition point n_CF shown in Fig. 5.12 using an op-amp noise adder circuit. The peak-to-peak voltage noise levels used for these measurements are varied from 200 mV to 800 mV in steps of 200 mV.

Figure 5.21 shows the response of the PLL when a baseband white noise is added to the output of an active control filter. The red curve shows the phase noise response of the system without additional noise. Adding strong noise makes the bandpass noise floor of the system higher as shown by the black curves. Comparing the output spectrum with the simulation results where noise is added to an active filter as shown in Fig. 4.4, depicts that the theoretical and measurement results agree. In both cases the response of a PLL to noise after the active control filter is that of a bandpass type.

Fig. 5.22 shows the response of a PLL where a baseband white noise is added to the output of a passive control filter. The red curve is again the system response without additional noise. The black curves show the increase in the system noise floor as noise power is increased. The measurement results and the simulation results from Fig. 4.3 shows that the PLL has a lowpass response when a baseband noise is added to the control filter output.

From Fig. 5.22, it can be observed that adding white noise at the passive control filter output shifts the whole system noise floor upwards. As discussed in a previous section, the $1/\sqrt{f}$ noise behavior due to the XCO can be observed up to a frequency offset of approximately 5 kHz from the center frequency.

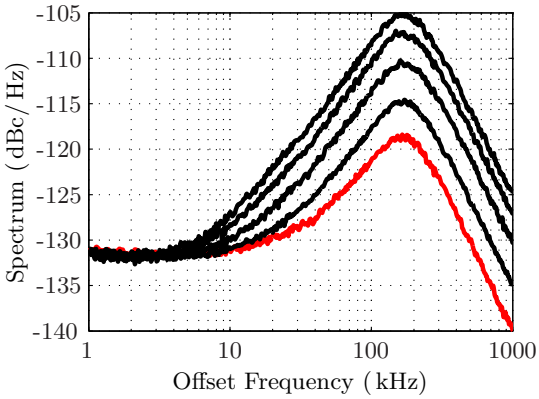

Fig. 5.21: SSB noise spectrum with baseband white noise added after an active CF. The red curve is the PLL noise floor without additional noise. The black curves show that stronger noise at the CF output results in a higher bandpass-shaped noise floor of the system.

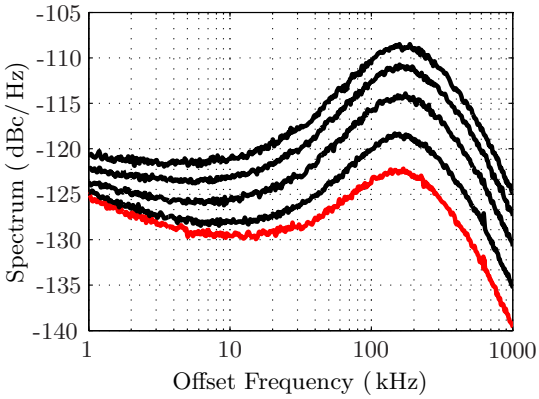

Fig. 5.22: SSB noise spectrum with baseband white noise added after a passive CF. The red curve is the PLL noise floor without additional noise. The black curves show that stronger noise at the CF output results in a higher lowpass-shaped noise floor of the system.

5.4.4 Noise Added to the VCO Power Supply

The phase noise injected after the VCO is studied in two different ways. In this section, the influence on the PLL of a noise source in the forward path after the VCO, representing the internal noise of the VCO, will be shown. In the next section, the influence of the noise coming after the VCO in the feedback path of the system will be demonstrated. Depending on where the noise is added after the VCO, the response of the system will be different.

The transfer function relating the bandpass phase noise source $n_{vp}(t)$ placed directly after the VCO in forward path standing for the internal noise of the VCO is derived from (3.3.1) as follows:

$$\Theta_o(s) = \frac{s(s\tau_1 + b)}{\tau_1 s^2 + (b + K_D K_o \tau_2)\, s + K_D K_o} n_{vp}(s)\,. \tag{5.4.4}$$

As expected, the PLL acts as a second order highpass filter with respect to the internal noise of the VCO.

In order to demonstrate this experimentally, a lowpass filtered white noise with a cutoff frequency of 1.28 MHz and a peak-to-peak level of 3 V is added to the power supply of the VCO. The black curve in Fig. 5.23 shows the highpass system response to this noise source. The red curve serves as reference and shows the system noise floor without additional noise. The results obtained here are in agreement to the simulation results from Fig. 4.5 where bandpass white noise was added directly after the VCO in the forward path.

5.4.5 Noise Added to the VCO Output in the Feedback Path

In order to demonstrate the influence of noise coupled into the feedback path on the output of the synthesizer, a bandpass filter was placed on the feedback as shown in the system block diagram in Fig. 5.12 and noise was added after it at the noise insertion point n_VCO. Noise is added after this filter by using a fast TTL/CMOS comparator. The purpose of the bandpass is to convert the square wave signal into analog signal so that noise can be coupled. As it was mentioned before, the output of the 10 MHz VCO is a square wave signal.

In order to explain the system response to the noise source in the feedback path, the transfer function relating noise in the feedback path $n_N(t)$ to the output of the PLL can be derived from the results found in (3.3.1):

$$\Theta_o(s) = -\frac{K_D K_o (s\tau_2 + 1)}{\tau_1 s^2 + (b + K_D K_o \tau_2)\, s + K_D K_o} n_N(s)\,. \tag{5.4.5}$$

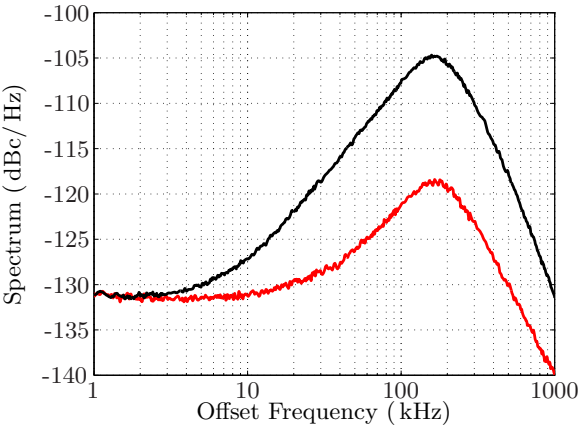

Fig. 5.23: SSB phase noise spectrum for a PLL with active control filter where baseband white noise is added to the power supply of the VCO. The red curve is the output without additional noise. The black curve shows the system highpass response to the power supply noise.

The system here exhibits a lowpass characteristic, similar to the case where noise is added after the reference and after the PD shown by transfer functions (5.4.1) and (5.4.2), respectively. The only difference between (5.4.5) and the transfer function of the reference is the negative sign.

Note that in the case where a synthesizer is being considered, difference between transfer functions relating feedback noise to the output and the transfer function relating reference noise to the output would be constant factors $-N$ and N/M, respectively.

In order to investigate the noise addition to the feedback path experimentally, bandpass white noise with a center at 10.7 MHz and bandwidth extending from 9.5 MHz to 11.5 MHz is added in the feedback path after the VCO at the point n_VCO in Fig. 5.12. The peak-to-peak noise levels used for this experiment are 50 mV, 100 mV, 200 mV and 400 mV.

Figure 5.24 shows the measurement results where an active control filter is used. Note that the active and passive filter in this case have similar response, as expected from the theory. The red curve is the phase noise response without any additional noise. The black curves show the lowpass response of the system as strong noise is added. As expected, the system noise floor goes higher as

stronger noise is added.

The results obtained here are similar to the results of adding noise after the loop divider as both of these sources are inserted into the feedback path of the system as also shown by the simulation curve in Fig. 4.7. In the case of a loop divider, the phase noise coming from the source before the divider will be divided by a factor of $^1/_N$ before appearing at the phase detector compared to the source that lies after the divider.

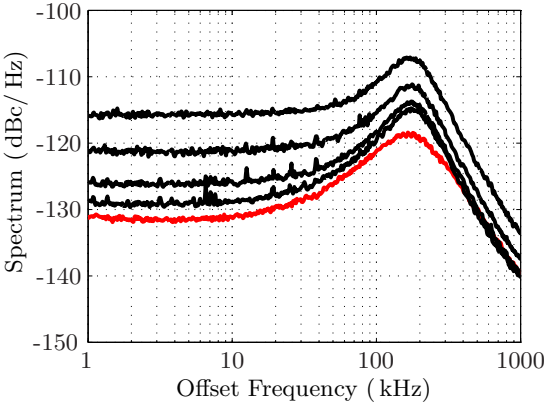

Fig. 5.24: SSB phase noise spectrum for a PLL with active control filter where bandpass white noise is added to the VCO output in the feedback path. The red curve is the output without additional noise. The black curves show that adding strong noise to the feedback path makes the system's lowpass-shaped noise floor go higher.

5.4.6 Noise Multiplied to the VCO Output

In order to study effects of amplitude fluctuations of the VCO on the synthesizer, an amplitude modulator circuit is built into the loop as shown in Fig. 5.12 through the noise insertion point n_VCO_AM. The output of the VCO is bandpass filtered and the resulting signal is passed through an amplitude modulator circuit built around a double balanced mixer on an extra adapter board in the noise analysis system shown in Fig. 5.13. Using this technique, the output of the VCO is multiplied by a baseband white noise filter with a lowpass having

a cutoff frequency of 1.28 MHz. The peak-to-peak noise voltage levels used for this measurement start from 1 V to 4 V with a step of 1 V.

Figure 5.25 shows the measurement result where an active filter was used in the PLL. The red curve is the system phase noise response without additional noise. The black curves show how the system noise floor goes higher as stronger noise is multiplied to the VCO output.

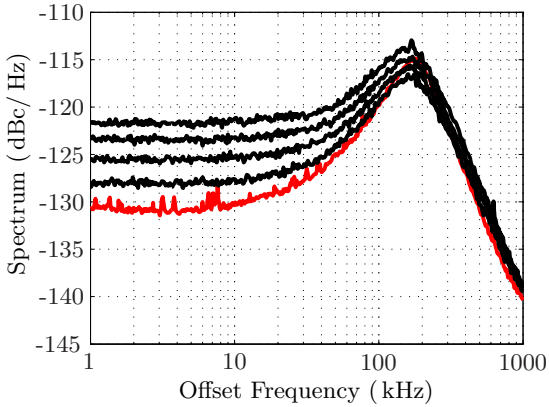

Fig. 5.25: SSB phase noise spectrum of a PLL with an active control filter where a baseband white noise is multiplied to the VCO output. The red curve is the system output without additional noise. The black curves show that the phase noise floor of the system goes higher as strong noise is multiplied.

In order to explain the results, (3.3.1) can be used to derive the influence of amplitude fluctuations of the VCO on the output phase of a synthesizer:

$$\Theta_o(s) = \frac{K_o K_{RN}(s\tau_2 + 1)}{\tau_1 s^2 + (b + K_D K_o \tau_2)\, s + K_D K_o} \left(R_N(s) - \frac{R_{N0}}{s} \right) . \qquad (5.4.6)$$

This is a transfer function of a second order lowpass filter. This transfer function is the same as the PLL transfer function, which relates the input phase to the output phase, except for the scaling factor is K_{RN}/K_D.

These measurement results prove the theory and shows that inside the PLL system a part of the amplitude noise is converted into phase noise. Figure 5.25 shows the phase noise measurements done with R&S FSUP. The measurement curves show that increasing the amplitude noise at the output of the VCO results in higher phase noise floor of the PLL system.

The simulations in Fig. 4.6 are in agreement with the measurement results. Both show that the amplitude fluctuations result in a lowpass phase noise characteristic at the output of a PLL.

5.4.7 Comparing the Noise Floor of a PLL and a Frequency Synthesizer

A PLL-based frequency synthesizer system employing an active control filter and having a fixed divider with a division ratio of 16 for both the loop and the reference dividers is used for the measurements. A 10 MHz reference signal will be running at 625 kHz after the reference divider. The output frequency of the system is at 10 MHz, since a prescalar with division ratio of 16 is used in the feedback path.

Due to the reduced reference frequency of 625 kHz, a new control filter having a characteristic similar to the system running at 10 MHz is used. The filter is designed for a synthesizer system bandwidth of 30 kHz instead of the 100 kHz system bandwidth in the case where the frequency at the phase detector was at 10 MHz.

Figure 5.26 shows the measurement results where an active control filter is employed. The measurements are done without any additional noise. The red curve shows the phase noise response for the system with an active control filter where no dividers are used and the frequency at the phase detector is 10 MHz. The black curves shows the system with an active control filter where dividers with fixed division ration of 16 are used in reference and feedback path so that the frequency at the phase detector is 625 kHz.

The black curve shows that the system with a loop divider gives a $20\log(N)$ dB increase in the noise floor compared to the red curve that shows the system without feedback divider. The system with feedback divider has a worse system noise behavior than the system without a feedback divider. The noise floor of the system is shift up by the divider.

This is a general fact and something that a designer have to care for when designing synthesizer systems. This curve shows the importance of using low noise components in the system and the importance of reducing coupling and supply noise on the system board. In many cases, even for systems producing output frequency in the Gigahertz range, the basic PLL would be running in some hundred Megahertz range. This is most often due to the limitations on the PFD (phase frequency detector) operation frequency. In these systems, the higher output frequency is produced by using a high feedback division factor. Additionally, mixers would also be used after the synthesizer to raise the system frequency to the desired value. In systems where a very high frequency has to

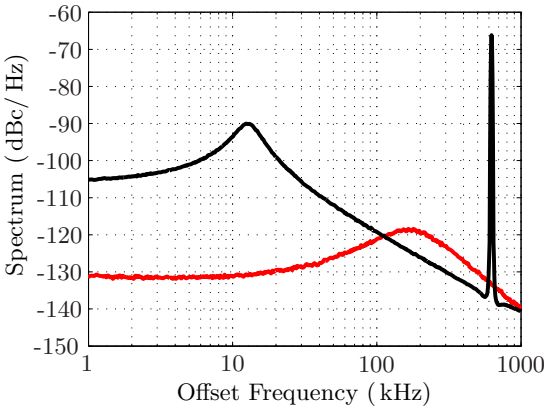

Fig. 5.26: SSB noise spectrum for a synthesizer with an active filter showing a $20\log(N)$ dB increase in the noise floor with the black curve where there is a divider with division ratio of 16 in feedback compared to the red curve where there is no divider in the loop.

be generated at the output of the synthesizer, care should be taken that the basic noise floor of the PLL used in the synthesizer system is low enough so that the output which would have $20\log(N)$ dB higher noise is still within the required design specifications.

In Fig. 5.26, there is a spur at 625 kHz. This is due to the fact that the first order *RC* lowpass placed between the phase detector and the control filter has not a sufficient attenuation. A second order lowpass filter would be more adequate.

6 Conclusion

This works deals with noise analysis of a PLL-based frequency synthesizer circuit considering a complex combination of intrinsic and extrinsic noise sources. The new analysis methodologies shown in this work lead to a deeper understanding of the complex noise phenomena affecting the output of the synthesizer. It shows how each point in the synthesizer circuit is contributing to the overall noise behavior. It gives deeper insight that can help in fine tuning the synthesizer circuit to reduce the total noise which appears in the output spectrum of the PLL signal.

A complete set of analysis techniques starting from new theoretical modeling to simulations and to new experimental methods for analyzing noise in a PLL-based frequency synthesizer system were developed.

In addition to the use of the non-standard Rice's noise model for modeling the noise sources mathematically, new and improved models for the phase detector and for the frequency divider were presented. These new models help to demonstrate the effects of amplitude fluctuations at the output of a synthesizer. Additionally, effects of sampling and delay were also considered in the modeling.

This mathematical setup led to the derivation of a very general mathematical description for the output voltage, as well as for the output average power while taking into consideration noise sources at different points in the circuit. This setup helps to study effects of different types of noise sources in the loop.

A new simulation set was built and a new experimental method was found in order to study effects of noise. The simulations are in agreement with the measurements. Both of these show how the noise from different components affects the output of the system. It was shown using simulations and experiments, that the amplitude noise is converted into phase noise at the output of the system. Furthermore, the importance of having low noise and low ripple power supply in the synthesizer was demonstrated. The noise from the DC power supply leads to a higher phase noise floor of the system, and the ripple on DC leads to spurs in the output.

Some other setups were also developed but were not included due to limited time and are left for future works. These includes the study of noise behavior of a fractional-N synthesizer. Some measurements were performed in a Diplom Thesis [94] supervised by the author. These indicated that the noise behavior is

similar to that of an integer-N synthesizer except for the existence of fractional spurs.

An experimental study of effects of $^1/_f$ noise on the system can also be done. A $^1/_f$ noise source based on OPA301 [62] was built and the initial analysis, not shown here, indicated that it gives a different influence on the output than the white noise source.

Furthermore, a 5-state frequency phase detector having a linear region extending from $(-4\pi,4\pi)$ was built and tested. It can be used in a synthesizer circuit to study the behavior of the system.

A low noise oscillator using a SAW-resonator and running at 433 MHz was also built [95]. This oscillator has a better noise floor than a general purpose XCO and it can be considered in future as an alternative reference source for a synthesizer to investigate the noise behavior.

A Mathematical Treatments

A.1 Linearization Technique for the Non-ideal Limiter

Figure A.1 shows a piecewise linear approximation of a non-ideal limiter. This section presents a complete derivation procedure for the output signal taking in account a sinusoidal signal at the input of a piecewise linear limiter circuit:

$$y(t) = f(x(t)) = \begin{cases} b & \text{if} \quad x(t) \geq a \\ mx(t) & \text{if} \quad -a < x(t) < a \\ -b & \text{if} \quad x(t) \leq -a\,, \end{cases} \tag{A.1.1}$$

where $m{=}\dfrac{b}{a}$ is the slope of the linear part and the parameters a and b describe the x-y-axis amplitude limiting factors. Given is the following sinusoidal signal at the input:

$$x(t) = A(t)\cos(\omega_c t + \phi(t) + \phi_c)\,, \tag{A.1.2}$$

where $\phi(t)$ is a random process uniformly distributed in the interval $[0, 2\pi)$. The output signal of this limiter can be derived by application of the Fourier series method with respect to the phase. But in order to accomplish this, the time has to be fixed at $t{=}t_0$:

$$\begin{aligned} x(t_0) &= A(t_0)\cos(\omega_c t_0 + \phi(t_0) + \phi_c)\,, \\ x_t &= A_t \cos(\alpha_t)\,, \end{aligned} \tag{A.1.3}$$

where $A_t{=}A(t_0)$ and $\alpha_t{=}\omega_c t_0{+}\phi(t_0){+}\phi_c$. After fixing the time α_t becomes a random variable uniformly distributed in the interval $[0, 2\pi)$. Equation (A.1.3) represents a harmonic signal that can be described using Fourier series. Cosine is an even function which implies that $b_k{=}0$ and only the coefficients a_k need to be determined:

$$f(A_t\cos(\alpha_t)) = \frac{a_0}{2} + \sum_k a_k \cos(k\alpha_t)\,, \tag{A.1.4}$$

$$\text{where} \qquad a_k = \frac{1}{\pi}\int_0^{2\pi} f(A_t\cos(\alpha_t))\cos(k\alpha_t)\mathrm{d}\alpha_t\,. \tag{A.1.5}$$

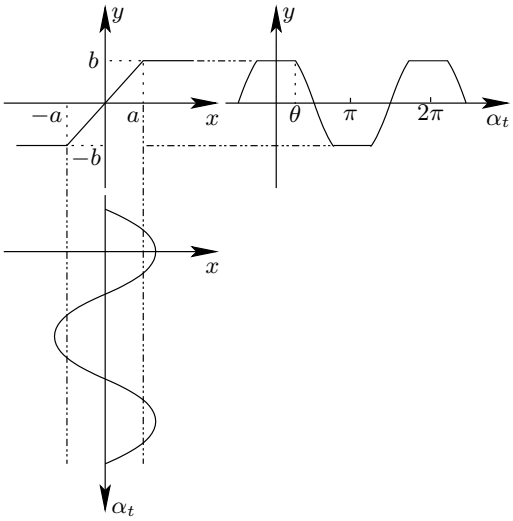

Fig. A.1: Characteristic curve for a piecewise linear limiter.

As shown in Fig. A.1, θ is the conduction angle. This corresponds to the point where the piecewise linear limiter function has a value of $x{=}a$ and $y{=}b$. An expression for the angle θ in terms of input and output can be derived. The conduction angle θ in terms of input signal is:

$$\begin{aligned} x_t(\alpha_t) = A_t \cos(\alpha_t) \quad &\Rightarrow \quad x_t(\theta) = A_L \cos(\theta) = a\,, \\ \Rightarrow \theta = \arccos\left(\frac{a}{A_L}\right) + 2k\pi \quad &\text{with} \quad \left|\frac{a}{A_L}\right| \leq 1\,, \end{aligned} \tag{A.1.6}$$

where A_L is the limiting amplitude value of the input signal. The conduction angle in terms of output is:

$$\begin{aligned} y_t = m x_t \quad &\text{with} \quad x_t = a = A_L \cos(\theta)\,, \\ \Rightarrow y_t = m A_L \cos(\theta) &= b\,, \\ \Rightarrow \theta = \arccos\left(\frac{b}{m A_L}\right) + 2k\pi \quad &\text{with} \quad \left|\frac{b}{m A_L}\right| \leq 1\,. \end{aligned} \tag{A.1.7}$$

Having found the conduction angle θ, the coefficients a_k of the Fourier series

can be derived as:

$$\begin{aligned} a_k &= \frac{1}{\pi}\int_0^{2\pi} f(A_t\cos(\alpha_t))\cos(k\alpha_t)\mathrm{d}\alpha_t \\ &= \frac{1}{\pi}\int_0^{\theta} b\cos(k\alpha_t)\mathrm{d}\alpha_t + \frac{1}{\pi}\int_{\theta}^{\pi-\theta} mA_t\cos(\alpha_t)\cos(k\alpha_t)\mathrm{d}\alpha_t \\ &- \frac{1}{\pi}\int_{\pi-\theta}^{\pi+\theta} b\cos(k\alpha_t)\mathrm{d}\alpha_t + \frac{1}{\pi}\int_{\pi+\theta}^{2\pi-\theta} mA_t\cos(\alpha_t)\cos(k\alpha_t)\mathrm{d}\alpha_t \\ &+ \frac{1}{\pi}\int_{2\pi-\theta}^{2\pi} b\cos(k\alpha_t)\mathrm{d}\alpha_t\,. \end{aligned} \tag{A.1.8}$$

The integral above can be solved to find the coefficients a_k:

$$\begin{aligned} a_k =& \frac{b}{k\pi}\{\sin[k\theta]+\sin[k(\pi-\theta)]-\sin[k(\pi+\theta)]-\sin[k(2\pi-\theta)]\} \\ &+\frac{mA_t}{2\pi(k+1)}\{-\sin[(k+1)\theta]+\sin[(k+1)(\pi-\theta)] \\ &\qquad -\sin[(k+1)(\pi+\theta)]+\sin[(k+1)(2\pi-\theta)]\} \\ &+\frac{mA_t}{2\pi(k-1)}\{-\sin[(k-1)\theta]+\sin[(k-1)(\pi-\theta)] \\ &\qquad -\sin[(k-1)(\pi+\theta)]+\sin[(k-1)(2\pi-\theta)]\}\,. \end{aligned} \tag{A.1.9}$$

It can be proved that a_0=0.
After the Fourier series with respect to random phase α_t has been derived by fixing the time, now the time can be allowed to vary again resulting in:

$$f\left(A(t)\cos(\omega_c t+\phi(t)+\phi_c)\right) = \sum_k a_k\cos(k\omega_c t + k\phi(t) + k\phi_c)\,, \tag{A.1.10}$$

where the coefficients a_k are now time-dependent:

$$\begin{aligned} a_k =& \frac{b}{k\pi}\{\sin[k\theta]+\sin[k(\pi-\theta)]-\sin[k(\pi+\theta)]-\sin[k(2\pi-\theta)]\} \\ &+\frac{mA(t)}{2\pi(k+1)}\{-\sin[(k+1)\theta]+\sin[(k+1)(\pi-\theta)] \end{aligned}$$

$$-\sin[(k+1)(\pi+\theta)]+\sin[(k+1)(2\pi-\theta)]\}$$

$$+\frac{mA(t)}{2\pi(k-1)}\{-\sin[(k-1)\theta]+\sin[(k-1)(\pi-\theta)]$$

$$-\sin[(k-1)(\pi+\theta)]+\sin[(k-1)(2\pi-\theta)]\}\,. \qquad \text{(A.1.11)}$$

The output consists of a sum of infinitely many harmonic components. If the output is passed though a bandpass filter centered around the angular frequency ω_c, i.e when k=1, then, the output signal can be described as:

$$y_{\text{out}} = a_1 \cos(\omega_c t + \phi(t) + \phi_c)\,, \qquad \text{(A.1.12)}$$

where the amplitude term a_1 is defined as:

$$a_1 = \frac{4b}{\pi}\sin(\theta) - \frac{mA(t)}{\pi}\sin(2\theta) + \frac{mA(t)}{\pi}(\pi - 2\theta)\,,$$

and the conduction angle θ is:

$$\theta = \arccos\left(\frac{b}{mA_L}\right) + 2k\pi\,.$$

The above equations show that a part of the amplitude fluctuations $A(t)$ will pass through the limiter circuit when the rise time is finite. It also shows that the phase noise term $\phi(t)$ is passed unsuppressed through the limiter.

Note that when $a \to 0$ which is equivalent to say that the conduction angle $\theta \to \pi/2$, this model gives results that are in agreement with the ideal limiter model [49], i.e. $a_1 = 4b/\pi$.

A.2 Second Order Frequency Synthesizer Transfer Function Taking into Account Delay, Noise, and Non-ideal Limiter

The derivation procedure for the transfer function of a second order synthesizer including noise and delay is very similar to what was illustrated in Section 2.6 on page 16 for the case of a first order synthesizer with delay. Figure A.2 shows a phase model for a PLL-based frequency synthesizer with delay and noise where the dividers contain a non-ideal limiter. As indicated in the block diagram, each device in the frequency synthesizer is contributing to the total output noise. The analysis is based on a second order synthesizer employing a first order lag-lead control filter having the transfer function:

$$F(s) = \frac{s\tau_2 + 1}{s\tau_1 + b}\,. \qquad \text{(A.2.1)}$$

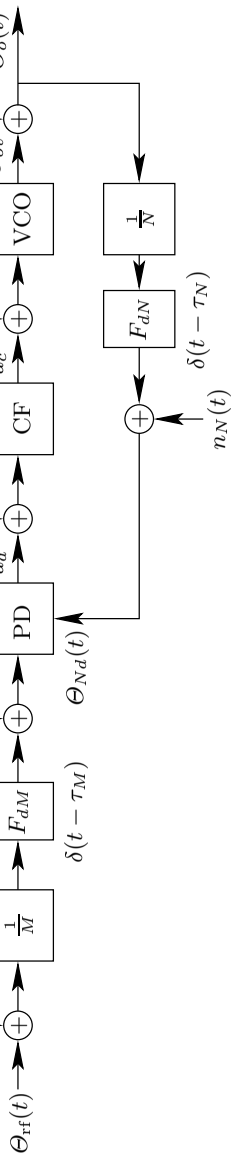

Fig. A.2: Phase model of a frequency synthesizer taking into account the noise coming from different components. The divider is modeled including delay and a non-ideal limiter, where the limiter is approximated by a piecewise linear characteristic discussed in the previous section.

The reference signal at the synthesizer input is:

$$\begin{aligned} u_{\text{in}}(t) &= \hat{u}_{\text{in}}(1 + R(t))\cos(\omega_c t + \phi_c + n_i(t))\,, \\ &= A(t)\cos(\Theta_{\text{rf}}(t) + n_i(t)) = A(t)\cos(\Theta_i(t))\,, \end{aligned} \tag{A.2.2}$$

where $R(t)$ and $n_i(t)$ are random variables representing amplitude fluctuations and phase noise of the reference signal, respectively, and ϕ_c is a constant offset. In a similar way the output of the VCO can be described as:

$$\begin{aligned} u_o(t) &= \hat{u}_o(1 + n_{VA}(t))\cos(\omega_o t + \phi_o + n_{vp}(t))\,, \\ &= n_o(t)\cos(\Theta_o(t))\,, \end{aligned} \tag{A.2.3}$$

where $n_{VA}(t)$ describes the amplitude fluctuations of the VCO signal and $n_{vp}(t)$ represents the phase noise of the VCO. Using results from Section 2.3 on page 12, it can be shown that a part of the amplitude fluctuations will pass through the dividers. The reference and the VCO signals after the bandpass soft limiter can be described as:

$$\begin{aligned} u_M(t) =& R_M(t)\cos(\Theta_{iM}(t)) = R_M(t)\cos\left(\frac{\Theta_i(t)}{M} + n_M(t)\right)\,, \\ =& \left\{\frac{4b}{\pi}\sin(\theta_1) - \frac{A(t)b}{a\pi}\sin(2\theta_1) + \frac{A(t)b}{a\pi}(\pi - 2\theta_1)\right\}\cdot \\ & \cos\left(\frac{\omega_c t}{M} + \frac{n_i(t)}{M} + n_M(t) + \frac{\phi_c}{M}\right)\,, \end{aligned} \tag{A.2.4}$$

$$\begin{aligned} u_N(t) =& R_N(t)\cos(\Theta_{oN}(t)) = R_N(t)\cos\left(\frac{\Theta_o(t)}{N} + n_N(t)\right)\,, \\ =& \left\{\frac{4d}{\pi}\sin(\theta_2) - \frac{n_o(t)d}{c\pi}\sin(2\theta_2) + \frac{n_o(t)d}{c\pi}(\pi - 2\theta_2)\right\}\cdot \\ & \cos\left(\frac{\omega_o t}{N} + \frac{n_{vp}(t)}{N} + n_N(t) + \frac{\phi_o}{N}\right)\,, \end{aligned} \tag{A.2.5}$$

with θ_1 and θ_2 being the conduction angles for the limiters in the reference and feedback dividers, respectively. Parameters a, b, c and d describe corresponding the x-y-axis amplitude limiting factors. $n_M(t)$ and $n_N(t)$ represent additional noise due to the reference and the feedback dividers, respectively.

Taking the reference and the feedback dividers' ideal delay into account by using the results from (2.5.2) on page 16, the two input signals to the phase detector can be expressed as:

$$u_{Md}(t) = R_{Md}(t)\cos(\theta_{iMd}(t))\,, \tag{A.2.6}$$

$$u_{Nd}(t) = R_{Nd}(t)(\cos(\theta_{oNd}(t))\,, \tag{A.2.7}$$

where

$$R_{Md}(t) = R_M(t-\tau_M)\,, \tag{A.2.8}$$

$$R_{Nd}(t) = R_N(t-\tau_N)\,, \tag{A.2.9}$$

$$\theta_{iMd}(t) = \frac{\Theta_i(t-\tau_M)}{M} + n_M(t)\,, \tag{A.2.10}$$

$$\theta_{oNd}(t) = \frac{\Theta_o(t-\tau_N)}{N} + n_N(t)\,. \tag{A.2.11}$$

As shown in (2.2.3) on page 10, the phase detector output depends on the amplitude fluctuations of the two input signals as well as the phase difference between them. The phase detector function including delay can be expressed as:

$$u_d(t) = g(R_{Md}(t), R_{Nd}(t), \varphi(t))\,, \tag{A.2.12}$$

where $\varphi(t)=\theta_{iMd}(t)-\theta_{oNd}(t)$ is the phase error function. The linearized output of the phase detector can expressed similar to (2.4.2) as:

$$\begin{aligned} u_d(t) \approx{}& \frac{b\Delta\Omega}{K_o} + K_D(\varphi(t)-\varphi_\infty) \\ &+ K_{RM}(R_{Md}(t)-R_{M0}) + K_{RN}(R_{Nd}(t)-R_{N0})\,. \end{aligned} \tag{A.2.13}$$

Note that $g(R_{M0}, R_{N0}, \varphi_\infty)=b\Delta\Omega/K_o$ with $\Delta\Omega=N\omega_c-\omega_o$ is the equation for the solution of the operating points and was derived in (2.2.10) on page 12. The corresponding Laplace domain expression for the output of the PD is:

$$\begin{aligned} U_d(s) \approx{}& \frac{b\Delta\Omega}{sK_o} + K_D\left(\Phi(s) - \frac{\varphi_\infty}{s}\right) \\ &+ K_{RM}\left(R_{Md}(s) - \frac{R_{M0}}{s}\right) + K_{RN}\left(R_{Nd}(s) - \frac{R_{N0}}{s}\right)\,, \end{aligned} \tag{A.2.14}$$

where

$$R_{Md}(s) = R_M(s)\mathrm{e}^{-s\tau_M}\,, \tag{A.2.15}$$

$$R_{Nd}(s) = R_N(s)\mathrm{e}^{-s\tau_N}\,. \tag{A.2.16}$$

The instantaneous phase angle of the VCO can be described as:

$$\theta_{oV}(t) = \omega_o t + K_o \int_0^t u_c(\tau)\mathrm{d}\tau + \phi_o \,, \tag{A.2.17}$$

and its corresponding Laplace domain expression is:

$$\Theta_{oV}(s) = \frac{\omega_o}{s^2} + K_o \frac{U_c(s)}{s} + \frac{\phi_o}{s} \,. \tag{A.2.18}$$

For a second order synthesizer, the output of the control filter $u_c(t)$ can be written as:

$$u_c(t) = (u_d(t) + n_{PD}(t)) * f(t) + n_{CF}(t) \,, \tag{A.2.19}$$

and the corresponding Laplace domain expression is:

$$U_c(s) = (U_d(s) + n_{PD}(s))F(s) + n_{CF}(s) \;. \tag{A.2.20}$$

Inserting the output of the control filter (A.2.20) into the expression for the VCO phase angle (A.2.18) taking into account that $\Theta_o(s)$=$\Theta_{oV}(s)$+$n_{vp}(s)$ results in:

$$\begin{aligned} \Theta_o(s) = {} & \frac{\omega_o}{s^2} + \frac{\phi_o}{s} + \frac{K_o}{s} F(s) n_{PD}(s) \\ & + \frac{K_o}{s} F(s) U_d(s) + \frac{K_o}{s} n_{CF}(s) + n_{vp}(s) \,. \end{aligned} \tag{A.2.21}$$

Inserting $U_d(s)$ from (A.2.14) into the expression for $\Theta_o(s)$ results in:

$$\begin{aligned} \Theta_o(s) = {} & \frac{\omega_o}{s^2} + \frac{\phi_o}{s} + \frac{K_o}{s} F(s) n_{PD}(s) + \frac{K_o}{s} n_{CF}(s) \\ & + n_{vp}(s) + \frac{K_o}{s} F(s) \left\{ \frac{b\Delta\Omega}{sK_o} + K_D \left(\Phi(s) - \frac{\varphi_\infty}{s} \right) \right. \\ & \left. + K_{RM} \left(R_{Md}(s) - \frac{R_{M0}}{s} \right) + K_{RN} \left(R_{Nd}(s) - \frac{R_{N0}}{s} \right) \right\} \,, \end{aligned} \tag{A.2.22}$$

and after inserting the phase error $\Phi(s)=\Theta_{iMd}(s)-\Theta_{oNd}(s)$, it becomes:

$$\begin{aligned}\Theta_o(s) = &\frac{\omega_o}{s^2} + \frac{b\Delta\Omega}{s^2}F(s) - \frac{K_D K_o}{s^2}F(s)\varphi_\infty + \frac{\phi_o}{s}\\ &+ \frac{K_o}{s}F(s)n_{PD}(s) + \frac{K_o}{s}n_{CF}(s) + n_{vp}(s)\\ &+ \frac{K_D K_o}{s}F(s)\Theta_{iMd}(s) - \frac{K_D K_o}{s}F(s)\Theta_{oNd}(s)\\ &+ \frac{K_{RM} K_o}{s}F(s)\left(R_{Md}(s) - \frac{R_{M0}}{s}\right)\\ &+ \frac{K_{RN} K_o}{s}F(s)\left(R_{Nd}(s) - \frac{R_{N0}}{s}\right).\end{aligned} \tag{A.2.23}$$

$\Theta_{oNd}(s)$ is the phase of the VCO after the feedback divider. The divider delays the VCO signal, divides it down by N, and adds extra noise $n_N(s)$ as:

$$\Theta_{oNd}(s) = \frac{\Theta_o(s)}{N}\mathrm{e}^{-s\tau_N} + n_N(s)\,. \tag{A.2.24}$$

Inserting $\Theta_{oNd}(s)$ into the expression for the synthesizer output phase (A.2.23), results in:

$$\begin{aligned}\Theta_o(s) = &\frac{\omega_o}{s^2} + \frac{b\Delta\Omega}{s^2}F(s) - \frac{K_D K_o}{s^2}F(s)\varphi_\infty + \frac{\phi_o}{s}\\ &+ \frac{K_o}{s}F(s)n_{PD}(s) + \frac{K_o}{s}n_{CF}(s) + n_{vp}(s)\\ &+ \frac{K_D K_o}{s}F(s)\Theta_{iMd}(s)\\ &- \frac{K_D K_o}{s}F(s)\left(\frac{\Theta_o(s)}{N}\mathrm{e}^{-s\tau_N} + n_N(s)\right)\\ &+ \frac{K_{RM} K_o}{s}F(s)\left(R_{Md}(s) - \frac{R_{M0}}{s}\right)\\ &+ \frac{K_{RN} K_o}{s}F(s)\left(R_{Nd}(s) - \frac{R_{N0}}{s}\right).\end{aligned} \tag{A.2.25}$$

Expressing the reference phase $\theta_{iMd}(t)$ from (A.2.10) in the Laplace domain results in:

$$\theta_{iMd}(s) = \frac{\theta_i(s)}{M}\mathrm{e}^{-s\tau_M} + n_M(s)\,, \tag{A.2.26}$$

$$= \left(\frac{\Theta_{\mathrm{rf}}(s)}{M} + \frac{n_i(s)}{M}\right)\mathrm{e}^{-s\tau_M} + n_M(s)\,. \tag{A.2.27}$$

The instantaneous phase angle of the reference containing phase noise is delayed by the reference divider and divided by the factor M. The divider also adds additional noise to the reference signal.

The instantaneous output phase angle $\Theta_o(s)$ from (A.2.25) can be reorganized in order to obtain the following equation relating the different input phase quantities to the output:

$$\begin{aligned}
\Theta_o(s) = {} & \frac{\frac{K_D K_o}{s} F(s)}{1 + \frac{K_D K_o}{Ns} F(s) \mathrm{e}^{-s\tau_N}} \left(\frac{\Theta_{\mathrm{rf}}(s)}{M} + \frac{n_i(s)}{M} \right) \mathrm{e}^{-s\tau_M} \\
& + \frac{\frac{K_D K_o}{s} F(s)}{1 + \frac{K_D K_o}{Ns} F(s) \mathrm{e}^{-s\tau_N}} n_M(s) \\
& + \frac{\frac{K_o}{s} F(s)}{1 + \frac{K_D K_o}{Ns} F(s) \mathrm{e}^{-s\tau_N}} n_{PD}(s) \\
& + \frac{\frac{K_o}{s}}{1 + \frac{K_D K_o}{Ns} F(s) \mathrm{e}^{-s\tau_N}} n_{CF}(s) \\
& + \frac{1}{1 + \frac{K_D K_o}{Ns} F(s) \mathrm{e}^{-s\tau_N}} n_{vp}(s) \\
& - \frac{\frac{K_D K_o F(s)}{s}}{1 + \frac{K_D K_o}{Ns} F(s) \mathrm{e}^{-s\tau_N}} n_N(s) \\
& + \frac{\frac{K_o K_{RM} F(s)}{s}}{1 + \frac{K_D K_o}{Ns} F(s) \mathrm{e}^{-s\tau_N}} \left(R_M(s) \mathrm{e}^{-s\tau_M} - \frac{R_{M0}}{s} \right) \\
& + \frac{\frac{K_o K_{RN} F(s)}{s}}{1 + \frac{K_D K_o}{Ns} F(s) \mathrm{e}^{-s\tau_N}} \left(R_N(s) \mathrm{e}^{-s\tau_N} - \frac{R_{N0}}{s} \right) \\
& + \frac{\frac{\omega_o}{s^2} + \frac{b\Delta\Omega}{s^2} F(s) - \frac{K_D K_o}{s^2} F(s) \varphi_\infty + \frac{\phi_o}{s}}{1 + \frac{K_D K_o}{Ns} F(s) \mathrm{e}^{-s\tau_N}} \,. \qquad \text{(A.2.28)}
\end{aligned}$$

Equation (A.2.28) gives the relationship for the output instantaneous phase angle of the VCO with respect to the reference signal as well as different noise sources. The part that describes the relationship of the VCO output phase $\Theta_o(s)$ to the synthesizer reference phase $\Theta_{\mathrm{rf}}(s)$ is called the transfer function of the synthesizer.

Introducing the filter transfer function $F(s)$ from (A.2.1) into (A.2.28) results in the equation of a second order frequency synthesizer:

$$
\begin{aligned}
\Theta_o(s) = {} & \frac{K_D K_o (s\tau_2 + 1)}{\tau_1 s^2 + \left(b + \frac{K_D K_o \tau_2 \mathrm{e}^{-s\tau_N}}{N}\right) s + \frac{K_D K_o \mathrm{e}^{-s\tau_N}}{N}} \left(\frac{\Theta_{\mathrm{rf}}(s)}{M} + \frac{n_i(s)}{M}\right) \mathrm{e}^{-s\tau_M} \\
& + \frac{K_o K_{RM} (s\tau_2 + 1)}{\tau_1 s^2 + \left(b + \frac{K_D K_o \tau_2 \mathrm{e}^{-s\tau_N}}{N}\right) s + \frac{K_D K_o \mathrm{e}^{-s\tau_N}}{N}} \left(R_M(s) \mathrm{e}^{-s\tau_M} - \frac{R_{M0}}{s}\right) \\
& + \frac{K_o K_{RN} (s\tau_2 + 1)}{\tau_1 s^2 + \left(b + \frac{K_D K_o \tau_2 \mathrm{e}^{-s\tau_N}}{N}\right) s + \frac{K_D K_o \mathrm{e}^{-s\tau_N}}{N}} \left(R_N(s) \mathrm{e}^{-s\tau_N} - \frac{R_{N0}}{s}\right) \\
& + \frac{K_D K_o (s\tau_2 + 1)}{\tau_1 s^2 + \left(b + \frac{K_D K_o \tau_2 \mathrm{e}^{-s\tau_N}}{N}\right) s + \frac{K_D K_o \mathrm{e}^{-s\tau_N}}{N}} n_M(s) \\
& + \frac{K_o (s\tau_2 + 1)}{\tau_1 s^2 + \left(b + \frac{K_D K_o \tau_2 \mathrm{e}^{-s\tau_N}}{N}\right) s + \frac{K_D K_o \mathrm{e}^{-s\tau_N}}{N}} n_{PD}(s) \\
& + \frac{K_o (s\tau_1 + b)}{\tau_1 s^2 + \left(b + \frac{K_D K_o \tau_2 \mathrm{e}^{-s\tau_N}}{N}\right) s + \frac{K_D K_o \mathrm{e}^{-s\tau_N}}{N}} n_{CF}(s) \\
& + \frac{s(s\tau_1 + b)}{\tau_1 s^2 + \left(b + \frac{K_D K_o \tau_2 \mathrm{e}^{-s\tau_N}}{N}\right) s + \frac{K_D K_o \mathrm{e}^{-s\tau_N}}{N}} n_{vp}(s) \\
& - \frac{K_D K_o (s\tau_2 + 1)}{\tau_1 s^2 + \left(b + \frac{K_D K_o \tau_2 \mathrm{e}^{-s\tau_N}}{N}\right) s + \frac{K_D K_o \mathrm{e}^{-s\tau_N}}{N}} n_N(s) \\
& + \frac{(s\tau_2 + 1)}{\tau_1 s^2 + \left(b + \frac{K_D K_o \tau_2 \mathrm{e}^{-s\tau_N}}{N}\right) s + \frac{K_D K_o \mathrm{e}^{-s\tau_N}}{N}} \frac{b\Delta\Omega}{s} \\
& - \frac{K_D K_o (s\tau_2 + 1)}{\tau_1 s^2 + \left(b + \frac{K_D K_o \tau_2 \mathrm{e}^{-s\tau_N}}{N}\right) s + \frac{K_D K_o \mathrm{e}^{-s\tau_N}}{N}} \frac{\varphi_\infty}{s} \\
& + \frac{(s\tau_1 + b)}{\tau_1 s^2 + \left(b + \frac{K_D K_o \tau_2 \mathrm{e}^{-s\tau_N}}{N}\right) s + \frac{K_D K_o \mathrm{e}^{-s\tau_N}}{N}} \frac{\omega_o}{s} \\
& + \frac{(s\tau_1 + b)}{\tau_1 s^2 + \left(b + \frac{K_D K_o \tau_2 \mathrm{e}^{-s\tau_N}}{N}\right) s + \frac{K_D K_o \mathrm{e}^{-s\tau_N}}{N}} \phi_o \,. \qquad \text{(A.2.29)}
\end{aligned}
$$

A.3 Active Filter Calculation

As an example on calculating the filter parameter, consider the structure of a non-ideal active filter with resistor R_3 for limiting the DC gain as shown in Fig. A.3.

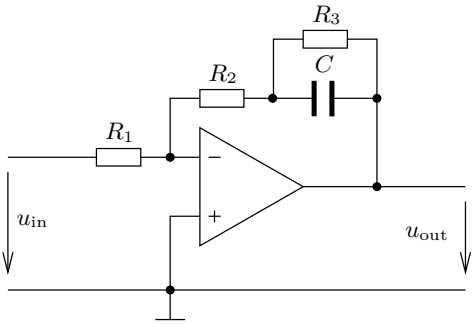

Fig. A.3: Circuit diagram of a non-ideal active control. When $R_3 \to \infty$ this filter acts as a perfect integrator.

This is an inverting operational amplifier with:

$$Z_1 = R_1, \qquad Z_2 = R_2 + \frac{1}{\mathrm{j}\omega\, C + \dfrac{1}{R_3}},$$

$$\Longrightarrow \qquad U_{\text{out}}(\mathrm{j}\omega) \approx -\frac{Z_2}{Z_1} U_{\text{in}}(\mathrm{j}\omega) = -\left(\frac{R_2}{R_1} + \frac{1}{\mathrm{j}\omega\, R_1\, C + \dfrac{R_1}{R_3}} \right) U_{\text{in}}(\mathrm{j}\omega)\,.$$

The transfer function can be derived to be:

$$H(\mathrm{j}\omega) \approx \frac{U_{\text{out}}}{U_{\text{in}}} = -\Big(\underbrace{\frac{R_2}{R_1}}_{\text{prop. part}} + \underbrace{\frac{1}{\mathrm{j}\omega\, R_1\, C + \dfrac{R_1}{R_3}}}_{\text{lowpass}} \Big),$$

$$= -\frac{R_2 + R_3}{R_1}\, \frac{1 + \mathrm{j}\omega\, C \dfrac{R_2\, R_3}{R_2 + R_3}}{1 + \mathrm{j}\omega\, C\, R_3}\,.$$

It can be expressed in the normalized form as:

$$H(\mathrm{j}\omega) = -K \frac{1 + \mathrm{j}\omega\, \tau_2}{1 + \mathrm{j}\omega\, \tau_1}, \tag{A.3.1}$$

with

$$\tau_1 = C\,R_3\,, \qquad \tau_2 = C\frac{R_2\,R_3}{R_2+R_3}\,, \qquad K = \frac{R_2+R_3}{R_1}\,,$$

For $R_3 \to \infty$ the filter acts as an ideal integrator for low frequencies. The transfer function reduces to:

$$H(\mathrm{j}\omega) = -\frac{1}{R_1}\;\frac{1+\mathrm{j}\omega\,CR_2}{\mathrm{j}\omega\,C} = -K_1\frac{1+\mathrm{j}\omega\,\tau_2}{\mathrm{j}\omega\,\tau_1}\,, \tag{A.3.2}$$

with

$$\tau_1 = C\,R_1\,, \qquad \tau_2 = CR_2\,, \qquad K_1 = -1\,.$$

Bode diagram for both the ideal and non-ideal integrator filter with ($\tau_1 > \tau_2$) is given below:

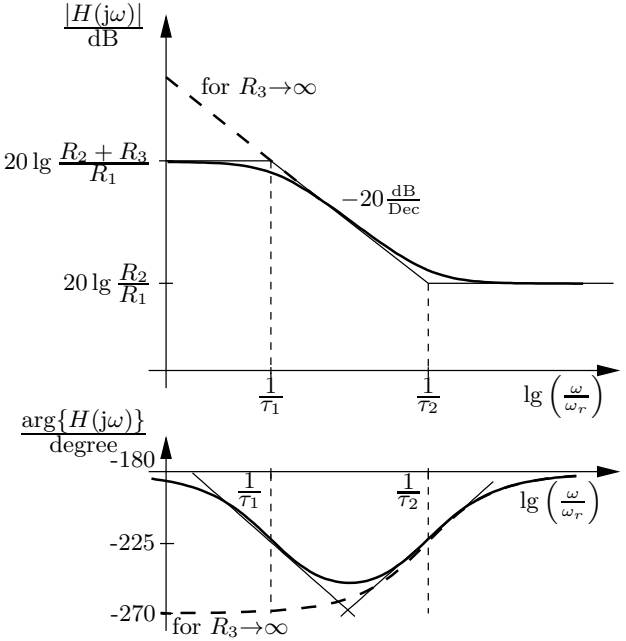

Fig. A.4: Bode diagram for the non-ideal active control filter. In the case of a perfect integrator the gain at DC goes to infinity.

The filter used in this work was of the type shown here but with R_3 not connected in general. The disadvantage of not using R_3 is that a small DC-offset at the input could lead to an increasing output voltage. The amplifier can saturate resulting in other frequency components not passing the filter. In this case the proportional part of the transfer function is suppressed leading to problems during the lock-in process. The purpose of R_3 is to limits the DC-gain to avoid these problems.

A.4 Average Power Spectrum of a PLL Including Effects of Noise

Given is the average power spectrum for a synthesizer taking into account the following noise sources: noise from reference oscillator A_{1i}, reference divider A_{2j}, phase detector A_{3k}, control filter A_{4l}, VCO phase noise A_{5m}, feedback divider A_{6n}, and VCO amplitude noise A_{7p}.

The solution here is showing a simplified case where only the first order approach for the solution of the Bessel functions shown in Section 3.3.1 is taken. It does not include effects of sampling and delay. Additionally, the influence on the loop of the amplitude fluctuations of the reference and the VCO signal are not taken into account. The amplitude noise of the VCO is only considered as a multiplicative term $(1+n_{va}(t))$ to the output signal of the VCO but its influence inside the loop is ignored:

$$
\begin{aligned}
\left\langle \overline{u_o(t)^2} \right\rangle &= \frac{\left\langle \overline{u_{o1}(t)^2} \right\rangle}{2} + \frac{\left\langle \overline{u_{o2}(t)^2} \right\rangle}{2}, \\
&= \frac{\hat{u}_o^2}{2} + \frac{\hat{u}_o^4}{4} \sum_{p=1}^{\infty} A_{7p}^2 \\
&+ \frac{\hat{u}_o^2 K_o^2 K_D^2}{4M^2} \sum_{i=1}^{\infty} \frac{A_{1i}^2}{\gamma_{1i}^2} \left(\alpha_{1i}^2 + \beta_{1i}^2\right) \\
&+ \frac{\hat{u}_o^2 K_o^2 K_D^2}{4} \sum_{j=1}^{\infty} \frac{A_{2j}^2}{\gamma_{2j}^2} \left(\alpha_{2j}^2 + \beta_{2j}^2\right) \\
&+ \frac{\hat{u}_o^2 K_o^2}{4} \sum_{k=1}^{\infty} \frac{A_{3k}^2}{\gamma_{3k}^2} \left(\alpha_{3k}^2 + \beta_{3k}^2\right) \\
&+ \frac{\hat{u}_o^2 K_o^2}{4} \sum_{l=1}^{\infty} \frac{A_{4l}^2}{\gamma_{4l}^2} \left(\alpha_{4l}^2 + \beta_{4l}^2\right)
\end{aligned}
$$

$$
\begin{aligned}
&+ \frac{\hat{u}_o^2}{4} \sum_{m=1}^{\infty} \frac{A_{5m}^2}{\gamma_{5m}^2} \left(\alpha_{5m}^2 + \beta_{5m}^2\right) \\
&+ \frac{\hat{u}_o^2 K_o^2 K_D^2}{4} \sum_{n=1}^{\infty} \frac{A_{6n}^2}{\gamma_{6n}^2} \left(\alpha_{6n}^2 + \beta_{6n}^2\right) \\
&+ \frac{\hat{u}_o^2 K_o^2 K_D^2}{8M^2} \sum_{i=1}^{\infty} \sum_{p=1}^{\infty} \frac{A_{1i}^2 A_{7p}^2}{\gamma_{1i}^2} \left(\alpha_{1i}^2 + \beta_{1i}^2\right) \\
&+ \frac{\hat{u}_o^2 K_o^2 K_D^2}{8} \sum_{j=1}^{\infty} \sum_{p=1}^{\infty} \frac{A_{2j}^2 A_{7p}^2}{\gamma_{2j}^2} \left(\alpha_{2j}^2 + \beta_{2j}^2\right) \\
&+ \frac{\hat{u}_o^2 K_o^2}{8} \sum_{k=1}^{\infty} \sum_{p=1}^{\infty} \frac{A_{3k}^2 A_{7p}^2}{\gamma_{3k}^2} \left(\alpha_{3k}^2 + \beta_{3k}^2\right) \\
&+ \frac{\hat{u}_o^2 K_o^2}{8} \sum_{l=1}^{\infty} \sum_{p=1}^{\infty} \frac{A_{4l}^2 A_{7p}^2}{\gamma_{4l}^2} \left(\alpha_{4l}^2 + \beta_{4l}^2\right) \\
&+ \frac{\hat{u}_o^2}{8} \sum_{m=1}^{\infty} \sum_{p=1}^{\infty} \frac{A_{5m}^2 A_{7p}^2}{\gamma_{5m}^2} \left(\alpha_{5m}^2 + \beta_{5m}^2\right) \\
&+ \frac{\hat{u}_o^2 K_o^2 K_D^2}{8} \sum_{n=1}^{\infty} \sum_{p=1}^{\infty} \frac{A_{6n}^2 A_{7p}^2}{\gamma_{6n}^2} \left(\alpha_{6n}^2 + \beta_{6n}^2\right) . \qquad \text{(A.4.1)}
\end{aligned}
$$

$$
\begin{aligned}
M_i &= i\Delta\omega \,, \\
\alpha_{1i} &= bM_iN^2 + \tau_1\tau_2 M_i^3 N^2 \,, \\
\beta_{1i} &= b\tau_2 M_i^2 N^2 - \tau_1 M_i^2 N^2 + K_o K_D \tau_2^2 M_i^2 N + K_o K_D N \,, \\
\gamma_{1i} &= b^2 M_i^2 N^2 + 2bK_o K_D \tau_2 M_i^2 N + K_o^2 K_D^2 \tau_2^2 M_i^2 + \tau_1^2 M_i^4 N^2 \\
&\quad - 2K_o K_D \tau_1 N M_i^2 + K_o^2 K_D^2 \,, \\
\alpha_{1i} &= \alpha_{2j} = \alpha_{3k} = \alpha_{6n} \,, \\
\beta_{1i} &= \beta_{2j} = \beta_{3k} = \beta_{6n} \,, \\
\gamma_{1i} &= \gamma_{2j} = \gamma_{3k} = \gamma_{6n} \,, \\
\alpha_{4l} &= K_o K_D bN + K_o K_D N M_l^2 \tau_1\tau_2 \,, \\
\gamma_{4l} &= b^2 N^2 M_l - K_o K_D N M_l \tau_1 + K_o K_D bN M_l \tau_2 + N^2 M_l^3 \tau_1^2 \,, \\
\alpha_{5m} &= K_o K_D bN M_m + K_o K_D N M_m^3 \tau_1\tau_2 \,, \\
\gamma_{5m} &= b^2 N^2 M_m^2 - K_o K_D N M_m^2 \tau_1 + K_o K_D bN M_m^2 \tau_2 + N^2 M_m^4 \tau_1^2 \,.
\end{aligned}
$$

Bibliography

[1] W.C. Lindsey and M.K. Simon, editors. *Phase-Locked Loops & Their Application*. IEEE Press, 1978.

[2] J.A. Crawford. *Frequency Synthesizer Design Handbook*. Arctech House, 1994.

[3] V.F. Kroupa. *Phase Lock Loops and Frequency Synthesis*. John Wiley & Sons Ltd, 2003.

[4] R.E. Best. *Phase-Locked Loops: Design, Simulation, and Applications*. McGraw-Hill Professional, 2003.

[5] A. Blanchard. *Phase-Locked Loops: Applications to Coherent Receiver Design*. John Wiley & Sons, Inc., 1976.

[6] W.F. Egan. *Frequency Synthesis by Phase Lock*. Wiley New York, 1981.

[7] F.M. Gardner. *Phaselock Techniques*. John Wiley & Sons, Inc., 2005.

[8] B.G. Goldberg. *Digital Frequency Synthesis Demystified: DDS and fractional-N PLLs*. Newnes, 1999.

[9] B. De Muer and M. Steyaert. *CMOS fractional-N synthesizers: design for high spectral purity and monolithic integration*. Kluwer Academic Publishers, 2003.

[10] D.H. Wolaver. *Phase-Locked Loop Circuit Design*. Printice Hall, Inc., 1991.

[11] K. Shu and E. Sánchez-Sinencio. *CMOS PLL synthesizers: analysis and design*. Springer Verlag, 2005.

[12] D. Banerjee. *PLL performance, simulation and design*. Dog Ear Publishing, 2006.

[13] C.S. Vaucher. *Architectures for RF frequency synthesizers*. Kluwer Academic Publishers, 2002.

[14] S.R. Al-Araji, Z.M. Hussain, and M.A. Al-Qutayri. *Digital phase lock loops: architectures and applications*. Springer, 2006.

[15] D.R. Stephens. *Phase-locked loops for wireless communications: digital, analog, and optical implementations*. Kluwer Academic Publishers, 2002.

[16] J. Craninckx and M. Steyaert. *Wireless CMOS frequency synthesizer design*. Kluwer Academic Publishers, 1998.

[17] Y. Tang, Y. Zhou, S. Bibyk, and M. Ismail. A low-noise fast-settling PLL with extended loop bandwidth enhancement by new adaptation technique. In *14th Annual IEEE International ASIC/SOC Conference: proceedings: September 12-15, 2001, Hyatt Regency Crystal City, Arlington, VA*, page 93. IEEE, 2001.

[18] T. Lee and B. Razavi. A stabilization technique for phase-locked frequency synthesizers. In *in Symp. VLSI Circuits Dig. Tech. Papers*, pages 39–42, 2001.

[19] S.T. Moon, A.Y. Valero-López, and E. Sánchez-Sinencio. Fully integrated frequency synthesizers: A tutorial. *International Journal of High Speed Electronics and Systems*, 15(2):353–376, 2005.

[20] D. Vye. Performing Transient Analysis on PLL Frequency Synthesizers. *Microwave Journal*, 45(1):62, 2002.

[21] J.J Gribble. Modified Root Locus Plots for SISO Systems with Time Delay. *IEEE Control Systems Magazine*, 13(1):54–56, 1993.

[22] S. Sancho, A. Suarez, and T. Fernandez. Nonlinear dynamics of microwave synthesizers–stability and noise. *IEEE Transactions on Microwave Theory and Techniques*, 49(10):1792–1803, 2001.

[23] P. Heydari. Analysis of the PLL jitter due to power/ground and substrate noise. *IEEE Transactions on Circuits and Systems I: Regular Papers*, 51(12):2404–2416, 2004.

[24] K.A. Jenkins, W. Rhee, J. Liobe, and H. Ainspan. Experimental analysis of the effect of substrate noise on PLL performance. In *Proc. Digest of Papers Silicon Monolithic Integrated Circuits in RF Systems 2006 Topical Meeting*, 2006.

[25] A. Mehrotra. Noise Analysis of Phase-Locked Loops. *Computer-Aided Design, International Conference on*, 0:277, 2000.

[26] B. Razavi. Predicting the Phase Noise and Jitter of PLLBased Frequency Synthesizers. In *Phase-Locking in High-Performance Systems:From Devices to Architectures*, pages 46–69. IEEE, 2003.

[27] M. Sanchez, M. A. del Casar, C. Briso, and J. I. Alonso. Application of the fractional synthesizers to SFCW radars. In *Proc. 33rd European Microwave Conf*, volume 3, pages 1207–1210, 2003.

[28] L. Lascari. Accurate phase noise prediction in PLL synthesizers. *Applied Microwave and Wireless*, 12(5):90–94, 2000.

[29] W. Lin. Arrival-time detection reduces PLL jitter. *RF DESIGN*, 30(2):40, 2007.

[30] Mini-Circuits Inc. Characterizing Phase Noise. *RF DESIGN*, 101:58–59, 2003.

[31] W. Kester. Converting oscillator phase noise to time jitter. *MT-008 TUTORIAL, Rev. A, Oct*, 2008.

[32] K. Kundert. Predicting the phase noise and jitter of PLL-based frequency synthesizers. *Phase-Locking in High-Performance Systems*, pages 46–69.

[33] P. Smith. Little known characteristics of phase noise. *Application Note AN-741. Analog Devices, Inc.(August). AN05225–0–1*, 2004.

[34] A. Hajimiri. Noise in Phase-Locked Loops [Invited]. *Proc. SSMSD*, pages 1–6, 2001.

[35] M. Curtin and P. O'Brien. Phase-Locked Loops for High-Frequency Receivers and Transmitters–Part 2. *Analog Dialogue*, 33(5):123–126, 1999.

[36] V. Ivo and H. Josef. Phase Noise Measurement. *Proceedings of the Radioelectronika 2001, BRNO 2001*, pages 131–134, 2001.

[37] M. de Queiroz Tavares and P. Semiconductors. PLL Frequency Synthesizers: Phase Noise Issues and Wide Band Loops. *Analog circuit design: high-speed analog-to-digital converters, mixed-signal design, PLL's and synthesizers*, page 357, 2000.

[38] T.C. Weigandt. *Low-Phase-Noise, Low-Timing-Jitter Design Techniques for Delay Cell Based VCOs and Frequency Synthesizers*. PhD thesis, Citeseer, 1998.

[39] J. Besse. Effects of synthesizer phase noise on BER performance. *EE: Evaluation Engineering*, 39(4):4, 2000.

[40] J. Craninckx and M.S.J. Steyaert. A 1. 8-GHz low-phase-noise CMOS VCO using optimized hollow spiral inductors. *IEEE Journal of Solid-State Circuits*, 32(5):736–744, 1997.

[41] M.H. Perrott, M.D. Trott, and C.G. Sodini. A Modeling Approach for Fractional-N Frequency Synthesizers Allowing Straightforward Noise Analysis. *IEEE J. Solid-State Circuits*, 37(8):1028–1038, 2002.

[42] T. H. Lee and A. Hajimiri. Oscillator phase noise: a tutorial. *IEEE Journal of Solid-State Circuits*, 35(3):326–336, 2000.

[43] D. Eric. Model PLL Dynamics And Phase-Noise Performance. *Microwaves & RF*, 39(2):73–82, 2000.

[44] S.O. Rice. Mathematical analysis of random noise. *Bell Systems Tech. J., Volume 23, p. 282-332*, 23:282–332, 1944.

[45] G.S. Sangha and M.H.W. Hoffmann. Analysis and Design of a Frequency Synthesizer with Internal and External Noise Sources. In *Conf. Proceedings*, volume 780, pages 521–524. AIP, 2005.

[46] G.S. Sangha and M.H.W. Hoffmann. Analysis and simulations of a frequency synthesizer with internal and external noise sources. *Advances in Radio Science*, 4:175–178, 2006.

[47] G.S. Sangha and M.H.W. Hoffmann. Investigation of the Effects of Noise on a Frequency Synthesizer. In *Conf. Proceedings*, volume 922, pages 716–719. AIP, 2007.

[48] G.S. Sangha and M.H.W. Hoffmann. Experimental Study of Noise in a Frequency Synthesizer. In *Conf. Proceedings*, volume 1129, pages 505–508. AIP, 2009.

[49] W.B. Davenport and W.L. Root. *An Introduction to the Theory of Random Singnals and Noise*. McGraw-Hill, 1958.

[50] D.D. Carpenter. The effect of time delays on the stability of practical phase locked receivers with multiple conversion by utilizing root locus with positive feedback. In *Conf. Rec.*, volume II of *Int. Conf. Commun.*, pages 33.14–33.19, 1973.

[51] J.W.M. Bergmans. Effect of loop delay on stability of discrete-time PLL. *IEEE Transactions on Circuit and Systems-I*, 42:229–231, 1995.

[52] J.E. Marshall. *Control of time-delay systems*. Peter Peregrinus Ltd., 1979.

[53] VA Baikov and KR Khusnutdinova. Formal Linearization and Exact Solutions of Some Nonlinear Partial Differential Equations. *Nonlinear Mathematical Physics*, 3(1-2):139–146, 1996.

[54] B. Krishnan. An existence theorem for nonlinear delay differential equations. *International Journal of Stochastic Analysis*, 2(2):85–89, 1900.

[55] A. Papachristodoulou, J.C. Doyle, and S.H. Low. Analysis of nonlinear delay differential equation models of TCP/AQM protocols using sums of squares. *Atlantis*, 2004.

[56] R.W. Lardner and G.N. Bojadziev. Non-linear differential equations with damping and large time delay. *IMA Journal of Applied Mathematics*, 18(1):25, 1976.

[57] L.F. Shampine and S. Thompson. Solving delay differential equations with dde23. *Appl. Numer. Math*, 37(4):441–458, 2001.

[58] Matlab R2010a. MathWorks, USA.

[59] J. Engberg and T. Larsen. *Noise theory of linear and nonlinear circuits*. John Wiley & Sons Ltd., 1995.

[60] R. Pettai. *Noise in Receiving Systems*. Wiley-Interscience, 1984.

[61] W.R. Bennett. *Electrical Noise*. New York: McGraw-Hill, 1960.

[62] Texas Instruments. OPA301: Low-Noise, High-Speed,16-Bit Accurate CMOS Operational Amplifier, USA.

[63] H. Akabane, M. Agu, and A. Yoshida. Fractal Characters of 1/2-order Integration of White Noise and $1/f$ Resistance Fluctuation. *Japanese Journal of Applied Physics*, 38(Part 1, No. 5A):3007–3010, 1999.

[64] M.H.W. Hoffmann. *Hochfrequenztechnik*. Springer, 1997.

[65] Maple V13. MapleSoft, Canada.

[66] M. Abramowitz and I.A. Stegun. *Handbook of Mathematical Functions with Formulas, Graphs and Mathematical Tables*. U.S. Department of Commerce, National Bureau of Standards, Applied Mathematic series 55, 1972.

[67] O. Kallenberg. *Foundations of modern probability*. Springer Verlag, 2002.

[68] A. Vretblad. *Fourier analysis and its applications*. Springer Verlag, 2003.

[69] H.T. Davis, H.T. Davis, and K.T. Thomson. *Linear algebra and linear operators in engineering with applications in Mathematica*. Academic Press, 2000.

[70] E.T. Jaynes and G.L. Bretthorst. *Probability Theory: The Logic Of Science*. Cambridge University Press, 2003.

[71] R.M. Gray. *Probability, random processes, and ergodic properties*. Springer Verlag, 2006.

[72] R.S. Burns. *Advanced control engineering*. Butterworth-Heinemann, 2001.

[73] B.R. Hunt, R.L. Lipsman, and J. Rosenberg. *A guide to MATLAB: for beginners and experienced users*. Cambridge Univ Pr, 2006.

[74] R.E. White. *Computational mathematics: models, methods, and analysis with MATLAB and MPI*. CRC Press, 2004.

[75] M. Hoffmann and H. Weiß. Systematic measurements for testing the influence of an internal noise source on the phase noise of an oscillator. In *Proceedings of German Microwave Conference (GeMiC)*, 2006.

[76] D. Self. *Audio power amplifier design handbook*. Newnes, 2006.

[77] A.S. Sedra and K.C. Smith. *Microelectronic circuits*. Oxford University Press, USA, 1998.

[78] Analog Devices. AD8061: Low Cost, 300 MHz Rail-to-Rail Amplifier, USA.

[79] MIC5209 Data Sheet: 500 mA Low-Noise LDO Regulator, USA. Micrel. Micrel.

[80] Rohde&Schwarz. Signal Source Analyzer R&S FSUP, Munich.

[81] Analog Devices. AD8616: Precision 20 MHz CMOS Dual Rail-to-Rail Operational Amplifier, USA.

[82] M.H.W. Hoffmann. *Verrauschte FM-Signale und Ihre Demodulation durch PLL-FM-Demodulatoren*. PhD thesis, Universität Saarland, 1980.

[83] Mini-Circuits. TUF-3: Frequency Mixer, USA.

[84] Analog Devices. ADCMP601: Rail-to-Rail, Very Fast, 2.5 V to 5.5 V, Single-Supply TTL/CMOS Comparator, USA.

[85] Texas Instruments. SN74LV4046A: High-Speed CMOS Logic Phase-Locked Loop with VCO, USA.

[86] Analog Devices. ADF4002: Phase Detector/PLL Frequency Synthesizer, USA.

[87] MAXIM. MAX2605: 45 MHz to 650 MHz, Integrated IF VCOs with Differential Output.

[88] Analog Devices. ADF4156: 6 GHz Fractional-N Frequency Synthesizer, USA.

[89] STMicroelectronics. TS922: Rail-to-rail high output current dual operational amplifier, Switzerland.

[90] Analog Devices. ADA4841-2: Dual Low Power, Low Noise and Distortion, Rail-to-Rail Output Amplifier, USA.

[91] Kay, A. Analysis and Measurement of Intrinsic Noise in Op Amp Circuits, Texas Instruments, USA. In *http://www.en-genius.net/site/zones/audiovideoZONE/technical_notes/avt_032910*.

[92] LTSpice IV. Linear Technology, USA.

[93] Tektronix. AFG3102: Dual Channel Arbitrary/Function Generator, USA.

[94] S. Großklaß. *Comparison of Integer-N and Fractional-N PLLs*. Institute for Microwave Techniques, University of Ulm, Diplomarbeit, September 2009.

[95] A. Vollmer. *Design of an Ultra Low Noise SAWR Feedback Oscillator at 433 MHz*. Institute for Microwave Techniques, University of Ulm, Studienarbeit, May 2009.

Curriculum Vitae

Name:	Gurpreet Singh Sangha
Date of Birth:	13.03.1976
Place of Birth:	Hissar, India
Family status:	married, one child

School Education

1982–1986	Government Senior Secondary School, Dharsul Kalan, Haryana, India
1986–1994	Ramouz College, Antelias, Lebanon
1994–1996	Beirut Evangelical School for Boys and Girls, Rabiya, Lebanon Degree: Lebanese Bacheloriate

University Education

1996–2002	Notre Dame University, Zouk Mikael, Lebanon Degree: Bachelor in Electrical Engineering
2002–2004	University of Ulm, Germany Degree: M.Sc. in Communications Technology

Work Experience

2004–2010	Research assistant at the Institute of Microwave Techniques, University of Ulm, Germany